DISSERTATION FOR THE DEGREE OF DOCTOR OF PHILOSOPHY (PHD)

Ruxolitinib-mediated Modulation and Dynamic Expression of P-glycoprotein in Human CD8+ T Cell Memory Subsets During Differentiation

by Kipchumba Biwott

UNIVERSITY OF DEBRECEN
DOCTORAL SCHOOL OF MOLECULAR CELLULAR AND IMMUNE BIOLOGY

DEBRECEN, 2025

DISSERTATION FOR THE DEGREE OF DOCTOR OF PHILOSOPHY (PHD)

Ruxolitinib-mediated Modulation and Dynamic Expression of P-glycoprotein in Human CD8+ T Cell Memory Subsets During Differentiation

by Kipchumba Biwott

Supervisor: Zsolt Bacso, M.D., Ph.D.

UNIVERSITY OF DEBRECEN
DOCTORAL SCHOOL OF MOLECULAR CELLULAR AND IMMUNE BIOLOGY

DEBRECEN, 2025

TABLE OF CONTENTS

LIST OF FIGURES

LIST OF TABLES

LIST OF ABBREVIATIONS

ABC – ATP-binding cassette

ABCB1 – ATP-binding cassette subfamily B member 1

ANOVA – Analysis of variance

APC – Antigen-presenting cell

ATP – Adenosine triphosphate

BCL-6 – B-cell lymphoma 6 protein

BLIMP-1 – B lymphocyte-induced maturation protein 1

CFTR – Cystic fibrosis transmembrane conductance regulator

CSA – Cyclosporine A

CTL – Cytotoxic T lymphocyte

EGTA – Ethylene Glycol-bis(β-aminoethyl ether)-N,N,N′,N′-tetraacetic acid

ET – Essential thrombocythemia

FACS – Fluorescence-activated cell sorting

FDCP – Factor-dependent cell progenitors

FERM – Four-point-one, ezrin, radixin, moesin domain

FlowSOM – Flow cytometry self-organizing maps

FOXO1 – Forkhead box protein O1

G-CSF – Granulocyte colony-stimulating factor

GVHD – Graft-versus-host disease

HDL – High-density lipoprotein

ID2/ID3 – Inhibitor of DNA binding 2/3

IFN – Interferon

IL – Interleukin

JAK1/2 – Janus kinase 1 and 2

JH – JAK homology domain

KS test – Kolmogorov-Smirnov test

MAIT – Mucosal-associated invariant T cells

MCP-1 – Monocyte chemoattractant protein-1

MDR-1 – Multidrug resistance protein 1

MHC – Major histocompatibility complex

MPN – Myeloproliferative neoplasm

mTOR – Mechanistic target of rapamycin

NBD – Nucleotide-binding domain

PBMC – Peripheral blood mononuclear cell

PC – Phosphatidylcholine

PD-1 – Programmed cell death protein 1

Pgp – P-glycoprotein

PMF – Primary myelofibrosis

PV – Polycythemia vera

RUX – Ruxolitinib

SH2 – Src homology 2 domain

STAT – Signal transducer and activator of transcription

TALL-1 – T-cell acute lymphoblastic leukemia cell line

TAP – Transporter associated with antigen processing

Tcm – Central memory T cell

TCR – T-cell receptor

Tem – Effector memory T cell

Temra – Effector memory T cells re-expressing CD45RA

Tex – Exhausted T cell

Th1/Th17 – T helper 1/17 cells

TKI – Tyrosine kinase inhibitor

TMD – Transmembrane domain

TNF – Tumor necrosis factor

Treg – Regulatory T cell

Tscm – Stem cell memory T cell

Tym – Young memory T cell

UMAP – Uniform Manifold Approximation and Projection

VLCFA – Very long-chain fatty acids

X-ALD – X-linked adrenoleukodystrophy

ZEB1/ZEB2 – Zinc finger E-box-binding homeobox

ZQ – Zosuquidar

1. INTRODUCTION

P-glycoprotein (Pgp), also known as multidrug resistance protein 1 (MDR1), is encoded by the *ABCB1* gene and is a prominent member of the ATP-binding cassette (ABC) transporter family. It functions primarily as an ATP-dependent efflux pump that exports a wide array of xenobiotics, toxins, and chemotherapeutic agents out of cells (Gottesman et al., 2002; Sarkadi et al., 2006; Ueda et al., 1986). Pgp is highly expressed in physiological barriers such as the blood-brain barrier, gastrointestinal tract, liver, kidneys, and placenta, where it plays a key detoxification role.

In the immune system, Pgp is expressed in various leukocyte subsets, including monocytes, dendritic cells (DCs), natural killer (NK) cells, mucosal-associated invariant T (MAIT) cells, antigen-presenting cells (APCs), B cells, and both CD4+ and CD8+ T lymphocytes (Alsuliman et al., 2017; Bossennec et al., 2018; Chen et al., 2020; Devine et al., 2023; Kooij et al., 2014; Neubauer, 2007; Pendse et al., 2003; Thurm et al., 2021). Beyond its well-known drug efflux activity, Pgp serves essential immunomodulatory functions. In CD8+T cells, it provides protection against reactive oxygen species (ROS) during early T cell receptor (TCR) activation, promotes activation and proliferation, and supports T cell persistence in hostile environments such as the tumor microenvironment (Boddupalli et al., 2016; Chen et al., 2020; Higgins, 1992; Mackay et al., 2012; Murata et al., 2016; Turtle et al., 2009; Wang et al., 2018). Additionally, Pgp is involved in cytokine secretion and cholesterol transport, which are crucial for immune signaling and homeostasis (Seelig, 2020).

Importantly, Pgp overexpression in tumor cells is a well-documented mechanism of chemotherapy resistance, including resistance to tyrosine kinase inhibitors (TKIs) such as imatinib in chronic myeloid leukemia (CML) (Bello-Reuss et al., 2000; Eadie et al., 2014). While high-dose chemotherapy can be effective in eliminating tumor cells, it often results in the depletion of tumor-infiltrating lymphocytes (TILs) and increased susceptibility to opportunistic infections (Ramos et al., 2021). Interestingly, memory CD8+T cells that express Pgp exhibit enhanced survival and resilience under stress, making them attractive candidates for adoptive immunotherapy and vaccine design (Mackay et al., 2012; Murata et al., 2016; Turtle et al., 2009).

The Janus kinase-signal transducer and activator of transcription (JAK-STAT) pathway is another central regulatory mechanism in immune signaling. Mutations in this pathway are common in hematologic malignancies, particularly in Philadelphia chromosome-negative myeloproliferative neoplasms (MPNs) such as essential thrombocythemia, polycythemia vera (PV), and primary myelofibrosis (MF), as well as in acute lymphoblastic leukemia (Bader & Meyer, 2022; Hammersen et al., 2023; Zhang et al., 2005). Dysregulated JAK1/2 activity contributes to cytokine hypersensitivity and malignant proliferation, which led to the development of JAK inhibitors like ruxolitinib (RUX), a selective JAK1/2 inhibitor approved for treating MPNs, MF, and graft-versus-host disease (GVHD) (Elli et al., 2019; Ivo et al., 2021; La Rosée et al., 2020; Verbeke et al., 2019).

RUX is metabolized primarily by cytochrome P450 enzymes CYP3A4 and CYP2C9 (Isberner et al., 2021). The potential for interaction with Pgp is clinically relevant, as Pgp may affect the bioavailability and immunosuppressive efficacy of RUX. In fact, genetic inactivation of *ABCB1* gen has been shown to enhance the anti-proliferative effects of RUX in T cells (Caroline et al., 2016), suggesting that Pgp may serve as a pharmacokinetic barrier to its action.

Programmed death-1 (PD-1, CD279) is an inhibitory receptor upregulated on T cells following activation. It plays a crucial role in limiting excessive immune responses and maintaining tolerance (Ortega et al., 2024; Rekik et al., 2015). In chronic inflammatory states such as myelofibrosis, sustained T cell activation can lead to immune exhaustion and high PD-1 expression. Notably, RUX has been shown to reduce PD-1 levels in T cells, potentially restoring immune function. Its therapeutic applications continue to expand, supported by promising outcomes in recent clinical studies. These include its use in protocols for managing the hyperinflammatory response in COVID-19 (Chen et al., 2020; Hammersen et al., 2023). However, it remains unclear whether RUX directly modulates Pgp expression or function, or whether it acts as a Pgp substrate, modulator, or inducer.

In this study, we investigated the relationship between RUX and Pgp in human CD8+ cytotoxic T lymphocytes under resting and antigen-primed conditions. We assessed *ABCB1* mRNA and protein expression, performed efflux assays using calcein-AM, and measured Pgp ATPase activity. Additionally, we evaluated CD8 and PD-1 expressions as markers of activation cytotoxicity and

immune exhaustion, respectively. Our findings show that RUX inhibits Pgp function in a dose-dependent manner, but only at high concentrations. Interestingly, RUX stimulated basal Pgp ATPase activity and suppressed verapamil-induced activation, indicating an interaction or modulation of the transporter.

Moreover, RUX delayed the downregulation of *ABCB1* mRNA in activated T cells and reduced PD-1 expression, suggesting it modulates both efflux activity and immune activation trajectories. Using an *in vitro* T cell priming model, we co-cultured human peripheral blood mononuclear cells (PBMCs) with JY cells, which are Epstein-Barr virus-transformed B-lymphoblastoid APCs that express MHC class I A2 and MHC class II DQ molecules (Bacsó et al., 1996; Biwott et al., 2025b). This long-term co-culture allowed us to track memory T cell development, and CD3/CD28 activation was used to study differentiation kinetics.

Our data revealed that ABCB1 expression is higher in unprimed Cytotoxic T lymphocytes (CTLs and declines following activation. However, RUX modifies this pattern by delaying mRNA downregulation, indicating its role as a transcriptional modulator. Furthermore, RUX promoted a shift in CD8+T cell subset distribution, enhancing the naive (Tn) and central memory (Tcm) populations while reducing effector memory (Tem) and terminal effector (Te) cells. It also expanded the pool of Pgp-expressing stem-like memory T cells and suppressed PD-1 upregulation.

In conclusion, these findings provide compelling evidence that RUX modulates Pgp expression and function, alters the course of T cell differentiation, and suppresses immune exhaustion markers such as PD-1. These dual effects on transporter activity and immune phenotype have important implications for optimizing immunosuppressive and anti-cancer therapies, especially in contexts such as GVHD, MPNs, and T cell exhaustion.

1.1. THE HUMAN ATP-BINDING CASSETTE TRANSPORTER SUPERFAMILY

ATP-binding cassette (ABC) transporters are a group of protein transporters that export substances from one side of the cell membrane to the other (Srikant, 2020). These transporters have been identified in sequenced genomes and have several paralogs across various species: for example,

there are 48 in humans, 79 in *Escherichia coli*, 23 in *Saccharomyces cerevisiae*, and more than 100 in *Arabidopsis thaliana* (Srikant, 2020). These efflux pump proteins utilize energy from ATP while transporting molecules across the cell membrane, working against the concentration gradient. They transport a wide range of substances, including sugars, amino acids, proteins, lipids, and metal ions (Higgins, 1992). Similar to Pgp, other ABC transporters are categorized based on their Nucleotide Binding Domains (NBDs). These NBDs feature specific motifs, namely the Walker A and Walker B motifs, separated by approximately 90 to 120 amino acids. Additionally, ABC genes contain a signature motif known as the C-loop, located upstream of the Walker B motif. These critical Walker motifs of the ATPase domain bind nucleotides.

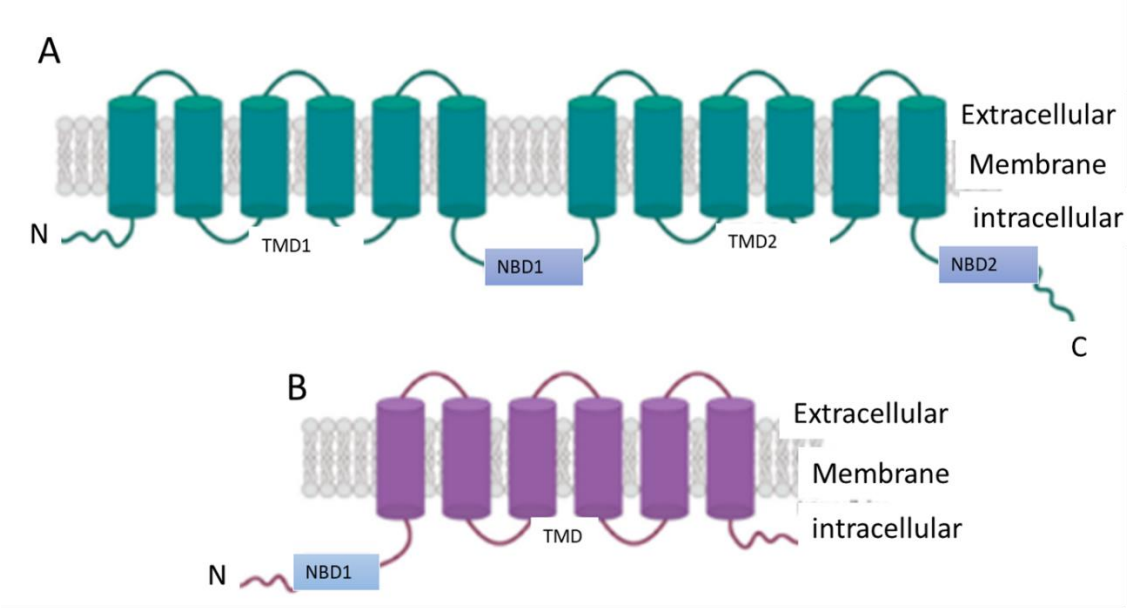

Figure 1: ABCB1 and ABCG2 protein structures. (A) Pgp is a full transporter, and (B) breast cancer resistance protein (BCRP/ABCG2) is a half transporter. NBD: nucleotide-binding domain; TMD: transmembrane domain (Skinner et al., 2023).

The Walker A and Walker B motifs are highly conserved sequences found in ATP-binding proteins, playing a pivotal role in ATP hydrolysis, a fundamental process for energy transduction in cells (Ambudkar et al., 2006; Stratford et al., 2006). The Walker A motif (P-loop)**,** with its characteristic GXXXX GK(T/S) sequence, binds the phosphate groups of ATP, where the lysine (K) residue interacts with the β- and γ-phosphates of ATP, stabilizing the negative charge, X is any amino acid repeated four times. The Walker B motif (hhhhD/E)**,** typically containing a conserved aspartate (D) or glutamate (E) residue, coordinates a magnesium ion (Mg^{2+}) and facilitates the nucleophilic attack on the γ-phosphate of ATP, h refers to any hydrophobic amino

acid. Together, these motifs enable the efficient hydrolysis of ATP into ADP and inorganic phosphate (Pi), releasing energy that drives conformational changes in ABC transporters (Oiwa & Sakakibara, 2005). The aspartate or glutamate residue in the Walker B motif acts as a catalytic base, deprotonating a water molecule to generate the nucleophilic hydroxide ion (OH^-) required for ATP hydrolysis. This mechanism underscores the critical role of these conserved residues in energy-dependent cellular processes (Dean et al., 2001).

Beyond the NBDs, ABC proteins possess transmembrane domains (TMDs) built from 6 to 12 hydrophobic transmembrane sequences that determine their substrate specificity. Mutations in ABC genes contribute to various human genetic disorders, such as cystic fibrosis, defects in bile and cholesterol transport, anemia, and neurological diseases (Dean et al., 2022). Their structural composition can categorize ABC proteins into full and half-transporters. Full-transporters generally include two TMDs and two nucleotide-binding domains (Figure 1 A). In comparison, half-transporters contain just one TMD and one NBD, requiring them to pair up as homodimers or heterodimers to function effectively (Figure 1 B) (Skinner et al., 2023).

1.1.1. Human ABC genes and associated diseases

The human ABC gene family includes the subfamilies ABCA, ABCB, ABCC, ABCD, ABCE, ABCF, and ABCG. The ABCA subfamily consists of 12 transporters, categorized into two groups based on their phylogenetic intron structures. The first subgroup includes ABCA1, ABCA2, ABCA3, ABCA4, ABCA7, ABCA12, and ABCA13, which are distributed across six chromosomes. The second group consists of five genes: ABCA5, ABCA6, ABCA8, ABCA9, and ABCA10 (Dean et al., 2001; Gottesman & Ambudkar, 2001).

Certain human diseases are closely linked to ABC genes. For example, ABCA1 is associated with cholesterol transport issues and disorders related to high-density lipoprotein (HDL) synthesis. Mutations in ABCA1 can lead to a rare genetic disorder known as Tangier Disease, characterized by low levels of HDL and Apoprotein A-I. Symptoms of this disorder include anemia, thrombocytopenia, neuropathy, and tonsillitis (Maranghi et al., 2019). The ABCA4 protein transports derivatives of vitamin A in rod photoreceptor cells. Mutations in ABCA4 can lead to Stargardt disease (Wang et al., 2023).

ABCB1 is a crucial transporter that exports xenobiotics from normal and tumor cells and is often linked to chemotherapy resistance. ABCB4 transports phosphatidylcholine (PC) in the liver, while ABCB11 transports bile salts. Mutations in ABCB11 are linked to pediatric hepatocellular cancer. ABCB2 (TAP1) and ABCB3 (TAP2) work together as heterodimers to transport peptides into the endoplasmic reticulum, presenting antigens via class I HLA molecules. Mutations in these genes are associated with autoimmune diseases, including ankylosing spondylitis, celiac disease, and Graves' disease (Dean et al., 2022). ABCB10 plays a role in protecting against reactive oxygen species.

The ABCC subfamily has varied functions such as ion transport and toxin efflux activity. Specifically, ABCC1 is a multidrug resistance protein, while the cystic fibrosis transmembrane conductance regulator (CFTR, also known as ABCC7) is implicated in the autosomal recessive disease cystic fibrosis. This disease primarily affects the mucosal lining of the lungs and digestive system (Dean et al., 2001; Moore et al., 2023). In addition, the *ABCC13* gene in other species encodes proteins responsible for transporting various molecules across cell membranes. However, in humans, *ABCC13* is likely nonfunctional due to accumulated mutations and deletions in the gene, preventing it from producing an active protein (Fan et al., 2023).

The ABCD subfamily comprises ABCD1, ABCD2, and ABCD3, which are in peroxisomes. These half-transporters function as homodimers or heterodimers. ABCD1 and ABCD2 regulate the transport of long-chain fatty acids. X-linked adrenoleukodystrophy (X-ALD) is associated with variants in ABCD1. This accumulation of very long fatty acids in peroxisomes results in myelin defects in neurons, as well as malfunctions in the adrenal glands and testes (Dean et al., 2022). ABCD2 is linked also to the transport of very long-chain fatty acids (VLCFAs), while ABCD3 is involved in transporting branched-chain acyl-CoA into peroxisomes. Additionally, ABCD4 transports compounds in mitochondria and lysosomes, and mutations in ABCD4 can result in cobalamin deficiency (Kawaguchi & Morita, 2016; Morita & Imanaka, 2012).

The ABCE and ABCF subfamilies contain ATP-binding domains but lack transmembrane domains. Therefore, they do not participate in membrane transport, they are involved in ribosome recycling after termination, facilitating 60S subunit maturation and ribosome assembly and translational elongation respectively (Dean et al., 2022). The ABCG1 protein is involved in cholesterol transport in macrophages, T cell proliferation, and protection from apoptosis. ABCG2

serves as a drug-resistance protein that effluxes xenobiotics out of cells. Finally, ABCG5 and ABCG8 function as heterodimers that transport sterols in the liver and intestine. Genetic alterations in ABCG5 and ABCG8 can lead to sitosterolemia, characterized by the accumulation of cholesterol and sterols (Dean et al., 2022; Lee et al., 2011).

1.1.2. P-glycoprotein and its structure

Pgp, also known as multidrug-resistance protein 1, is a member of the ABC transporter family, one of the largest groups of active transporter proteins (Seelig, 2020; Singh et al., 2021). It is a single polypeptide composed of two homologous TMDs, each consisting of six membrane-spanning α-helices and one cytoplasmic nucleotide-binding domain, linked by a 75-amino acid region that contains numerous phosphorylation sites (Johnston & Kennedy, 2024; Mora Lagares et al., 2022) (Figure 2). The TMDs form a central pocket for drug binding and provide a pathway for substrate translocation, while the NBDs are responsible for ATP hydrolysis. Binding of ATP to the NBDs triggers conformational changes that switch the TMDs from an inward-facing to an outward-facing orientation, thereby facilitating the release of substrates across the membrane (Singh et al., 2021). In humans, Pgp is encoded by the *ABCB1* gene, whereas in mice, it is encoded by the *Abcb1a* and *Abcb1b* genes (Chen et al., 2020). The molecular mass of ABCB1 is approximately 170 kDa (Seelig, 2020). Other ABC transporters that are involved in xenobiotic efflux include the multidrug-resistant protein MRP1/ABCC1, encoded by the *ABCC1* gene, the breast cancer-resistant protein BCRP/ABCG2, encoded by the *ABCG2* gene, (Fan et al., 2023; Moore et al., 2023). Pgp plays a crucial role in drug absorption, distribution, metabolism, and elimination and Toxicity (ADMET). Drug interactions with Pgp can significantly reduce drug levels in serum and tissues. Pgp was initially discovered during surface labeling of CHO cells, which displayed resistance to colchicine. The MDR1 protein influences the rate of cellular uptake of xenobiotic substances, as well as their distribution and elimination, thus affecting the ADMET properties of drugs and their bioavailability (Ahmed Juvale et al., 2022). Pgp substrates include lipophilic compounds and those containing hydrogen bonds, such as anti-neoplastic agents, antiepileptics, adrenoreceptor antagonists, calcium ion blockers, steroids, opioids, immunosuppressants, protease inhibitors, antiemetics, antiparasitics, antibiotics, lipid-lowering agents, and histamine antagonists (Ahmed Juvale et al., 2022).

In its inward-facing conformation (Figure 3), Pgp has an internal cavity measuring 60Å diameter, while in its outward-facing conformation, the cavity size ranking varies from 70 Å to 200 Å. The NBDs are separated by 30 Å (Ahmed Juvale et al., 2022). The inward-facing conformation of Pgp has binding pockets that feature aromatic and hydrophobic residues with polar side chains, such as similar Q343, Q721, Q942, Q986, and S975. These residues are organized to form hydrogen bonds and van der Waals interactions, which enable the protein to bind to a wide variety of molecules (Ahmed Juvale et al., 2022; Karthika et al., 2022). Substances ranging from 250 to 4000 Da have been identified as Pgp substrates. The key difference between ABC transporters and non-transporters lies in the conserved motif C (LSGGQ), which is present between the A and B motifs in ABC transporters. These motifs form the active site for ATPases, comprising Walker A and B motifs from one NBD and the C motif from the other NBD (Figure 4) (Ahmed Juvale et al., 2022; Johnston & Kennedy, 2024; Mora Lagares et al., 2022).

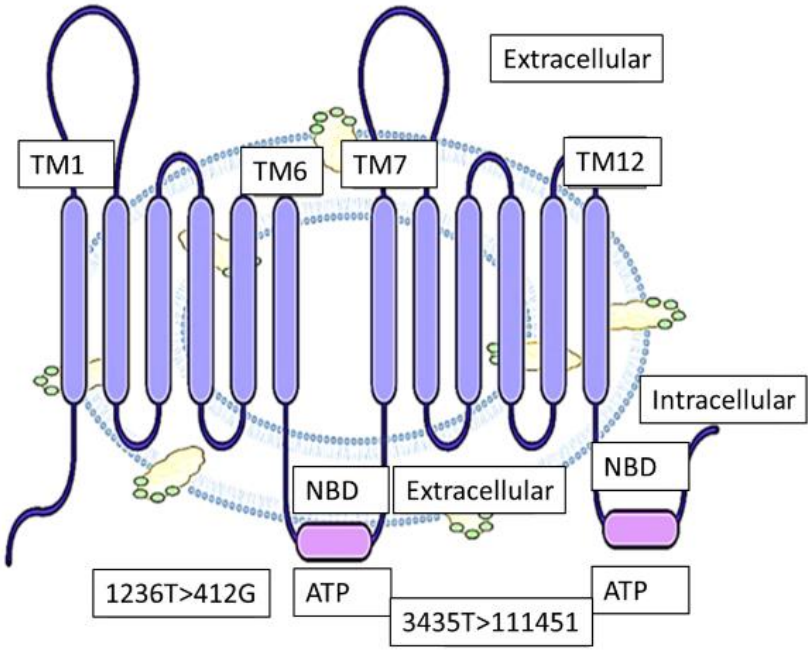

Figure 2: Structure of P-glycoprotein. The transmembrane domain spans from TM1 to TM6 and from TM7 to TM12. The nucleotide-binding domains (NBD) are associated with adenosine triphosphate (ATP) (Karthika et al., 2022).

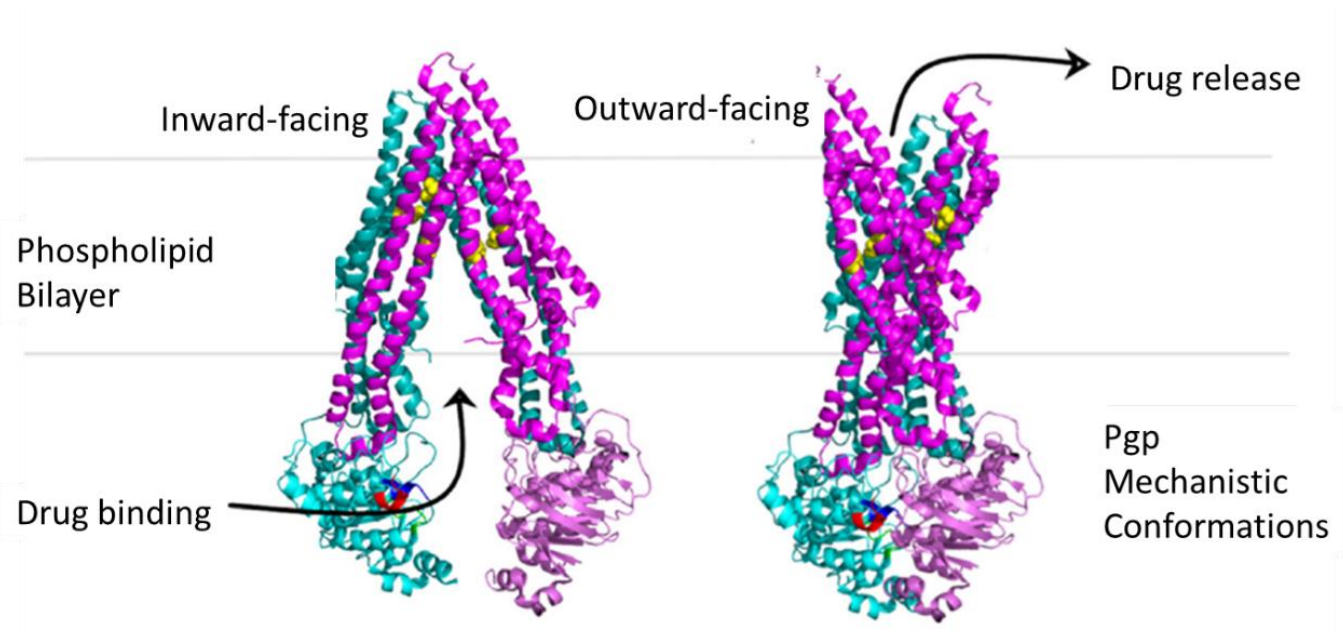

Figure 3: Ribbon structure of P-glycoprotein. Showing inward-facing and outward-facing conformations, with cavity dimensions, NBD separation, and binding pockets formed by aromatic, hydrophobic, and polar residues (Ahmed Juvale et al., 2022).

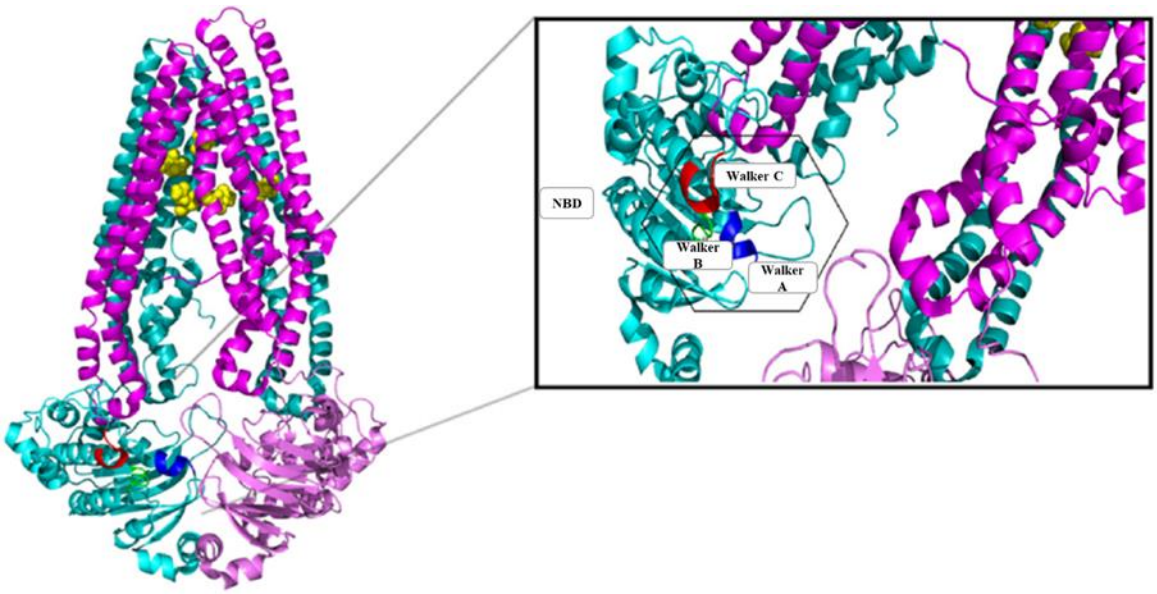

Figure 4: Shows the P-glycoprotein structure illustrated using ribbons. The nucleotide-binding domains are indicated, highlighting the ABC walker regions for ATP binding and hydrolysis. It is depicted in various colors: A in blue, B in green, and C in red (Ahmed Juvale et al., 2022).

1.1.3. Role of Pgp in the immune system cells and the rest of the organs

Pgp functions as an efflux pump, exporting xenobiotics and pharmacological drugs such as calcium channel blockers and protease inhibitors into compartments like bile ducts, the intestinal lumen, and renal proximal tubules, thereby contributing to systemic detoxification and tissue protection (Dean et al., 2022). It is highly expressed in barrier and excretory tissues, including the adrenal glands, kidneys, liver, colon, and blood-brain barrier, where it plays a protective role by limiting the accumulation of harmful substances. According to the Protein Atlas (Figure 5), Pgp shows particularly high expression in adrenal tissue, where it regulates hormone secretion and steroid transport. Its expression in the brain, lungs, skin, and heart underscores its critical role in maintaining physiological homeostasis and defending against toxic insults across multiple organ systems (Fan et al., 2023). In the liver, Pgp facilitates cholesterol transport, homeostasis, and bile excretion, and its downregulation has been associated with disrupted lipid bioavailability and metabolic imbalance (Ahmed Juvale et al., 2022). In renal proximal tubule epithelial cells, Pgp responds to endotoxemia by increasing efflux activity to support renal detoxification (Heemskerk et al., 2007). Notably, during *Listeria monocytogenes* infection, Pgp mediates the efflux of bacterial proteins from the basal to apical surfaces of intestinal villi, suggesting a specialized role

in intestinal immune defense (Neudeck et al., 2004). In the placenta, Pgp facilitates glucocorticoid transport, thereby protecting the developing fetus by limiting excessive fetal hormone exposure through redirection to maternal circulation (Devine et al., 2023; Ge et al., 2021).

Beyond its classical roles in drug transport and detoxification, Pgp is increasingly recognized for its involvement in immune regulation. It is expressed in various immune cell types, including dendritic cells, CD4+ regulatory T cells (Tregs), effector T cells, CD8+ cytotoxic T cells, B cells, natural killer (NK) cells, and macrophages (Ahmed Juvale et al., 2022; Bossennec et al., 2018; Chaudhary et al., 1992; Ge et al., 2021). In dendritic cells, Pgp modulates activation, migration, proliferation, and cytokine production (Lee et al., 2011; Randolph et al., 1998). It has been implicated in the regulation of type I interferon responses, particularly IFN-β, suggesting a broader role in innate immunity (Ahmed Juvale et al., 2022). In T cells, Pgp facilitates migration by transporting sphingosine-1-phosphate and is essential for the development and function of Tregs, which are critical for maintaining immune tolerance. It also protects T helper cells (Th1 and Th17) in the small intestine from oxidative stress induced by bile acids. Importantly, CD8+ T cells expressing Pgp display enhanced effector memory characteristics, improved survival, and increased resistance to oxidative stress, highlighting Pgp's contribution to adaptive immunity and immune cell fitness (Chen et al., 2020). Additionally, in macrophages, Pgp promotes the shift from pro-inflammatory M1 to anti-inflammatory M2 phenotypes, further emphasizing its immunoregulatory capabilities (Cory et al., 2016; Pavlova et al., 2023).

In the context of stem cell biology, Pgp is highly expressed in CD34+ hematopoietic stem cells (HSCs), where it plays a key role in regulating differentiation and survival. ABCB1 supports the proliferation and repopulation of actively cycling Side Population cells, distinguishing it from ABCG2, which marks quiescent stem cells and contributes to self-renewal by exporting differentiation-inducing substrates (Koh et al., 2023; Yin et al., 2008). This functional distinction positions ABCB1 as a marker of active proliferation and tissue regeneration, while ABCG2 identifies stem cell quiescence and long-term maintenance. Overall, Pgp plays a multifaceted role not only in xenobiotic efflux and barrier function but also in lipid regulation, hormone transport, immune cell function, and stem cell biology, making it a critical component in maintaining physiological integrity and immune competence across tissue development and function of regulatory T cells (Tregs)**,** which are vital for maintaining immune tolerance. Furthermore, Pgp

provides a protective function for T helper cells (Th1 and Th17) in the small intestine, shielding them from oxidative stress caused by bile acids. This underscores the multifaceted role of Pgp in immune regulation and cellular protection, particularly within the intestinal environment (Ahmed Juvale et al., 2022). Notably, CD8+ T cells expressing Pgp exhibit enhanced effector memory, contributing to cell survival and oxidative stress resistance (Chen et al., 2020).

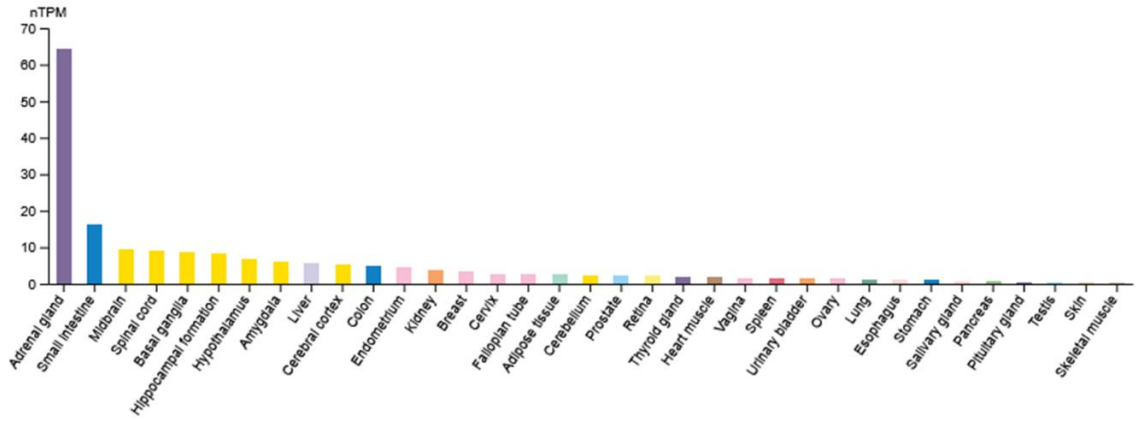

Figure 5: The expression levels of the ABCB1 gene across various tissues. Pgp is measured in normalized Transcripts Per Million (nTPM) on the Y-axis, ranging from 0 to 70, while the X-axis lists tissues including the adrenal gland, small intestine, midbrain, spinal cord, basal ganglia, hippocampus, hypothalamus, amygdala, liver, cerebral cortex, endometrium, colon, breast, cervix, fallopian tube, adipose tissue, cerebellum, prostate, retina, thyroid gland, heart muscle, vagina, spleen, urinary bladder, ovary, lung, esophagus, stomach, salivary gland, pituitary gland, pancreas, testis, and skeletal muscle, with each bar's height indicating the gene expression level in nTPM and varying colors used for visual differentiation without representing a specific categorical distinction (The Human Protein Atlas) (Devine et al., 2023).

1.2. CD8+ T CELLS AND INFECTIONS

CD8+ T cells are essential for combating intracellular pathogens and targeting and destroying cancer cells (Kaech & Wherry, 2007; Raskov et al., 2021). Upon antigen recognition, naive CD8+ T cells undergo activation with significant expansion and maturation into effector and memory T cell subsets (Figure 6). After eliminating infected or tumor cells, the expanded populations contract by apoptosis, and only the memory cells remain. Effector CD8+ T cells, also known as cytotoxic T lymphocytes, induce the death of target cells by engaging Fas/Fas ligand interactions and releasing the cytolytic protein perforin, which forms pores in the target cell membrane, allowing

granzymes (serine proteases) to enter and initiate apoptosis, similar to caspases. Memory CD8+ T cells are crucial for providing swift and robust immune responses upon re-exposure to antigens, thereby contributing to long-term immunity (Kaech & Wherry, 2007; Sun et al., 2023).

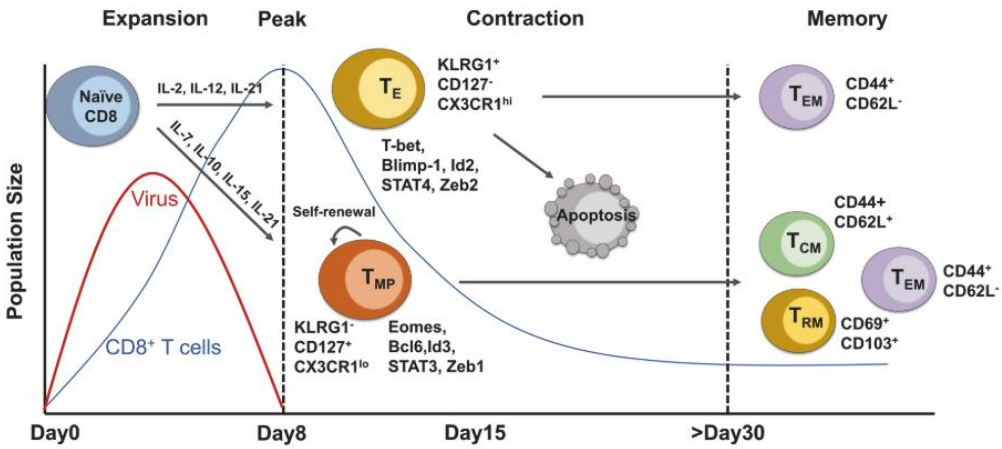

Figure 6: Dynamics of CD8+ T cell response and differentiation during acute viral infection.

At this point, CD8+ T cells differentiate into effector T cells (Te), which target and destroy infected cells, and T memory precursor (Tmp), which can develop into long-lasting memory T cells. Differentiation into effector or memory cells is regulated by specific transcription factors and cytokines. After the peak, most effector cells undergo apoptosis, with some transitioning into Tem cells, while Tmp cells persist and give rise to central memory T cells and resident memory T cells (Trm). This process ensures long-term immunity by maintaining a diverse pool of memory T cells capable of providing rapid protection upon re-infection (Sun et al., 2023).

During CD8+ T cell final differentiation, multiple effector and memory cell subsets arise, each with distinct characteristics, differentiation potentials, and immune roles. These subsets include short-lived effector T cells (Te), exhausted T cells (Tex), long-lived memory T cells (Tm), Tmp, and both Tcm and Tem (Muroyama & Wherry, 2021). Additionally, tissue-resident memory T cells (Trm) are localized in specific tissues to provide immediate, localized immune responses. These populations are defined by their phenotypes, developmental pathways, and specific immune roles (Kaech et al., 2003; Kaech & Wherry, 2007; Muroyama & Wherry, 2021).

1.2.1. Heterogeneity of CD8+ T cells

Naive CD8+ T cells become activated upon encountering antigens presented by antigen-presenting cells (APCs) after migrating to lymphoid tissues. Upon activation, CD8+ T cells rapidly proliferate

(clonal expansion) into effector cells to fight chronic infections or tumors. This response is triggered by antigen recognition and co-stimulation. After the threat is controlled, most effector cells die in the contraction phase**,** but a few differentiate into memory T cells, such as T memory precursors, which persist and can mount rapid responses upon future antigen exposure. During the differentiation of antigen-reactive cells, both phenotypical and functional changes occur (Stemberger et al., 2009). $CD8^+$ T cells can be categorized into short-lived and long-lived effector and memory T cells, which differ in effector functions, homing potential, and proliferative capacity (Sallusto et al., 1999); short-lived effectors migrate to peripheral organs to display effector functions, whereas long-lived memory cells are subdivided into effector memory T cells (Tem) and central memory T cells (Tcm).

Tem cells mainly migrate to peripheral tissues, whereas Tcm is home to and recirculate to secondary lymphoid organs, expanding vigorously upon encountering antigens compared to Tem. Tcm cells produce IL-2 and display effector functions, including the production of IFN-γ, along with constant self-renewal activity (Stemberger et al., 2009). Markers have been used to identify CD8+ subsets, such as the homing receptor CD62L and IL-7 receptor. Tcm cells are characterized as CD62L high, Tem cells as CD62L low, and effector cells as CD62L low (Jameson & Masopust, 2018). Stem cell memory T (Tscm) cells, defined by markers CD45RA+CD62L+CCR7 and memory marker CD95+, lie between naive and Tcm cells (Flynn & Gorry, 2014; Mahnke et al., 2013; Restifo & Gattinoni, 2013). Previous studies have shown that the CD73+ marker and ALDH1 activity decline with age (Murata et al., 2016). Cells expressing CD45RA+CD62L+ contain CD8+CD73+ cells, which comprise a novel memory T cell population, young memory T cells (Tym) with proliferative capacity and drug resistance (Murata et al., 2016). Chronic infection leads to excessive signals that reduce T cell effector function, resulting in the expression of inhibitory receptors like PD1+ and LAG3 (Ivo et al., 2021). This condition is associated with lower metabolism, homeostatic proliferation, and responses to antigens (Kurachi, 2019; Xia et al., 2021). Temra cells are terminally differentiated effector memory T cells characterized by CD8+ expression (T effector memory cells re-expressing CD45RA), which are a subset of T cells involved in immune memory and rapid immune responses, particularly important in chronic infections, aging, and immune surveillance. CD45RA serves as a marker to distinguish Temra from central memory and effector memory T cells, which have CD45RO. Temra cells gradually lose co-stimulatory markers CD27 and CD28 (Lugli et al., 2020; Türk et al., 2024).

1.2.2. CD8+ T cell exhaustion

Exhausted CD8+ T cells (Tex) represent a subset of differentiated cells exhibiting distinct phenotypic characteristics, heterogeneity, and varying functional capabilities. During the exhaustion process, these CD8+ T cells lose their ability to produce IL-2 and TNF-α, and there is a decline in cytotoxic functionality (Wherry et al., 2003). Additionally, impaired production of IFN-γ generally occurs at a later stage of exhaustion, which is frequently associated with terminally differentiated T cells (Böhm et al., 2021).

Terminal CD8+ T effector memory cells have been observed to retain the capability to degranulate and produce various chemokines and cytokines, including MIP-1α, MIP-1β, RANTES, and IL-10 (Wherry et al., 2007). In contrast to tissue memory (Tm) cells during acute infections, which undergo consistent homeostatic self-renewal in response to cytokines such as IL-7 and IL-15, Tex cells demonstrate significant defects in their responsiveness to these homeostatic cytokines. This impairment can be attributed to deficiencies in the signaling pathways associated with IL-7Rα and IL-2/15Rβ (Sun et al., 2023).

The defining characteristic of CD8+ Tex cells is their upregulated and sustained expression of multiple immune regulators (IRs) such as PD-1, CTLA-4, LAG-3, TIGIT, Tim-3, CD39, and 2B4 (Blackburn et al., 2009; Wherry et al., 2007). The extent of IR expression and co-expression is directly correlated with the degree of T cell exhaustion. Additionally, Tex cells express costimulatory molecules that may contribute to T cell exhaustion in the context of chronic infections and tumors. For instance, co-stimulation of CD27 and CD28 can enhance the process of T-cell exhaustion (Sun et al., 2023). CD28 signaling is further compromised due to diminished competition with CTLA-4 for B7 family ligands. PD-1 signaling plays a crucial role in suppressing T cell functionality by specifically inducing the dephosphorylation of the TCR and CD28, thereby decreasing downstream signaling and impairing T cell activation (Hui et al., 2017).

Persistent antigen exposure reduces TCF-1 expression, driving stem-like (early precursor, late progenitor) Tpex, into transitory effector (Teff)-like states and terminal cells (Figure 7). Teff-like cells, which are crucial for viral and tumor control, express CX3CR1, produce IFN-γ, TNF-γ,

granzyme B, and exhibit high cytotoxicity and proliferation. Their generation depends on CD4+ T cell help and IL-21 (Sun et al., 2023). Hudson *et al.* proposed a linear trajectory in which Tpex cells develop into CX3CR1+Tim-3+CD101− Teff-like cells, which then further differentiate into CX3CR1−Tim-3+CD101+ Terminal Tex cells (Hudson et al., 2019).

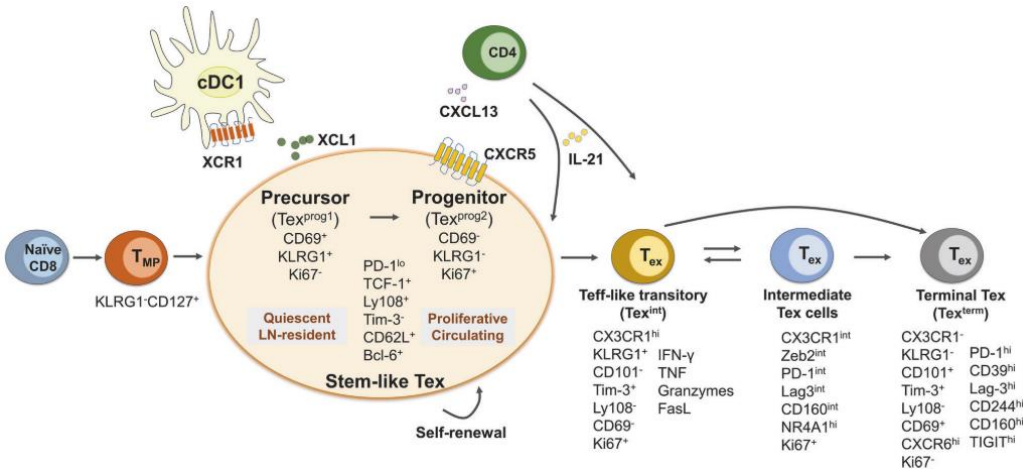

Figure 7: CD8+ T cell exhaustion trajectory in chronic infection and tumors. In chronic infections or tumors, CD8+ T cells undergo a progressive exhaustion process, transitioning through distinct stages: naive, Tmp, stem-like T cell precursors (Tpex, including early precursors and late progenitors), effector-like transitory, intermediate, and Tex. Each stage is characterized by unique surface markers, effector molecule expression, proliferation capacity, and tissue localization. CD4+ T cells play a critical role in shaping these subsets by producing CXCL13, which promotes the differentiation of CXCR5+ Tpex cells, and IL-21, which drives the formation of CX3CR1+ transitory Tex cells. Additionally, Tpex cells interact with conventional type 1 dendritic cells (cDC1s) through the XCL1/XCR1 signaling axis, facilitating their development and function (Hudson et al., 2019; Sun et al., 2023; Tsui et al., 2022).

1.2.3. Transcriptional regulation of cytotoxic T-cell differentiation

The transcriptional regulation of CD8+ T cell development is orchestrated by a network of transcription factors (TFs) that balance the differentiation of effector and memory CD8+ T cells. These TFs often function in pairs, creating a counter-regulatory axis that fine-tunes cell fate decisions. Notably T-box transcription factors T-bet and Eomesodermin (EOMES), drive the differentiation of activated CD8+ T cells into cytotoxic T lymphocytes (Kaech & Cui, 2012). CTLs express effector molecules such as IFN-γ, granzyme B, perforin, and chemokine receptors

CXCR3, and CXCR4. The chemokine receptor CXCR4 expressed on activated T cells, binds chemokines like CXCL9, CXCL10, and CXCL11, guiding cells to sites of inflammation and playing a role in autoimmune diseases. CXCR4, expressed on various cell types, binds CXCL12 (SDF-1) and is critical for cell migration, stem cell homing, and cancer progression, making it a target for therapeutic interventions such as stem cell mobilization and cancer treatment. Conversely, CD8+ T cells lacking T-bet and EOMES can differentiate into IL-17-producing CD8+ T cells, losing their CTL identity (Kallies et al., 2009).

The expression of T-bet and EOMES is regulated by TCR activation, along with cytokines such as IL-12 and signaling pathways like mTOR (Hu et al., 2024). These factors induce T-bet expression in a RUNX3-dependent manner, while IL-2 further enhances their expression. However, IL-12 and mTOR inhibit the transcriptional activator FOXO1, creating a dynamic regulatory network. T-bet and EOMES also cooperate to maintain memory CD8+ T cells by promoting IL-15 signaling, which supports their proliferation and survival. Effector CD8+ T cells with high T-bet levels exhibit elevated KLRG1 and reduced IL-7Rα, marking them as terminal effector cells. In contrast, cells with high EOMES and low KLRG1 and IL-7Rα are poised to develop into memory cells, expressing markers like CD62L, CXCR3, and CXCR4, which facilitate homing to lymph nodes and bone marrow (Intlekofer et al., 2008; Kaech & Cui, 2012). The absence of EOMES impairs the persistence and homeostatic turnover of memory CD8+ T cells (Banerjee et al., 2010). Notably, T-bet and EOMES exhibit reciprocal expression patterns, with high levels in effector cells and reduced levels in memory cells (Kaech & Cui, 2012).

Effector CD8+ T cells express the transcriptional repressor B lymphocyte induced maturation protein-1 (BLIMP-1), which is induced by IL-2 and IL-12 (Kaech & Cui, 2012). BLIMP-1 enhances KLRG1 expression while suppressing IL-7Rα, a pattern that reverses in memory CD8+ T cells. In contrast, BCL-6, a transcriptional repressor that antagonizes BLIMP-1, is highly expressed in memory cells and supports the development of self-renewing central memory T cells (Ichii et al., 2004). Additionally, ID2 and ID3, inhibitors of DNA-binding proteins, play crucial roles in CD8+ T cell differentiation. ID2 supports the transition from naive to effector cells, while ID3 is essential for the transition from effector to memory cells (Kaech & Cui, 2012; Yang et al., 2011). These TFs inhibit E-protein transcription factors, further shaping the differentiation trajectory of CD8+ T cells (Zook et al., 2018).

The regulation of CD8+ T cell fate involves a complex interplay of opposing TFs, including T-bet vs. EOMES, BLIMP-1 vs. BCL-6, ID2 vs. ID3, STAT4 vs. STAT3, and ZEB2 vs. ZEB1 (Sandu et al., 2020; Sun et al., 2023). Generally, T-bet, BLIMP-1, ID2, STAT4, and ZEB2 promote effector differentiation and CTL function, while EOMES, BCL-6, ID3, STAT3, and ZEB1 support memory development and maintenance. These TFs engage in intricate cross-regulatory interactions; for example, ID2 promotes T-bet, which in turn enhances ZEB2 expression, while STAT3 sustains BCL-6 and EOMES expression. BLIMP-1 represses ID3, and BLIMP-1 and BCL-6 mutually inhibit each other, creating a finely balanced regulatory network (Joshi et al., 2007; Sun et al., 2023; Xin et al., 2016).

Effector differentiation is primarily driven by TCR signals, costimulatory signals, and cytokines such as IL-2, IL-12, type I IFN, IFN-γ, IL-21, and IL-27 (Chen et al., 2018; Kallies et al., 2009; Xin et al., 2016). For instance, IL-2 and IL-12 induce BLIMP-1, T-bet, and ID2 expression, while IFN-α/β supports CD8+ T cell expansion and IFN-γ production via STAT4. IFN-γ synergizes with IFN-α to further amplify T-bet expression (Chen et al., 2018; Curtsinger et al., 2005). Additionally, IL-21 and IL-27 promote BLIMP-1 expression in effector CD8+ T cells (Zhang & Bevan, 2011). In contrast, memory differentiation is supported by cytokines like IL-7, IL-10, IL-15, and IL-21 (Sun et al., 2023). TCF-1, a downstream effector of the Wnt signaling pathway, and FOXO1, associated with metabolic regulation, are critical for memory CD8+ T cell differentiation and longevity (Zhao et al., 2022). Further research is needed to elucidate how TCR and cytokine signaling sequentially activate these TFs and how their cross-regulation shapes CD8+ T cell fate.

Subset	Key Transcription Factors	Roles and Characteristics	Markers and Functions
Naive CD8+ T Cells	Tcf1, LEF1	Maintain an undifferentiated state, self-renewal capacity.	CD45RA, CD62L await activation by antigens.
Stem Cell Memory T cells	Tcf1, LEF1, BCL6	Self-renewal, long-term survival, and potential to differentiate.	CD45RO, CD62L; generate other subsets upon antigen re-encounter.
Young Memory T cells	Tcf1, LEF1, EOMES	Maintain a transitional state between naive and central memory T cells, high proliferative potential.	CD45RA+, CD44int, CD73, CD62L+; exhibit rapid recall responses and robust expansion upon antigen exposure.
Central Memory T cells	BCL6, Tcf1, EOMES	Long-lived, strong antigen recall responses proliferate rapidly.	CD45RO, CD62L, CD44hi; enhanced immune recall.
Effector Memory Tcells	Blimp-1, T-bet	Rapid effector response, strong cytotoxicity, cytokine production.	CD45RO, CD44hi, CD62Llo; secrete IFN-γ, TNF-α.

Effector Memory Re-expressing CD45RA T cells	T-bet, EOMES,	Fully differentiated, robust cytotoxicity.	CD45RA, CD57+; contribute to tumor immunity.
Terminal Effector Tcells	Blimp-1, T-bet	Short-lived, produce perforin, granzyme B, and IFN-γ for rapid action.	CD45RA, CD8+; strong cytotoxicity.
Tc1 Cells	T-bet, STAT4, EOMES	Cytotoxic cells eliminating tumor and infected cells.	CD29+, IFN-γ+, TNF-α+; depend on IL-12 for activation.
Memory Tc1 Cells	T-bet, EOMES, Tcf1	Retain cytotoxicity, produce IFN-γ on reactivation.	CD44hi, CD122hi; important for long-term immunity.
Exhausted Tc1 Cells	TOX, Blimp-1, BATF, IRF4	Impaired function due to chronic antigen exposure, express inhibitory receptors.	PD-1+, LAG3+, TOX+; poor prognosis in cancers.
Progenitor Exhausted Tc1	Tcf1, CXCR5, PD-1	Less differentiated, responsive to immunotherapy.	PD-1int, CXCR5+, TCF-1+; reinvigorated by checkpoint inhibition.

Table 1. CD8+ T cell subsets and their key transcription factors, roles, and markers (Doan Ngoc et al., 2022; Liu et al., 2020; Murata et al., 2016; St. Paul & Ohashi, 2020; Sun et al., 2023; van den Broek et al., 2018; Wang et al., 2022; Willinger et al., 2006; Zhao et al., 2022; Zhou et al., 2010; Zu & Chen, 2024).

1.2.4. Models of T cell Differentiation

T cells differentiate through multiple stages. When naive CD8+ T cells encounter an antigen, they undergo specific developmental processes, giving rise to Tem and long-lasting Tcm cells. To explain the formation of memory CD8+ T cells, three main models have been suggested (Figure 8). These include the linear differentiation model, signal-strength model, and asymmetric-cell-fate model. In the linear differentiation model, naive T cells can differentiate into both effector and memory T cells (Harris & Drake, 2013; June, 2007). The signal strength model suggests that naive T cells undergo hierarchical differentiation based on the intensity and duration of signals received from APCs, where weak signals lead to cell death, strong signals drive terminal differentiation into short-lived effector T cells, and intermediate signals favor the development of central memory T cells with self-renewal capacity. In contrast, the stem cell model proposes that Tcm cells function as a reservoir of self-renewing cells capable of generating both effector and memory T cells, ensuring long-term immune protection. Together, these models explain how T cells balance immediate immune responses with the maintenance of immunological memory (Ahmed & Gray, 1996; Khanniche et al., 2022). The formation of heterogeneous effector cell populations is influenced by the strength of the signals received. This model posits that the signals encountered during T cell priming, such as antigen signals (Signal 1), co-stimulation (Signal 2), and pro-inflammatory cytokines (Signal 3), affect T cell heterogeneity. Weaker signals favors memory T cells formation, while stronger signals typically promote terminal effector T cells formation (Shakiba et al., 2021).

Asymmetric-cell-fate model: This model suggests that memory and effector cells can arise from a single precursor T cell during activation, resulting in the formation of self-renewing memory cells and terminally differentiated memory cells (Arsenio et al., 2015; Borsa et al., 2021; Kaech & Cui, 2012). Together, these models provide a deeper understanding of how various conditions and signals influence the differentiation and function of CD8+ T cells.

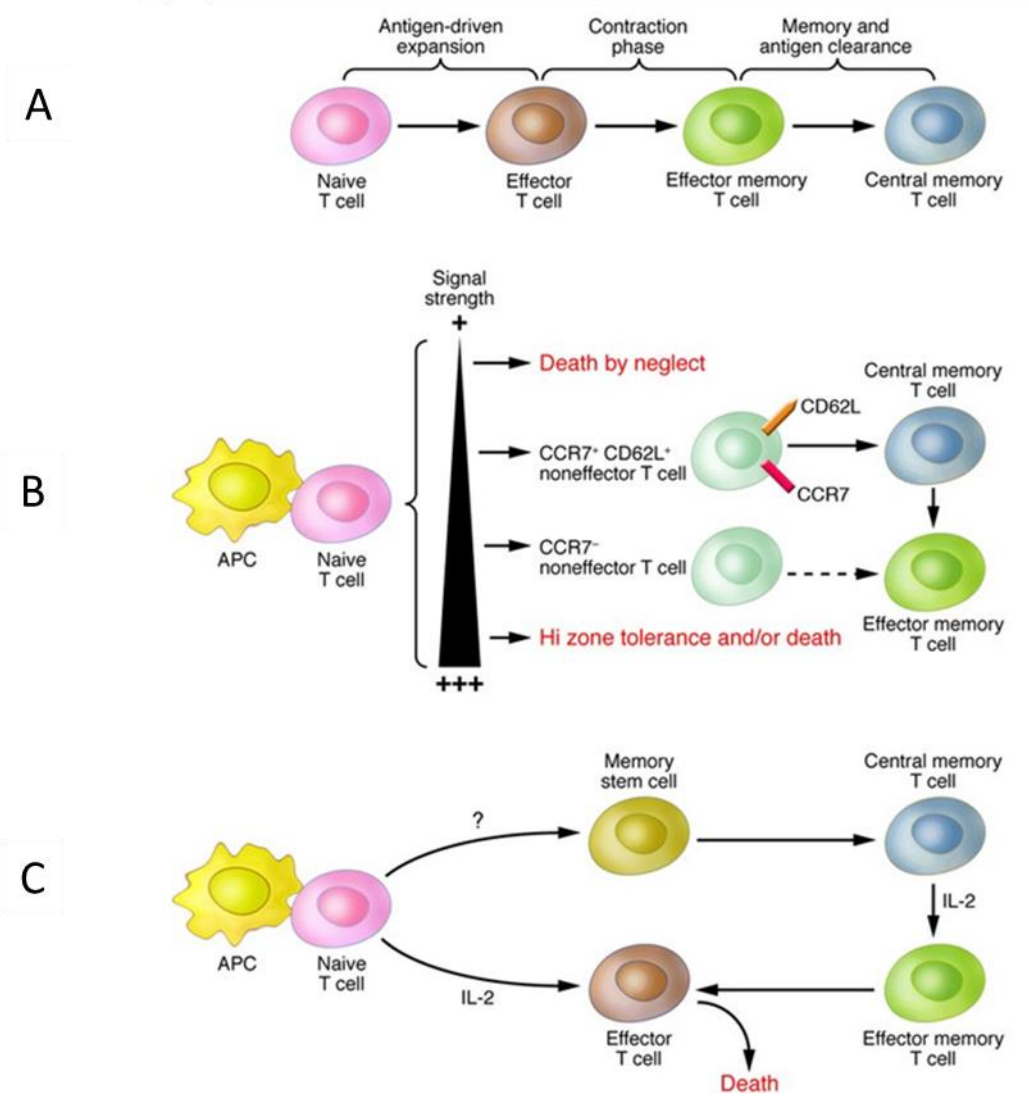

Figure 8: Models describing CD8+ T cell differentiation upon antigen encounter. CD8+ T cell differentiation into memory subsets follows three main models. The linear differentiation model suggests a stepwise transition from naive to effector-to-effector memory T cells, with some Tem cells reverting to central memory T cells after antigen clearance (A). The signal strength model proposes that differentiation depends on the strength and duration of signals from antigen-presenting cells, where weak signals lead to cell death, moderate signals produce memory cells, and strong signals create terminal effector cells (B). Asymmetric cell model *memory and effector cells can arise from a single precursor T cell during activation (C) (June, 2007).*

1.3. RUXOLITINIB JAK1/2 INHIBITOR FOR MULTIPLE DISEASES

RUX is a potent, selective oral inhibitor of JAK1/2 that has been approved for clinical use. Janus kinases (JAKs) serve as crucial mediators of cytokine signaling through the JAK-STAT pathway, regulating approximately 50 cytokines and hormones that govern hematopoiesis, immune function, and metabolic processes (Shawky et al., 2022). The JAK family comprises four members, JAK1, JAK2, JAK3, and TYK2, whose broad involvement in cellular signaling has positioned them as attractive therapeutic targets for diverse diseases. Their pivotal role in transmitting extracellular signals to intracellular responses has made JAK inhibition a promising strategy for modulating immune and inflammatory pathways (Shawky et al., 2022).

Chemically, RUX is identified as ([3R]-3-cyclopentyl-3-[4-(7H-pyrrolo[2,3-d]pyrimidin-4-yl)-1H-pyrazol-1-yl] propanenitrile), an orally bioavailable cyclopentyl-propionitrile derivative. It possesses a chiral carbon atom, resulting in the R and S enantiomers. Type I inhibitors are a class of small molecules that competitively inhibit enzymes by binding to their active sites. These inhibitors target the conserved active conformation of the adenosine 5-triphosphate (ATP) binding pocket within the kinase domain. As an ATP-competitive inhibitor, RUX is a potent and selective inhibitor of JAK1 (IC_{50}: 3.3 nM) and JAK2 (IC_{50}: 2.8 nM), with comparatively weaker inhibitory activity against TYK2 (IC_{50}: 19 nM) and JAK3 (IC_{50}: 428 nM), demonstrating modest to marked selectivity across JAK family members (Alim et al., 2021, Rosée et al., 2020).

JAK2 plays an explicitly crucial role in hematopoietic signaling related to myeloid cells and hormone receptors. RUX inhibits the signaling pathways of key inflammatory cytokines, providing anti-inflammatory benefits that are particularly advantageous in the treatment of myeloproliferative neoplasms and allogeneic transplantation (Shawky et al., 2022). By targeting JAK1 and JAK2, RUX suppresses the production of IL-1β, TNF-α, IL-6, IL-12, and chemokines CXCL10 and CXCL11 in TNF-α-treated human macrophages. It also reduces LPS-induced inflammatory responses by antagonizing the autocrine interferon IFN-β regulatory pathway triggered by LPS in human macrophages. These actions collectively contribute to the anti-inflammatory effects of RUX, offering significant therapeutic value by controlling excessive inflammation in MPNs and potentially other inflammatory conditions (Intlekofer et al., 2008).

RUX inhibits IL-6-induced STAT3 phosphorylation and limits the production of monocyte chemoattractant protein-1 (MCP-1/CCL2), a key chemokine involved in immune cell recruitment, particularly attracting monocytes, memory T cells, and dendritic cells to sites of inflammation. It also inhibits the proliferation of factor-dependent cell progenitors (FDCP) that rely on specific growth factors or cytokines for survival, proliferation, and differentiation, as well as pro-B-cell BA/F3 cells expressing JAK2-V617F (Ostojic et al., 2011).

Mutations in JAK2 have been implicated in malignancies, particularly Philadelphia-chromosome-negative myeloproliferative neoplasms (Böhm et al., 2021). MPNs are classified into polycythemia vera (PV) and essential thrombocythemia (ET). Activating mutations, such as JAK2-V617F, are associated with diseases like PV, ET, and primary myelofibrosis (PMF). Other mutations related to MPNs include alterations in the endoplasmic reticulum chaperone protein calreticulin and the thrombopoietin receptor. Additionally, JAK2 mutations have been linked to acute lymphoblastic leukemia, acute myeloid leukemia, and acute megakaryoblastic leukemia (Ivo et al., 2021).

Beyond its role in autoimmune and inflammatory diseases, JAK mutations also play crucial roles in myeloproliferative disorders, lymphomas, and leukemias. JAK1 mutations have been identified in acute lymphoblastic leukemia, while JAK2-V617F mutations are strongly associated with myeloproliferative neoplasms, particularly polycythemia vera, which occurs in nearly all PV patients (Ivo et al., 2021). The JAK3 mutant has been linked to leukemia induction in mice and a small percentage of patients with T-cell acute lymphoblastic leukemia. It has also been associated with severe combined immunodeficiency (O'Shea et al., 2004). Similarly, TYK2 mutations have been implicated in immunodeficiency with T-cell lymphopenia, increasing susceptibility to bacterial and viral infections. TYK2 deficiency has been linked to recurrent respiratory infections, highlighting the critical role of JAK kinases in immune regulation and disease pathology (Shawky et al., 2022).

Several JAK2 inhibitors, including RUX, fedratinib, pacritinib, and momelotinib, have been approved for treating MPNs (Shawky et al., 2022). RUX, in particular, is indicated for conditions such as myelofibrosis, hydroxyurea-resistant PV, graft-versus-host disease, and post-allogeneic hematopoietic stem cell transplantation (Appeldoorn et al., 2023; Ostojic et al., 2011).

The efficacy of RUX lies partly in its broad anti-inflammatory activity against the cytokine storm inherent to myeloproliferative neoplasms. It targets a wide range of pro-inflammatory cytokines and growth factors, helping to mitigate excessive immune responses. During treatment, RUX has been effective in reducing splenomegaly (Ostojic et al., 2011). Conversely, RUX also enhances the efficacy of immune checkpoint inhibitors by acting in the presence of myeloid cells, upregulating antigen-presenting molecules, including major histocompatibility complex class II (MHC-II), and improves the proliferative and inductive function of immune-stimulatory myeloid cells on cytokine-producing T cells. RUX significant effects include inhibition of specific immune cell proliferation, induction of apoptosis, and reduction in selected plasma cytokine levels, reducing the number of suppressive myeloid cells. Additionally, RUX downregulates granulocyte colony-stimulating factor (G-CSF). Furthermore, RUX has been shown to restore the activity of exhausted T cells (Zak et al., 2024).

1.3.1. Structure of Janus Kinases (JAKs)

Janus kinases are intracellular non-receptor tyrosine kinases with a conserved seven-domain architecture (JH1-JH7), sharing approximately 48% sequence homology among family members (Liau et al., 2019). The C-terminal JH1 domain functions as the catalytic kinase domain, while the adjacent JH2 pseudo-kinase domain serves a critical regulatory role despite lacking catalytic activity (Min et al., 2015). Structural studies have revealed that the central JH3 and JH4 domains share homology with SH2 domains (Figure 9), though their biological functions require further elucidation (Garrido-Trigo & Salas, 2019). The N-terminal FERM domain plays an essential role in receptor binding and membrane localization, facilitating interactions with cytokine receptors and subsequent signal transduction initiation (Ferrao & Lupardus, 2017). This sophisticated domain organization enables JAKs to effectively integrate regulatory functions with catalytic activity while maintaining stable receptor associations (Shawky et al., 2022).

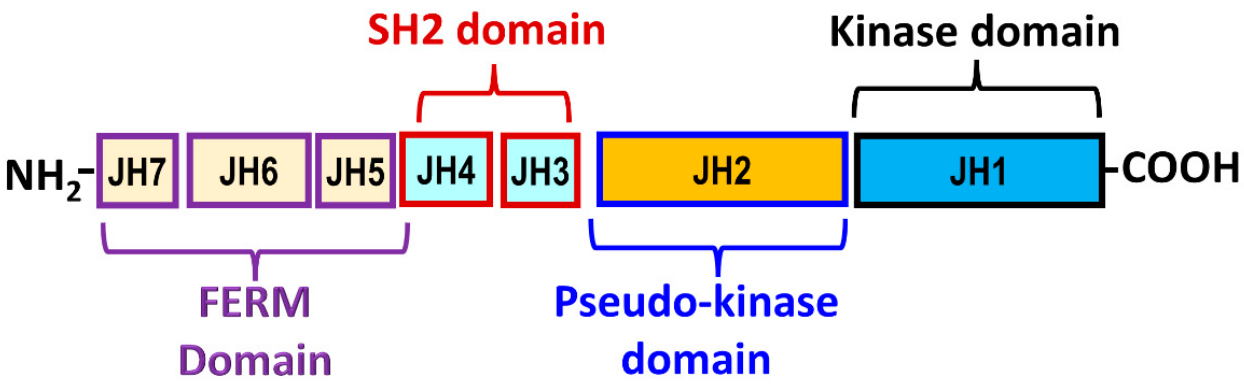

Figure 9: Structure of Janus Kinase domains (Shawky et al., 2022). Highlighting the FERM, SH2-like (JH3–JH4), pseudokinase (JH2), and kinase (JH1) domains that integrate receptor binding, regulatory, and catalytic functions.

1.3.2. Classification of JAK Inhibitors

JAK inhibitors represent an important class of targeted therapeutics that modulate cytokine signaling through specific inhibition of JAK family tyrosine kinases (Abroun et al., 2015). These compounds can be systematically classified based on three key characteristics: selectivity, binding mode, and binding site (Shawky et al., 2022). First-generation inhibitors such as tofacitinib and baricitinib are non-selective, broadly targeting multiple JAK isoforms (Figure 10 and Figure 11). In contrast, second-generation inhibitors, including upadacitinib and ritlecitinib, demonstrate improved selectivity for specific JAK family members, potentially reducing off-target effects (Vainchenker et al., 2018). These compounds can be categorized by their binding sites as ATP-competitive inhibitors (Types I-II), allosteric modulators (Types III-V), or covalent binders (Type VI). This comprehensive classification framework provides critical insights for developing JAK inhibitors with optimized therapeutic profiles for treating autoimmune, inflammatory, and oncological diseases (Min et al., 2015; Shawky et al., 2022).

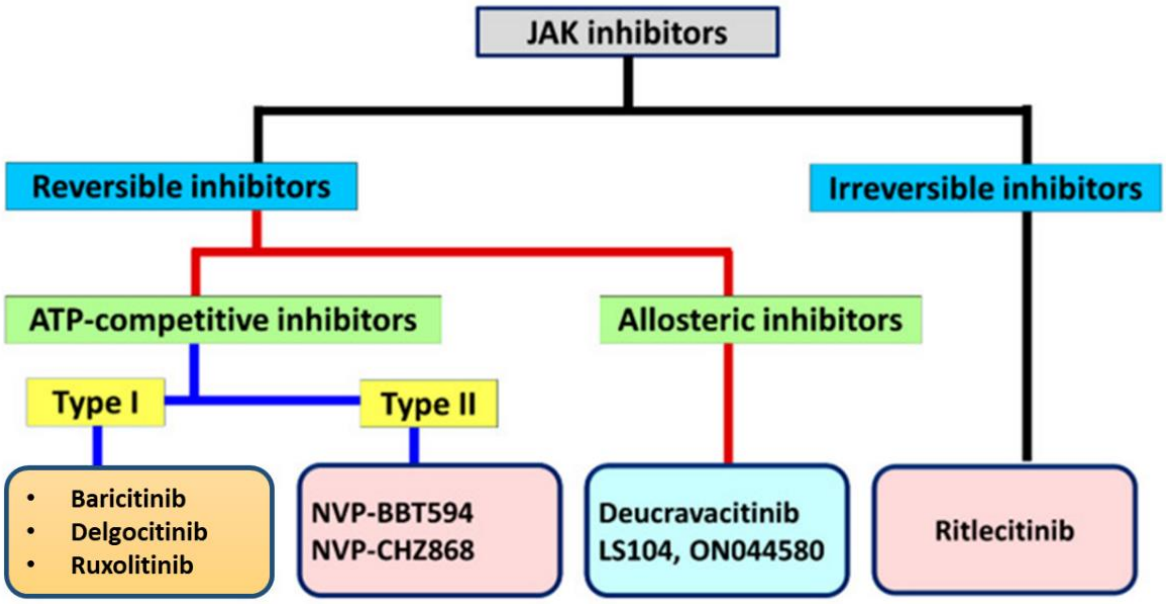

Figure 10: Classification of Janus kinases (Shawky et al., 2022). JAK inhibitors are categorized by selectivity, binding mode, and binding site. First-generation inhibitors target multiple JAK isoforms, whereas second-generation inhibitors show improved isoform selectivity. Based on binding site, they are further classified as ATP-competitive (Types I–II), allosteric (Types III–V), or covalent (Type VI).

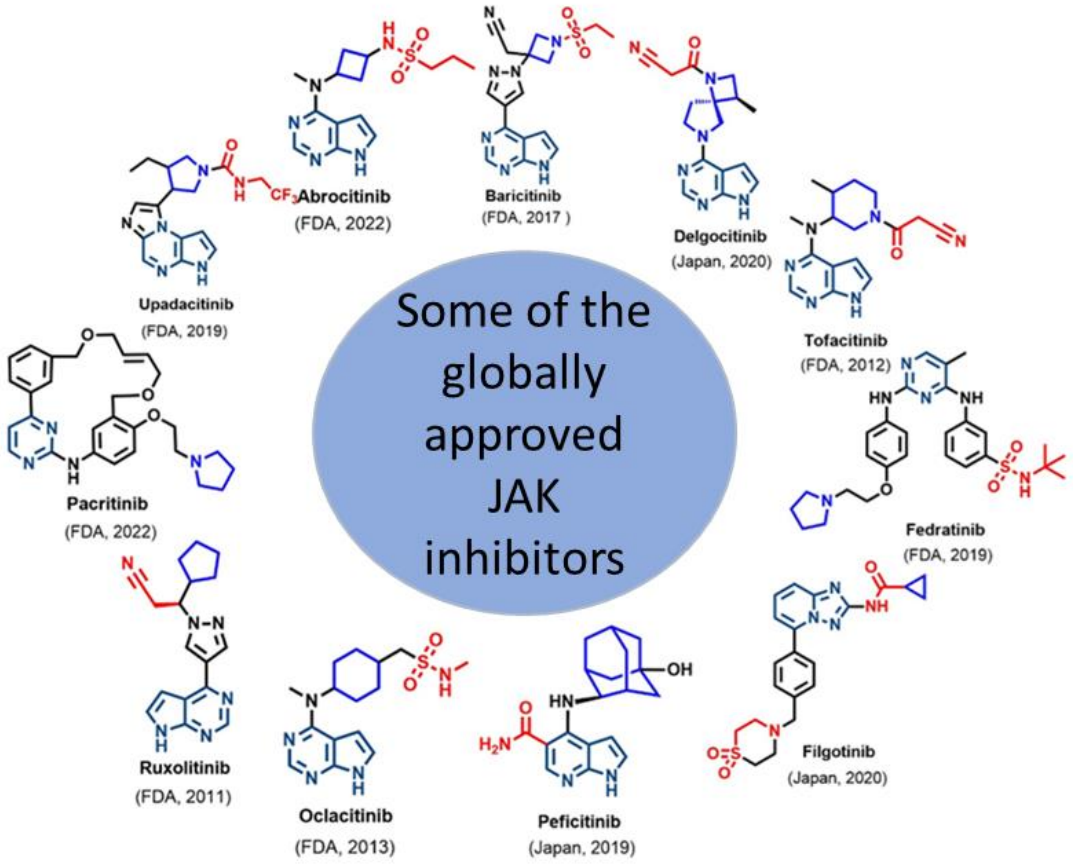

Figure 11: Structure of globally approved JAK inhibitors (Shawky et al., 2022).

2. JUSTIFICATIONS AND OBJECTIVES

2.1. Justifications

P-glycoprotein, encoded by the ABCB1 gene, plays a pivotal role in drug resistance and immune regulation. While its function in removing xenobiotics and chemotherapeutic agents is well established, its role in immune cell function, particularly in CD8+ T cells, remains less understood. Elevated expression of Pgp in tumor cells contributes to chemotherapy resistance, limiting the effectiveness of treatment. In immune cells, however, it can enhance resilience under challenging conditions. Understanding the mechanisms underlying Pgp-mediated resistance in T cells is essential for optimizing cancer immunotherapy, managing autoimmune diseases, and improving transplantation outcomes.

RUX, a JAK1/2 inhibitor, has demonstrated immunomodulatory properties in hematologic malignancies and inflammatory conditions. However, its potential impact on Pgp activity and T cell maturation remains incompletely understood. Investigating how RUX influences Pgp expression and function in cytotoxic T lymphocytes could provide valuable insights into its therapeutic implications, particularly in graft-versus-host disease and the efficacy of chemotherapeutic agents.

By elucidating the relationship between Pgp expression, T cell maturation, and RUX treatment, this study aims to contribute to developing targeted strategies for improving immune resilience, enhancing cancer treatment outcomes, and refining immunotherapeutic approaches.

2.2. Objectives

2.2.1. General objectives

To investigate Pgp presence, activity, and expression dynamics in cytotoxic T lymphocytes during maturation, and to determine whether the JAK inhibitor RUX modulates these parameters.

2.2.2. Specific objectives

1. To quantify Pgp expression and efflux activity in CTLs and assess how RUX alters them.

2. To characterize the temporal pattern of Pgp expression throughout CTL differentiation and evaluate its modulation by RUX.

3. MATERIALS AND METHODS

3.1. Antibodies and chemicals

All materials and chemicals, unless otherwise specified, were obtained from Thermo Fisher Scientific (Budapest, Hungary), Sigma-Aldrich and Merck Life Science Kft. (Budapest, Hungary), or MedChem Express (Budapest, Hungary).

The following fluorescently-labeled monoclonal antibodies (mAbs) were applied. Mouse anti-human CD16 Fluorescein isothiocyanate (FITC), CD19 Phycoerythrin (PE), CD56 Peridinin Chlorophyll Protein-Cyanine 7 (PC7), and CD62L Pacific Blue (Beckman Coulter, Beckman Coulter Magyarország Kft., Budapest, Hungary). Mouse anti-human CD3 Peridinin Chlorophyll Protein-Cyanine 5.5 (PerCP-Cy5.5), CD4 Pacific Blue, CD45 RA FITC, and CD8 Allophycocyanin-Hilite7 (APC-H7) (Becton Dickinson, Hungary). Mouse anti-human CD45 Pacific Orange (PO) (EXBIO Praha, Czech Republic). Mouse anti-human CD73 PE (Sony Biotechnology Inc., I.T.A. Life Science Kft., Budapest, Hungary). Mouse anti-human CD95 PE-Cyanine7 and CD127 PE-Cyanine5.5 (Thermo Fisher Scientific, Budapest, Hungary). Mouse anti-human CD279 (PD-1) Allophycocyanin-Cyanine7 (APC-Cy7) (BioLegend, Biomedica Hungária Kft., Budapest, Hungary). The anti-human CD8 (OKT8) PO and Pgp (15D3) Alexa Fluor 647 dye-labeled mouse mAbs were produced in-house from hybridoma and mouse ascites.

The anti-human CD8 mouse monoclonal antibody (mAb) was isolated from the supernatant of OKT8 hybridoma cells. OKT8 cells were cultured in RPMI medium, and the supernatant was collected and purified using a Protein A column at 4°C.

3.2. Isolation and purification of 15D3 and OKT8 antibodies

The 15D3 anti-human Pgp mouse mAb was purified from mouse ascites (Gellen et al., 2023). One million 15D3-hybridoma cells were injected intraperitoneally into ten-week-old female BALB/c and Swiss nude mice. Mice were housed in the animal facility of the University of Debrecen, Life Science Building, Hungary, under controlled conditions, with a temperature range of 21-25°C and a 12-hour light/dark cycle. They had free access to standard mouse pellets and water ad libitum within standard mouse cages. On day 14 post-injection, ascites were collected aseptically from the mice and stored at -80°C. The collected ascites were then purified using a protein-G column kit

(Thermo Fisher Scientific NAb™ Protein G Spin Kit), according to the manufacturer's instructions.

The protein concentration of the isolated 15D3 and OKT8 mAbs protein concentration was measured using a NanoDrop™ OneC microvolume UV-Vis Spectrophotometer at 280 nm. 0.02% sodium azide solution was added to the purified antibodies, which were then stored at 4°C for short-term use or at -20°C for long-term storage (Gellen et al., 2023). Furthermore, according to the manufacturer's instructions, Alexa Fluor and PO-labelled mAbs were prepared for direct immune-labelling purposes (Thermo Fisher Scientific, Budapest, Hungary).

3.3. Cell lines and generation of cytotoxic T lymphocytes

The following cells and cell lines were used in this study:

i) Peripheral blood mononuclear cells (PBMCs) from healthy donors

ii) NIH-MDR

iii) NIH-3T3

iv) JY cells (Human Epstein–Barr virus-transformed B-lymphoblastoid cell line).

The Pgp (MDR1/ABCB1)-expressing NIH-3T3 MDR1 cells and their parental NIH-3T3 mouse fibroblast counterparts were originally obtained from the laboratory of Dr. Michel Gottesman (NIH, USA). The JY cell line, a human Epstein-Barr virus-transformed B-lymphoblastoid cell line, expresses high levels of MHC class I A2 and class II DR molecules on its plasma membrane (Bacsó et al., 1996; Biwott et al., 2025b).

All cell lines were maintained in RPMI 1640 medium (Sigma-Aldrich, Merck Life Science Kft., Budapest, Hungary) supplemented with sodium bicarbonate, glucose, pyruvate, MEM non-essential amino acids, GlutaMAX, gentamycin or ampicillin, and 10% heat-inactivated fetal calf serum (FCS; SEBAC, Aidenbach, Germany). Cultures were incubated at 37 °C in a humidified atmosphere with 5% CO_2.

Cytotoxic T lymphocytes were derived from human peripheral blood lymphocytes (PBLs), which were obtained from leukocyte-enriched buffy coats of voluntary healthy donors. Peripheral blood mononuclear cells (PBMCs) were isolated using Ficoll-Paque Plus (Amersham Biosciences, Uppsala, Sweden) density gradient centrifugation. Blood samples were collected with written informed consent from individual donors at the Regional Blood Center of the Hungarian National

Blood Transfusion Service in Debrecen, Hungary. The study was conducted with the written approval of the Director of the National Blood Transfusion Service (OVSzK 3572-2/2015/5200) and the Regional and Institutional Ethics Committee of the University of Debrecen, Medical and Health Science Center.

Monocytes were removed by positive selection using anti-CD14-conjugated magnetic microbeads (Miltenyi Biotec, FRANK Diagnosztika Kft., Budapest, Hungary), according to the manufacturer's protocol. The resulting PBLs were cultured at a density of 2–5 × 10^6 cells/mL in T75 tissue culture flasks using complete RPMI medium supplemented with 10 mM Hepes buffer (pH 7.3) and 50 µM 2-mercaptoethanol (SERVA, Heidelberg, Germany). Cells were either used immediately or frozen for long-term storage. When required, human recombinant IL-2 (20 IU/mL; PeproTech) was added to the medium.

CTLs were generated by priming PBLs with heat-inactivated JY cells at a 4:1 PBL: JY cell ratio in mixed cultures, as described in previous studies. JY cells were heat-shocked at 45 °C for 2 hours to arrest proliferation. From day three onward, IL-2 (20 IU/mL) was added every third day. Cultures were maintained for 30 days, followed by a second 30-day priming cycle. This prolonged low-dose IL-2 stimulation supports the development of memory T cells (Kalia & Sarkar, 2018).

3.4. Measurement of Pgp and CD8 protein on cell surfaces

In this procedure, T cells were initially washed with PBS by centrifugation at 1200 rpm for 5 minutes. After the washing step, the cells were counted using a hemocytometer and adjusted to a concentration of 5 million cells per mL. Subsequently, 250,000 cells were plated in a 96-well format. To facilitate the detection of Pgp and CD8, we added 10 mg/mL of Alexa647-15D3 anti-Pgp antibody and 10 µg/mL of Alexa488-OKT8 anti-CD8 antibody to the cells. The mixture was gently vortexed and incubated on ice for 45 minutes. After incubation, the cells were washed twice with ice-cold glucose PBS to remove unbound antibodies. The cells were then resuspended in ice-cold glucose PBS containing 2 µM Hoechst dye. Pgp intensity measurements were subsequently performed using a Novocyte 3000 RYB flow cytometer.

3.5. Isolation of total RNA from CD8+ and CD8- cells

Human primary T cells were sorted into CD8+ and CD8- populations utilizing a FACS ARIA III instrument. Total RNA isolation was performed on various cell types, MDR1, 3T3 NIH cells, PBL-derived CD8+ and CD8- cells, and JY-preactivated CD8+ and CD8- cells. The process followed the manufacturer's guidelines for TRI Reagent® (catalog number: TR118, Molecular Research Center, Inc.). Initially, the cells were centrifuged, and 1 mL of Trizol™ reagent was added to lyse the samples, which contained approximately 1 x 10^6 cells each. The samples were homogenized by gently mixing them up and down. Following this, 200 µL of chloroform was added for every 1 ml of Trizol reagent. The tubes were capped, vortexed vigorously for 15 seconds, and incubated at room temperature for 3 to 5 minutes. Subsequently, the samples were centrifuged for 15 minutes at 15000 x rpm at 4°C. The upper aqueous phase was carefully transferred to fresh tubes, avoiding any disturbance to the interphase. To precipitate RNA, 500 µL of isopropanol (2-propanol) was added without vortexing, and gentle mixing was performed twice. The samples were left at room temperature for 15 to 20 minutes before centrifugation for 10 minutes at 15000 x rpm at 4°C. Following centrifugation, the supernatant was discarded, and the RNA pellet was washed with 800 µL of 70% ethanol. Each sample was briefly vortexed for 5 seconds and then centrifuged for 7 minutes at 15000 x rpm at 4°C. The supernatant was carefully discarded, and the RNA pellet was air-dried for 5 to 10 minutes. Subsequently, the RNA pellet was resuspended in 20-50 µL of RNase-free water (AccuGENE® LONZA) and incubated in a water bath set to 65°C for 10 minutes. RNA yield, purity, and integrity were assessed using a Nanodrop spectrophotometer, measuring A260/A280 and A260/A230 ratios. The isolated RNA samples were stored at -20°C for future use.

3.6. Real-time quantitative PCR

Real-time quantitative PCR TRIzolate Reagent (UD GenoMed) was used to isolate total RNA, and a High-Capacity cDNA Reverse Transcription kit (Applied Biosystems) was used to reverse transcribe the RNA to cDNA in accordance with the manufacturer's instructions. The TaqMan probes Hs00184500_m1 ABCB1 (Sorf et al., 2020), Hs00184500_m1 ACTB, Mm02619580_g1 Actb, Hs02786624_g1 GAPDH, and Mm99999915_g1 Gapdh were used in real-time q-PCR to measure the quantity of mRNA. A Roche LightCycler 480 Instrument II was used for real-time

monitoring. Human and mouse β-actin and GAPDH reference genes, chosen through housekeeping gene stability analysis with the RefFinder program, were used for gene expression normalization. The delta-delta cycle threshold (ΔΔCT) approach was used to measure gene expression.

3.7. Inhibitory effects of zosuquidar and RUX in NIH-3T3 Cells and CTLs

The functional activity of ABCB1 transporter was assessed through the inhibitory effects of specific inhibitors, to achieve this calcein accumulation assay was employed (Goda et al., 2020). The ABCB1 inhibitor Zosuquidar (ZQ), and RUX were investigated. ZQ and RUX were serially diluted (from high to low concentrations) across 12 U-bottom 96-well plates to assess their effects. NIH-3T3 mouse fibroblasts transfected with the human ABCB1 (MDR1) gene served as the positive control for evaluating the transport activity factor, while untransfected NIH-3T3 parental cells served as the negative control, maintained at 80-90% confluence. Calcein-AM, an ABC substrate, was added to achieve final concentrations of 5 nM for NIH-MDR cells and 1 nM for CTLs. Cells were evenly distributed in the wells, with and without calcein-AM, at a density of 0.5 x 10^6 cells per well. Subsequently, anti-CD8 Alexa647-OKT8 antibodies were added, and the treated cells were incubated at 37°C in a controlled environment with 5% CO2 for 30 minutes. After incubation, the cells were washed twice with 200 µL of ice-cold glucose-PBS containing 1% FBS to remove excess calcein-AM. This was performed at 1200 RPM for 5 minutes. The treated cells were then suspended in 150 µL of 20 µg/mL Hoechst 33342 (nuclear dye) and maintained on ice in dark conditions. Finally, the intensity of calcein was subsequently measured using the Novocyte 3000 RYB flow cytometer.

The transport activity factor of the Pgp pump was determined by analyzing the difference in dye accumulation within the cells in the presence versus the absence of the inhibitors.

TAF calculation: $TAF = (\mathrm{MFI(inh)} - \mathrm{MFI(0)})/\mathrm{MFI(inh)}$

MFI (inh): Mean Fluorescence Intensity with inhibitor, MFI (0): Mean Fluorescence Intensity without inhibitor. The TAF ranges from a maximum value of 1 to a minimum value of 0.0. (Goda et al., 2020; Sarkadi et al., 2006).

3.8. Experiment setup of T cell activation and treatment in human PBLs

To activate T cells via the TCR, wells of a 24-well plate were coated with 2 µg/mL anti-CD3/CD28 Dynabeads and incubated overnight at 4 °C. Afterwards, excess antibody was removed by washing with PBS. One million PBLs were added separately to the prepared wells to generate TCR-activated cells. RUX (100 µM) was added to some of the wells containing CD3/CD28-activated cells (activated + RUX), and to other wells containing cells without activation (RUX-only). Untreated and unstimulated cells served as controls. All activation and treatment conditions were maintained for 72 hours (as summarized in Table 2).

Following incubation, cells were counted, and 250,000 cells from each treatment group were stained in a 96-well U-bottom plate with the following antibodies: anti-PD1 (APC/allophycocyanin-tagged), anti-Pgp (Alexa488-conjugated UIC2 in combination with the Pgp inhibitor ZQ), and anti-CD8 (Pacific Orange-conjugated OKT8). Staining was performed on ice for 45 minutes in the dark. The cells were then washed with PBS, resuspended in glucose-PBS containing Hoechst dye, and analyzed by flow cytometry.

Activation status	Untreated	Drug treated
No	Human PBLs	Human PBLs + RUX
Yes	Human PBLs + CD3/CD28 beads	Human PBLs + CD3/CD28 beads + RUX

Table 2: CD3/CD28 activation of human primary peripheral blood lymphocytes over 72 hours. Each well was populated with two million human primary T cells. Additionally, the wells contained anti-CD3 and anti-CD28 at a concentration of 2 µg/ml. The design included wells with T cells treated solely with anti-CD3 and anti-CD28, as well as those treated with RUX as described.

3.9. Preparation of membranes from NIH 3T3 mouse fibroblast cells

In the preparation of cellular membranes, NIH 3T3 mouse fibroblast cells expressing wild-type Pgp (WT Pgp) and its mutant variants, as well as control cells lacking Pgp, were utilized (Krasznai et al., 2014). The membrane preparation method developed by Sarkadi was employed (Balazs

Sarkadi et al., 1992). Initially, the cells were collected from flasks and subjected to three washes with 10 ml of washing buffer containing 0.05 mg/ml phenylmethylsulfonyl fluoride (PMSF), followed by centrifugation at 300 × g for 5 minutes at 4°C. After washing, the cells were resuspended in 10 mL of ice-cold TMEP buffer, which contains 50 mM Tris-HCl, 50 mM mannitol, 2 mM EGTA, 2 mM dithiothreitol (DTT), and 1X protease inhibitor cocktail, with an additional 0.5 mM PMSF. The cell suspension was homogenized using a glass-Teflon tissue homogenizer for 25 minutes. Subsequently, the preparation was centrifuged at 500 × g for 10 minutes at 4°C to eliminate nuclear debris and intact cells, which formed a pellet. The membrane fractions in the supernatant were further isolated by conducting a centrifugation at 28,000 × g for 1 hour at 4°C, yielding a pellet comprising the membrane proteins. These membrane fractions were then resuspended in 1-2 ml of ice-cold TMEP buffer and stored at -80°C for future use. The concentration of proteins within these membrane fractions was determined utilizing the Lowry method (Lowry et al., 1951).

3.10. ATPase activity measurement

The ATPase activity specific to ABCB1 was evaluated by measuring the release of inorganic phosphate resulting from ATP hydrolysis (Bársony et al., 2016; Goda et al., 2020; Sarkadi et al., 1992). In addition to ABCB1, a variety of other ATPases are present in cellular environments. To isolate the specific activity of ABCB1, several inhibitors were utilized to inhibit the activities of these other ATPases: Na-azide was applied to target the F0F1 complex, Ouabain for the Na+/K+ ATPase, and EGTA specifically for Ca^{2+} ATPases. Furthermore, vanadate-sensitive ATPase activity was assessed, as vanadate selectively binds nucleotides within the nucleotide-binding domains of ABCB1, acting as an analog for inorganic phosphate. Membrane samples were prepared with an ATPase premix consisting of 51 mM MOPS, 64 mM KCl, 6.4 mM Na-azide, and 0.65 mM EGTA Tris, together with 2.6 mM DTT and 1.28 mM Ouabain. The treatment was carried out in the presence or absence of 100 µM Na-orthovanadate, utilizing a concentration of 5µg protein in 60 µL per sample in each well of a 96-well plate. The samples underwent initial treatment with various inhibitors, specifically RUX at concentrations of 100 µM, 10 µM, and 1 µM; ZQ at 10 µM; and CSA at 20 µM, conducted in the presence or absence of 40 µM verapamil for a duration of 10 minutes at 37 °C. After this treatment, 10 µL of ATP-Mg^{2+} (3.5 mM) was added to each well to initiate the ATPase reaction, which was subsequently incubated at 37 °C for

25 minutes. 40 µL of 5% SDS was added to terminate the reaction. The concentration of inorganic phosphate released during the ATPase response was determined using a colorimetric assay. This involved adding 105 µL of a color reagent prepared from 5 mL of Pi-reagent (comprised of 1% ammonium molybdate, 0.014% potassium antimony tartrate, and 2.5 M sulfuric acid), 3 mL of 20% acetic acid (CH_3COOH), and 2.5 mL of 1% ascorbic acid. The plate was then incubated for 30 minutes at a room temperature of 22°C. The released phosphate formed a chromogenic phosphomolybdate complex, which is directly proportional to the amount of inorganic phosphate present. This was quantified by measuring the absorbance at 700 nm using a spectrophotometer. The specific activity of ABCB1 was calculated by subtracting the ATPase activity of vanadate-positive samples from the ATPase activity of vanadate-free samples.

3.11. Experimental setup to measure the change in phenotypes and Pgp expression

The phenotypes of peripheral blood lymphocytes and Pgp expression were measured in PBLs that were unprimed (JY-non-exposed) and after JY-exposure (JY-primed). Multicolor flow cytometric measurements were carried out to determine the change in the population proportion and Pgp expression in different populations (T, B, NK, and NKT, CD4+ and CD8+ T cells). Four independent repeated experiments were carried out (Table 3A).

3.12. Experimental setup of the T cell activation and treatment in unprimed and JY-primed CTLs

CTL maturation experiments used the JY-primed PBLs (JY-exposed cells) after the one-month subset differentiation period. The unprimed (JY-non-exposed) control lymphocytes compared in the activation experiments were from the same two donor sources as the JY-exposed CTLs. The unprimed experiments were repeated 3 times, giving 12 FCS (flow cytometry standard) files in the 4 activation/treatment groups. The JY-primed experiments were repeated 4 times, giving 16 FCS files in the 4 activation/treatment groups. The experimental setup is shown in Table 3 B.

TCR-activation of cells was achieved by coating wells of a 24-well plate with 2µg/ml antibody of the CD3/CD28 Dynabeads and incubating overnight at 4°C. Then, excess Ab was removed with PBS wash, and one million cells from JY-exposed primed and JY-non-exposed unprimed

cells were added separately to individual wells (TCR-activated cells). RUX was added to wells separately containing CD3/28 (activated and RUX-treated cells). RUX was added to the wells that contained only the cells (RUX-only treated cells), and untreated/unstimulated cells (control cells) were used. The activations and treatments were done for 72 hours.

A

PBLs	Time of exposure	
Non-exposed to JY cells, unprimed PBLs (prior *in vivo* T cell maturation)	-	Flow cytometry measurements after the JY-priming were performed and the data was analyzed using sequential gating.
JY-priming (PBLs exposed to JY cells (*in vitro* CTL maturation)	28 days of JY-cell exposure (2 times of 14-day cycles)	

B

PBLs	Time of exposure	Activation/treatment (72 hours)	
Non-exposed to JY cells, unprimed PBLs (prior *in vivo* T cell maturation)	-	Unstimulated/untreated (control)	Flow cytometry measurements after the activation/treatment and multidimensional data analysis were performed
		Treated (RUX)	
		Activated (CD3/28)	
		Activated (CD3/28) and treated (RUX)	
JY-priming (PBLs exposed to JY cells (*in vitro* CTL maturation)	28 days of JY-cell exposure (2 times of 14-day cycles)	Unstimulated/untreated (control)	
		Treated (RUX)	
		Activated (CD3/28)	
		Activated (CD3/28) and treated (RUX)	

Table 3: *T-cell activation and treatment responses.*

The objective of the experiment was to evaluate T-cell activation and treatment responses. PBLs were divided into two groups: the unprimed (JY-non-exposed) and the JY-primed, which underwent a 14-day exposure. Subsequently, we assessed changes in population proportions and Pgp expression across various PBL phenotypes (A). Following JY exposure, the PBLs were activated using CD3/CD28 beads. The experimental treatments included: administration of RUX, activation with simultaneous treatment (CD3/CD28 + RUX), and a control group that remained unstimulated and untreated. CD8+ cytotoxic T lymphocytes were quantified using flow cytometry, and multidimensional data analysis was conducted to classify the CTL subsets (B).

3.13. Flow cytometry

Calcein intensity was systematically measured in NIH-3T3 MDR, NIH-3T3, and CTLs, alongside the expression levels of Pgp and CD8 in CTLs. These evaluations were performed utilizing the Novocyte 3000 RYB and the BD Biosciences FACS Aria III flow cytometer. The resulting data from the FACS and flow cytometry analyses were processed using FCS Express version 6.0 Flow Research Edition.

Cellular surface staining of lymphocytes was performed using mAbs, as detailed above. Briefly, cells were incubated with mAbs for 15 minutes at room temperature, followed by washing with PBS at 1600 RPM for 5 minutes. The cells were then suspended in 400 µL of PBS for acquisition. Samples were measured with FACS Canto II, using BD FACSDiva v6.1.3 (BD Bioscience). A total of 100, 000 events per sample were collected, and the data were analyzed using FlowJo v10.9.0 (TreeStar Inc., Ashland, OR, USA).

3.14. Sequential gating of T cells

Flow cytometry data were preprocessed through a series of steps, including data cleaning, quality control, gating, down-sampling, and concatenation, before undergoing machine learning analysis. Quality control was performed using PeacoQC to select good events. Doublets were removed sequentially by gating on forward scatter (FSC) area versus height and FSC area versus width (Figure 12 and Figure 13).

White blood cells (WBCs) were gated based on light scatter parameters (forward scatter, FSC, versus side scatter, SSC), followed by gating on CD45 versus SSC to isolate CD45+ lymphocytes. Within this population, major lymphocyte subsets were identified using lineage-specific markers: T cells (CD3+), B cells, and NK cells. T cell subsets (CD4+, CD8+, and NKT cells) were further delineated within the CD3+ gate. Pgp expression was analyzed within T cells and their subsets (CD4+, CD8+), as well as in B and NK cells (Figure 12).

To remove antibody precipitates, a clean gate was applied on CD45RA versus P-glycoprotein (Pgp) expression. CD8+ cytotoxic T lymphocytes (CTLs) were then sequentially gated from this clean population (Figure 13). For multidimensional analysis, 3,200 CD8+ T cells were down-sampled from each of the 28 individual files, yielding a total of 89,600 CD8+ T lymphocytes. These were concatenated into a single dataset for downstream multidimensional and machine learning analyses using the FlowJo plugin.

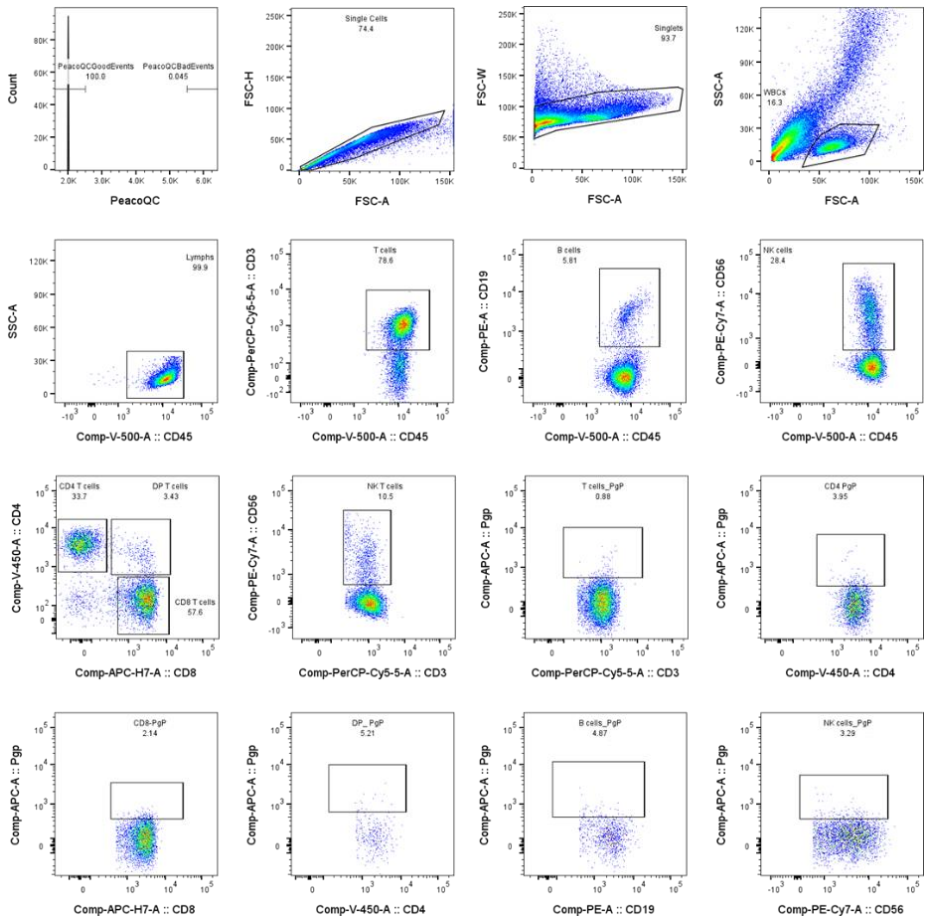

Figure 12: Sequential universal gating of T Lymphocytes. Sequential gating of cells from left to right and top to bottom. Events are gated on PeacoQC good events, followed by doublets being removed from FSC area vs height and area vs width. White blood cells were gated on light scatter parameters, and lymphocytes were gated on CD45 vs SSC. Lymphocyte subsets (T, B, and NK cells) were gated based on different markers within the CD45+ lymphocytes. T cells subsets (CD4, CD8, and NKT cells) were gated within CD3+ T cells. Later, the Pgp expression was gated within the T cells and their further subsets (CD4, CD8), B cells, and NK cells.

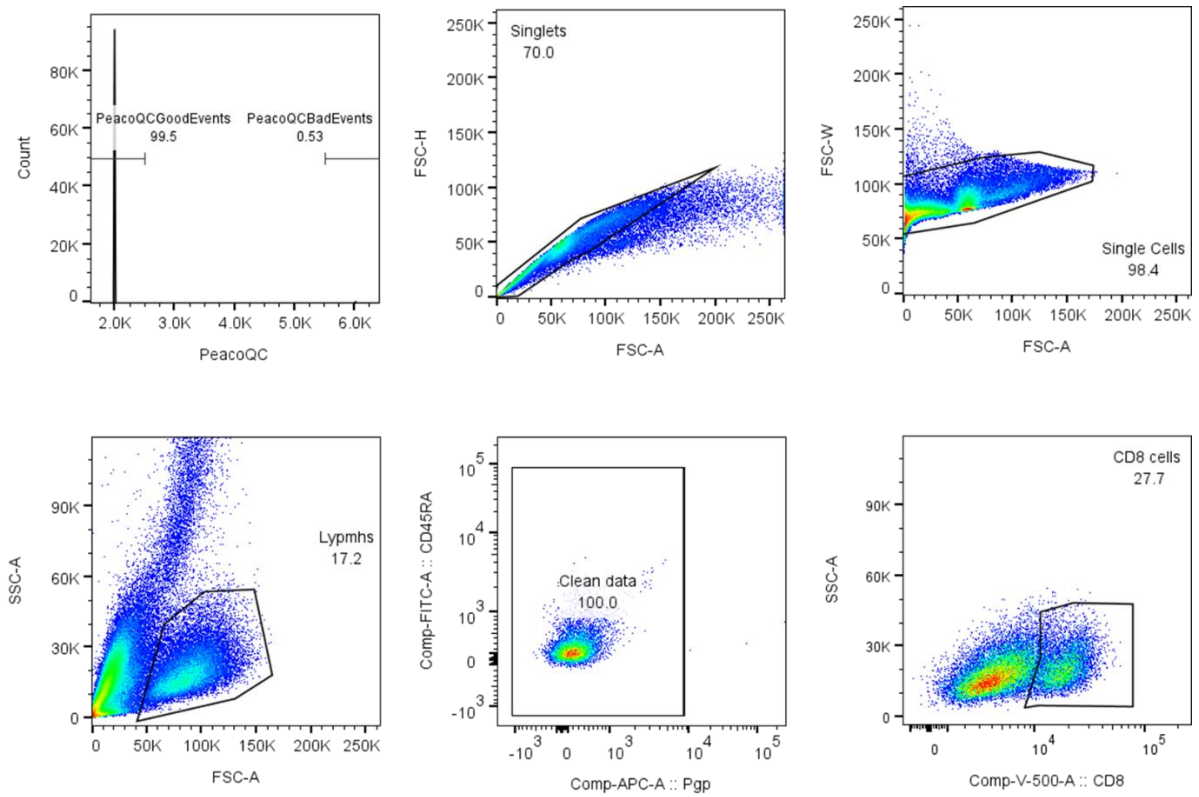

Figure 13: Sequential universal gating of CD8+ Lymphocytes. Sequential gating of cells from left to right and top to bottom. Events are gated on PeacoQC good events, followed by doublets removed from FSC area vs. height and area vs. width. Lymphocytes were gated on light scatter parameters. A clean gate on CD45RA vs. Pgp was applied to remove antibody precipitates, and CD8 cells were gated among clean gate data.

3.15. Multidimensional data analysis

Dimensionality reduction was performed using Uniform Manifold Approximation and Projection (UMAP) to visualize the high-dimensional data (McInnes et al., 2018). FlowSOM was utilized to construct self-organizing maps and identify meta-clusters of T cells (Van Gassen et al., 2015), and the number of clusters was optimized through multiple clustering iterations with different numbers of meta-clusters to prevent over- and under-clustering (Figure 14). A slight over-clustering approach was preferred to avoid missing out on less expressive clusters. The immune clusters identified by FlowSOM were overlaid onto individual samples, and the percentage of these clusters among CD8+ lymphocyte cells was exported for statistical comparison across different experimental conditions.

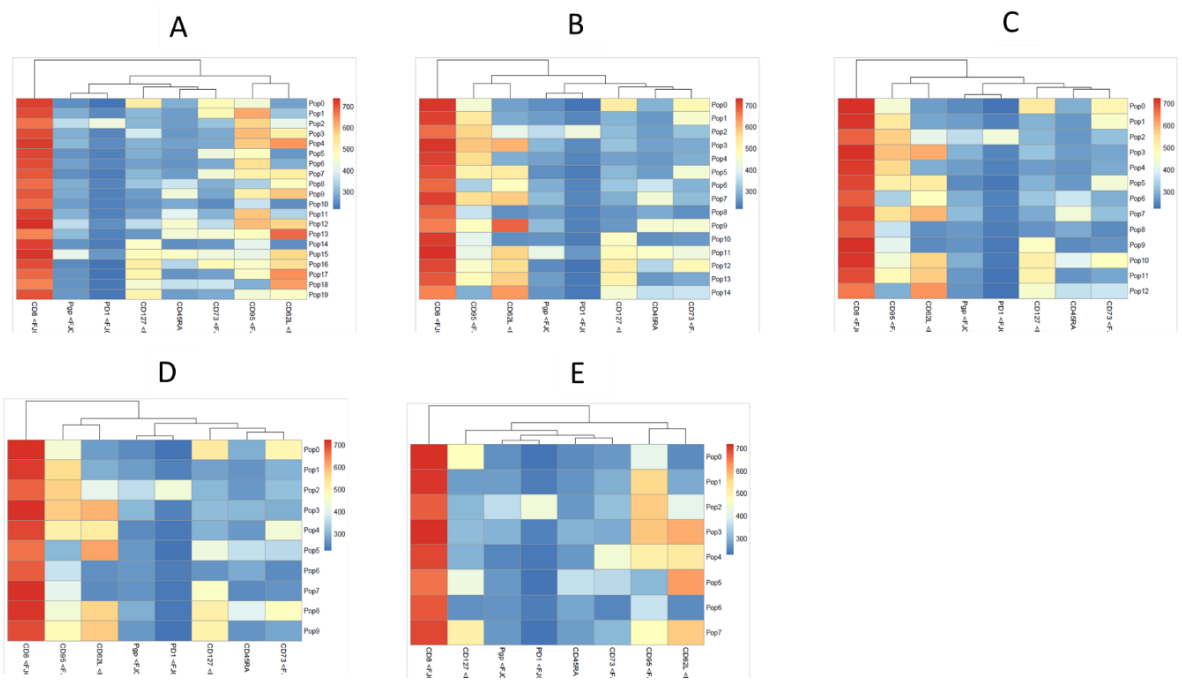

Figure 14: FlowSOM clustering. It was repeatedly performed on datasets to optimize meta clusters, decreasing clusters in each iteration. Heatmaps representing fluorescence expression in different channels from different clusters are shown. 20 meta-clusters were performed (A), which shows over-clustering, and multiple clusters show similar expressions. (B) meta clusters are reduced to 15, still similar expression was identified between several clusters. (D) 10 meta clusters show significant biological clusters that are getting merged. (E) 8 meta clusters also show biologically significant clusters are getting merged. 13 meta clusters were found to be optimal since it is slightly over cluster and not under cluster (C).

3.16. Statistical analysis

Kolmogorov–Smirnov (KS) and Shapiro–Wilk normality tests were used to assess the normality of data distribution. For non-normal distributed, nonparametric variables, the Mann-Whitney test, and the normally distributed parametric variables, Student's t-test was applied to calculate the significant differences.

One-way ANOVA with Tukey's post hoc test for multiple comparisons was employed for internal comparison with the level of significance set at $p<0.05$. Statistical analysis was conducted using GraphPad Prism v9.0 (GraphPad Software, Inc., San Diego, USA).

A chi-square test of independence was conducted in Excel to determine whether the measured magnitudes of CTL subsets varied significantly across different activations and treatments.

Post hoc comparisons were adjusted using the Bonferroni correction to account for multiple tests. The effect size was calculated using Cramer's V and interpreted as large, medium, small, or negligible based on established thresholds.

4. RESULTS

4.1. PART 1: The Presence and Functional Role of The Pgp in Cytotoxic T Lymphocytes

We conducted several cellular, biochemical, and molecular tests to systematically examine how RUX affects the phenotype and function of cytotoxic T lymphocytes. Following a description of baseline and antigen-induced alterations in Pgp and CD8 expression, we evaluated the impact of RUX on Pgp mRNA levels, transporter activity, ATPase activity, and PD1 alterations.

4.1.1. Dynamic expression of Pgp and CD8 in quiescent and antigen-primed human lymphocytes

Each blood sample came from a separate human donor, and Pgp expression was assessed in quiescent peripheral blood CD8+ lymphocytes (CTL13, CTL14) and compared with CD8+lymphocytes primed with JY cells (CTL1, CTL4) (Figure 15). To promote the development of mature cytotoxic T lymphocytes and memory T cells, the priming process entailed cultivating peripheral blood lymphocytes with JY cells once every two weeks for 28 days. Pgp expression was marginally but significantly higher in unprimed lymphocytes (CTL13, CTL14) than in JY-primed lymphocytes (CTL1, CTL4) (Figure 15A).

The marked shift of T cells from a naive to an effector phenotype, along with the production of memory cells, is probably responsible for the slight decline in average Pgp expression seen following repeated antigenic stimulation. Each population exhibits unique Pgp expression patterns. Conversely, compared to their unprimed counterparts (CTL13, CTL14), JY-primed CTLs (CTL1, CTL4) exhibited considerably higher levels of CD8 expression (Figure 15B). The rise in CD8 expression probably indicates increased T cell activation, differentiation, and cytotoxic capacity due to repeated antigen exposure, thus enhancing CD8+ immune responses in the mixed lymphocyte cultures. Notably, CD8 expression levels varied significantly across individual donors, highlighting donor-specific differences in protein expression. Conversely, the variability in Pgp expression among donors did not reach statistical significance.

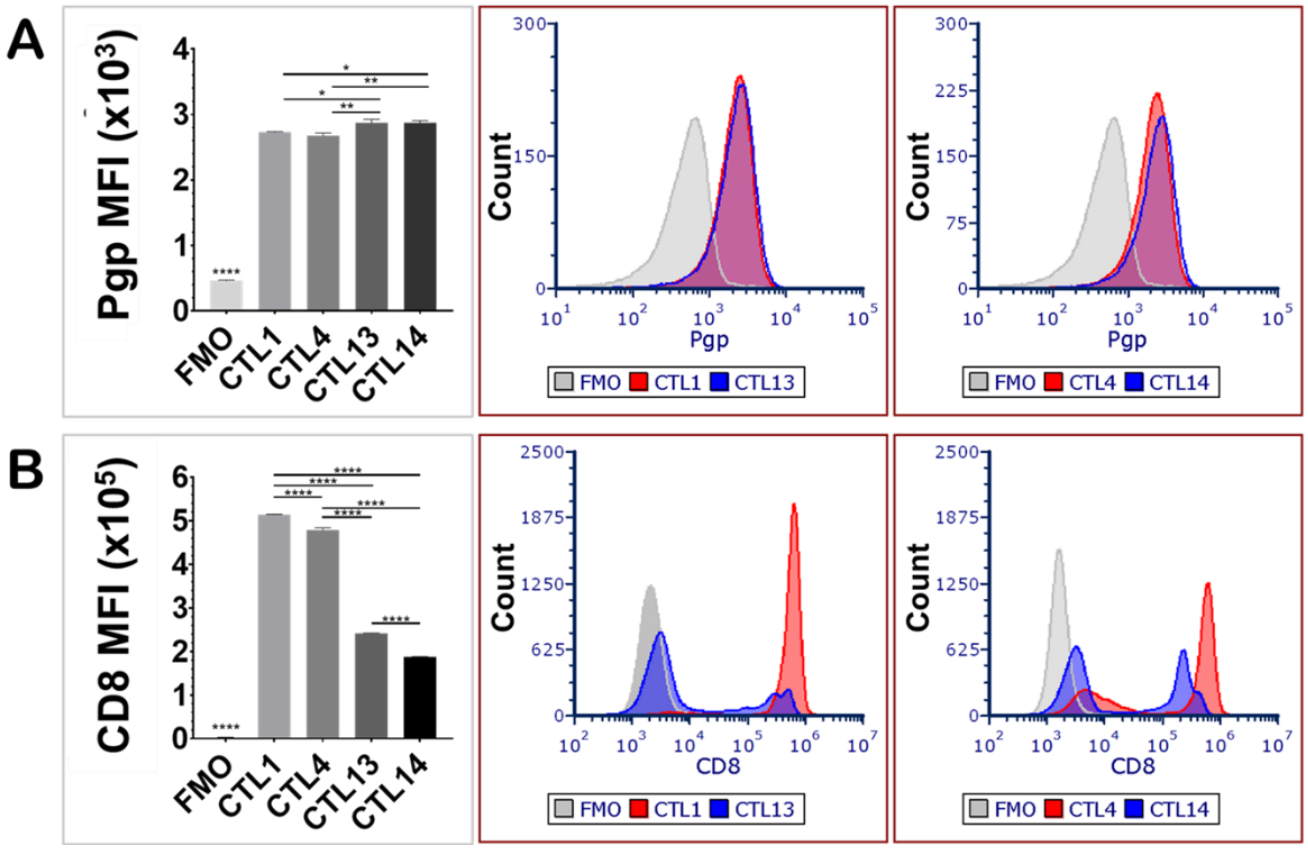

*Figure 15: Expression of Pgp and CD8 on JY-primed and unprimed human CD8+ T lymphocytes. Pgp expression decreased, while CD8 expression increased upon activation. (A) Mean fluorescence intensity (MFI) and fluorescence intensity distribution overlays of Pgp in JY-primed (CTL1, CTL4) and unprimed (CTL13, CTL14) cytotoxic T lymphocyte samples from different human donors. (B) MFI and fluorescence distribution overlays of CD8 expression in CTL1, CTL4, CTL13, and CTL14 donor samples. Statistical comparisons between groups were performed using one-way ANOVA followed by Tukey's multiple comparison test (n=3). Significance levels are indicated as *p < 0.05, **p < 0.01, ***p < 0.001. Error bars represent mean ± SEM.*

4.1.2. Ruxolitinib modulates Pgp mRNA expression in TCR-activated human T cells.

ABCB1 is crucial in chemoresistance and immune cell activity by facilitating the efflux of various xenobiotics. To explore the potential interaction between RUX and Pgp, we examined RUX's impact on ABCB1 mRNA expression in primary human T lymphocytes. We initially measured ABCB1 mRNA levels in JY-primed lymphocyte cultures, primarily consisting of CD8+ cytotoxic T lymphocytes, and compared these to a positive control cell line with high human Pgp expression. The NIH-3T3 MDR1 cell line, mouse fibroblasts transfected with the human ABCB1 gene, was

used as the positive control, while untransfected NIH-3T3 parental cells acted as the negative control (Figure 16A). When normalized to CTL expression levels, NIH-3T3 MDR1 cells showed about 500 times higher ABCB1 mRNA expression, whereas expression in the untransfected NIH-3T3 cells was undetectable. Gene expression was normalized using both human and mouse ACTB (β-actin) and GAPDH as reference genes, with all figures consistently normalized to ACTB due to its lower inter-treatment variability in human lymphocytes compared to GAPDH.

We investigated the baseline variability of ABCB1 mRNA levels in CD8+ T cells isolated from peripheral blood lymphocytes compared to those from JY-primed cytotoxic T lymphocyte cultures derived from five different human donors (Figure 16B). JY cells were used to provide alloantigenic stimulation, simulating physiological T cell priming. After this priming, ABCB1 mRNA levels decreased by about 95%, or to one-twentieth of the levels seen in naive CD8+ cells from PBMCs. Despite notable donor-to-donor variability in naive cell populations, a consistent reduction in ABCB1 expression was observed in nearly all donors following prolonged activation. This pattern aligns with our previous protein-level observations and reflects T cell maturation, where cells transition from naive and memory states to more differentiated effector phenotypes (Biwott et al., 2025b).

We examined the immediate effects of RUX on ABCB1 expression in CD8+ T lymphocytes during acute TCR stimulation (Figure 16C). Peripheral blood lymphocytes (PBL) were activated for 72 hours using anti-CD3/CD28 beads, resulting in reduced ABCB1 mRNA expression, consistent with the trend seen in the one-month JY-priming model. Notably, co-treatment with RUX mitigated this reduction, maintaining ABCB1 expression in both CD8+ and CD8- lymphocyte populations. These results indicate that RUX, may regulate Pgp expression by modulating TCR signaling pathways involved in T cell activation and differentiation. This effect is evident at both the protein and mRNA levels. The trends were consistent in both short-term activated naive T cells and long-term cultured JY-primed effector/memory CTLs (Biwott et al., 2025b).

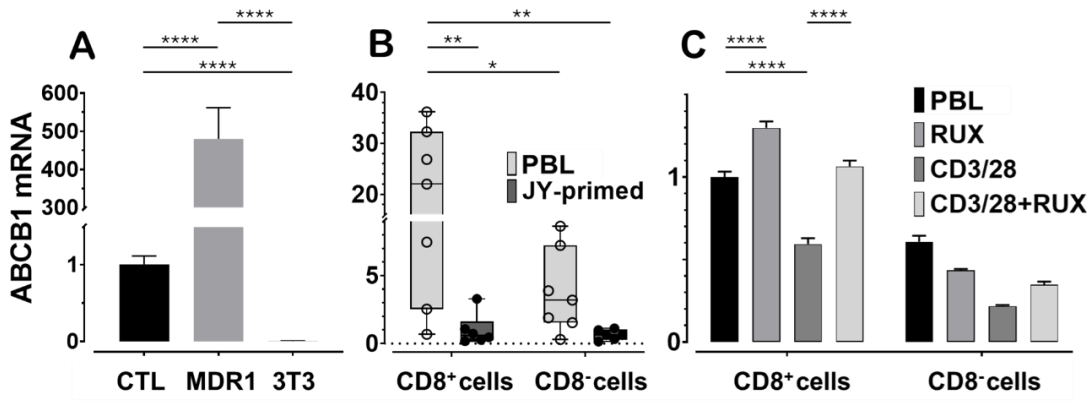

*Figure 16: Human P-glycoprotein transporter mRNA is expressed in cytotoxic T lymphocytes. Gene expression levels were standardized to ACTB (β-actin). (A) ABCB1 mRNA expression in JY-primed cultured human cytotoxic T lymphocytes was compared to control cell lines: ABCB1-transfected (MDR1, expressing human ABCB1) and un-transfected NIH-3T3 mouse fibroblasts. Expression values are reported as fold changes relative to the average mRNA levels in CTLs. (B) ABCB1 mRNA levels in CD8+and CD8- lymphocytes, sorted by flow cytometry, from freshly isolated peripheral blood lymphocytes (PBL) and JY-primed CTLs cultured for one month from the same donors. Values are expressed as fold changes relative to the average expression in JY-primed CD8+CTLs. (C) ABCB1 mRNA expression in flow cytometry-sorted CD8+and CD8- lymphocytes from freshly isolated PBL and in CTLs activated for 72 hours with anti-CD3/CD28 beads, with or without RUX. Expression values are shown as fold changes relative to the average in unstimulated PBL. Statistical analyses were conducted using one- or two-way ANOVA, followed by Dunnett's or Tukey's multiple comparison tests, as appropriate. Significance is denoted by asterisks (*p < 0.05; **p < 0.01; ****p < 0.0001). Error bars in panels A and C indicate the mean ± SEM (n = 3). In panel B, the median, interquartile range (second and third quartiles), and 95% confidence intervals are displayed (n = 6–7).*

4.1.3. Dose-dependent inhibition of P-glycoprotein activity by ruxolitinib and ZQ in cytotoxic T lymphocytes

To assess functional Pgp in human cytotoxic T lymphocytes, we measured its transporter activity with an optimized calcein efflux assay (Goda et al., 2020). Calcein-AM, a nonpolar fluorescent substrate of P-glycoprotein, becomes fluorescent after cleavage by intracellular esterases, with its accumulation inversely related to Pgp efflux activity. We quantified transporter function using the transport activity factor (TAF), which reflects the fractional increase in calcein accumulation with versus without a Pgp inhibitor. To validate Pgp activity and evaluate its pharmacological inhibition, we generated dose-response curves with ZQ, a third-generation Pgp-specific inhibitor, in NIH-3T3 cells overexpressing human MDR1 (NIH-3T3 MDR1) and primary human cytotoxic

T lymphocytes (CTLs). ZQ effectively blocked Pgp-mediated efflux in a dose-dependent manner in both cell types. NIH-3T3 MDR1 cells showed high sensitivity to ZQ, with an IC_{50} range of 1.779×10^{-7} to 2.847×10^{-7} M, while CTLs exhibited a right-shifted curve with an IC_{50} range of 1.809×10^{-6} to 3.498×10^{-6} M, consistent with lower Pgp expression in CTLs (Figure 17A and B). To enhance assay sensitivity in CTLs, we lowered the calcein-AM concentration to account for their reduced transporter expression compared to NIH-3T3 MDR1 cells. This adjustment allowed clear, quantifiable dose-dependent Pgp inhibition, confirming ZQ's effectiveness in primary CTLs, though at higher concentrations than in overexpressing cell lines.

We also assessed RUX's potential to modulate Pgp function. RUX induced dose-dependent inhibition of calcein efflux in both NIH-3T3 MDR1 cells and CTLs. In NIH-3T3 MDR1 cells, the IC_{50} for RUX ranged from 1.002×10^{-5} to 1.572×10^{-5} M, indicating moderate inhibitory potency (Figure 17A). In CTLs, the IC_{50} was higher, ranging from 3.003×10^{-5} to 8.543×10^{-5} M, suggesting lower affinity or indirect Pgp modulation (Figure 17B). Compared to ZQ, RUX dose-response curves were notably right-shifted in both systems, indicating weaker transporter

interaction. Nonetheless, the inhibition profile in CTLs suggests RUX may function as a low-affinity Pgp substrate or modulator.

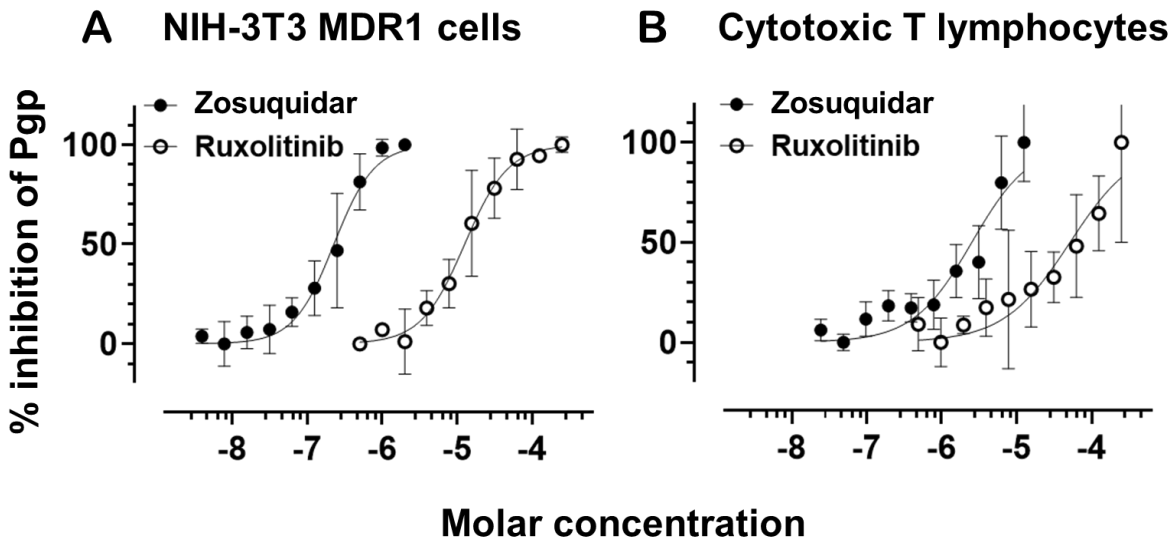

Figure 17: Dose-dependent inhibition of P-glycoprotein activity by RUX and ZQ. (A) A calcein-AM efflux assay was used to measure Pgp activity in NIH-3T3 cells that were stably expressing human MDR1 and (B) primary human cytotoxic T lymphocytes. The percentage inhibition of Pgp was calculated by measuring intracellular fluorescence after cells were treated with increasing concentrations of either RUX (open circles) or ZQ (filled circles). The mean ± SD of three measurements is represented in the data. In all cell types, ZQ demonstrated strong inhibition; NIH-3T3 MDR1 cells had lower IC_{50} values than CTLs. Pgp was inhibited by ruxolitinib with noticeably higher IC_{50} values, suggesting reduced potency in both cell types.

4.1.4. Ruxolitinib directly stimulates Pgp ATPase activity and interferes with verapamil-induced activation

Using membrane extracts from NIH-3T3 MDR1 cells, we conducted ATPase activity experiments to assess the direct interaction of RUX with Pgp. The ATPase assay offers a more direct readout of transporter interaction because variations in ATP hydrolysis reflect changes in the conformational cycling brought on by substrate or inhibitor binding, even though our fluorescent substrate accumulation experiment indicated functional inhibition of Pgp. To find out if RUX, ZQ, or CSA could alter basal ATPase activity, we first measured it. RUX increased basal Pgp ATPase activity in a concentration-dependent manner (measured at 1 µM, 10 µM, and 100 µM), as illustrated in Figure 18. When compared to control circumstances, the maximum dose (100 µM)

almost doubled the basal ATPase activity, and the increase was statistically significant ($p < 0.05$). Verapamil (40 μM), a well-known Pgp activator, had an effect similar to that of 100 μM RUX and similarly markedly increased ATPase activity ($p < 0.01$).

On the other hand, known Pgp inhibitors ZQ (10 μM) and CSA (20 μM) both decreased basal ATPase activity, although not to a statistically significant level at this sample number, still clearly demonstrating their inhibitory effect on transporter function.

We then investigated how RUX affects the ATPase stimulation induced by verapamil. When verapamil and increasing RUX concentrations were co-treated, interference was observed. The verapamil-induced ATPase activation was decreased by RUX; however, this decrease was relatively independent of the RUX concentration and statistically insignificant. In keeping with their substantial inhibitory impact, ZQ was also successful in inhibiting verapamil-induced ATPase activation on a significant manner ($p < 0.001$), while although with CSA the inhibitory effect was obvious it was not significant at one sample number.

All of these findings show that RUX can concentration-dependent and statistically significantly increase basal Pgp ATPase activity and this effect be affected by other inducers like the verapamil. This behavior strongly suggests that RUX directly interacts with Pgp. It likely acts as a substance that Pgp transports or alters its function, potentially influencing how various drugs interact with Pgp.

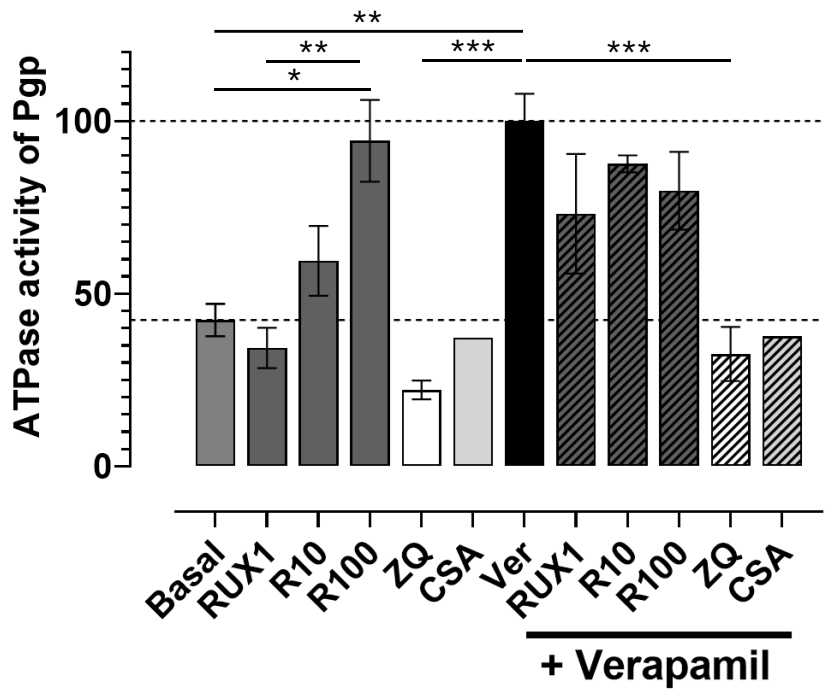

*Figure 18: RUX activates the ATPase activity of Pgp and interferes with other activators. RUX exhibited a dose-dependent increase in basal ATPase activity (lower dashed line) at concentrations of 1 μM (RUX1), 10 μM (R10), and 100 μM (R100). R100 considerably enhanced basal ATPase activity to levels that were equal to those caused by verapamil (Ver). For both basal and verapamil-stimulated ATPase activity, ZQ and cyclosporin A (CSA) decreased it. Verapamil and RUX co-treatment demonstrated probably a competitive effect. Mean ± SEM is used to depict the data, and post-hoc multiple comparisons are used to assess significance: *p < 0.05, **p < 0.01, and ***p < 0.001 (n = 3, except CSA n = 1).*

4.1.5. RUX impedes PD-1 expression and modulates CD8 and Pgp levels in human CD8+T cells following acute activation

Due to its ability to postpone lymphocyte maturation, RUX is used therapeutically in myeloproliferative diseases and graft-versus-host disease, where aberrant T cell proliferation is caused by altered JAK-STAT signaling. To ascertain whether the maturation-delaying effect of RUX could be replicated *in vitro*, we monitored the surface expression of PD-1, CD8, and Pgp after activating PBLs with CD3/CD28 beads for 72 hours. Since we were interested in CD8+ cytotoxic T cells, we used flow cytometry to examine the CD8+ and CD8- subsets independently. Fluorophore-conjugated antibodies against CD8, PD-1, and Pgp were used to stain cells, and the mean fluorescence intensity (MFI) was measured.

Acute CD3/CD28 activation confirmed effective T cell activation by dramatically upregulating PD-1 expression in CD8+ cells ($p < 0.0001$) compared to the control, as seen in Figure 19. With much lower PD-1 levels than activated, untreated controls ($p < 0.0001$), RUX administration dramatically slowed this induction, indicating that RUX attenuates or delays activation-associated phenotypic maturation.

An inhibitory effect on activation-induced alterations was further supported by the fact that CD8 expression levels were dramatically upregulated upon CD3/CD28 stimulation ($p < 0.0001$), but that this upregulation was partially blocked by RUX ($p < 0.0001$). CD3/CD28 stimulation also markedly increased surface expression for Pgp ($p < 0.0001$), while RUX administration markedly inhibited this induction, albeit not as much as for PD-1 (Figure 19).

The effects of RUX appear to be more noticeable in CD8+ T cells, as the CD8- population showed little changes in PD-1, CD8, or Pgp expression across circumstances, and the differences were not statistically significant when compared to control cells. Overall, these results corroborate RUX's function as an inhibitor of activation-associated maturation events in T cells by showing that it inhibits PD-1 induction and modifies CD8 and Pgp expression in activated CD8+ T lymphocytes.

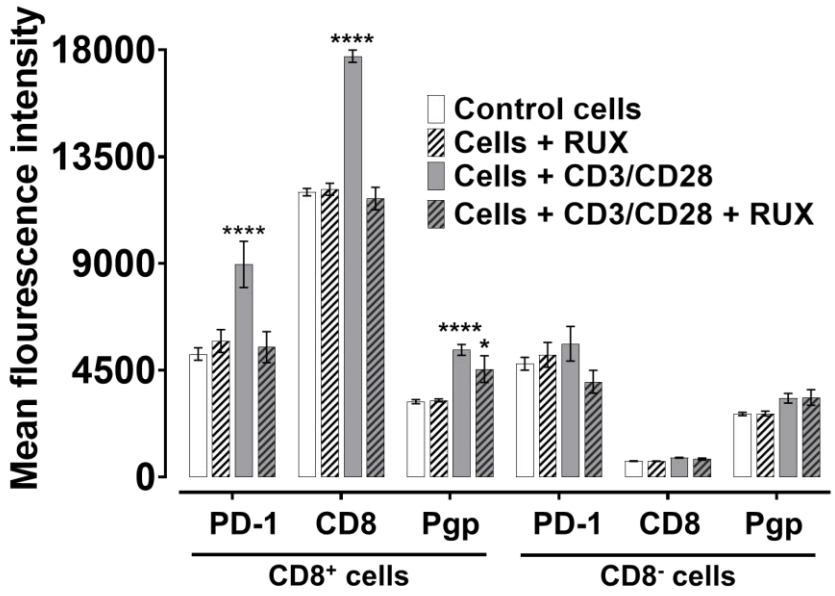

*Figure 19: RUX modulates Pgp and CD8 surface levels on sorted human cytotoxic T lymphocytes and inhibits PD-1 expression during acute CD3/CD28-mediated activation. After being stimulated for 72 hours using CD3/CD28 beads, peripheral blood mononuclear cells were either treated with RUX (100 nM) or left untreated. Fluorophore-conjugated anti-Pgp, anti-PD-1, and anti-CD8 antibodies were used to stain the cells after incubation, and flow cytometry was used for analysis. Each condition's fluorescence intensity was measured in 20,000 cells. Three separate experiments (n = 3) are represented by the mean ± SEM. Tukey's multiple comparison test was used to examine group differences after a one-way ANOVA (*p < 0.05; ****p < 0.0001).*

4.2. PART 2: P-glycoprotein expression in maturing CD8+ T cells and the effect of RUX

To investigate the expression of Pgp during T-cell maturation, we examined its expression in earlier and later memory states of human CD8+ T cells, as well as the maturation modulatory effect of RUX. Previous studies have shown that Pgp is expressed in young memory CD8+ T cells (Murata et al., 2016).

4.2.1. JY-priming predominantly generates specific CD8+ T cell phenotypes and increases Pgp expression in these populations

Peripheral blood lymphocytes from humans were cultured with proliferation-inhibited JY cells. The JY cell line, derived from B-lymphoblasts, exhibits a high surface expression of MHC class I A*02:01 proteins, making it an effective antigen-presenting cell. This interaction triggers a robust

CD8+ T-cell allotype immune response in mixed lymphocyte cultures. Previous research has shown that the resulting cytotoxic T lymphocyte clones exhibit strong and specific cytotoxic activity against JY target cells (Biwott et al., 2025b). In the present study, 8-color flow cytometry was primarily used to analyze live cells.

The overall frequency of T cells did not differ significantly between JY-primed lymphocytes and unprimed/non-exposed cells (Figure 20A). However, there was a marked upregulation of CD8+ T cells (Figure 20F) and a significant reduction in CD4+ T cells (Figure 20E), highlighting the effectiveness of MHC I restriction. Furthermore, the frequencies of NK and NKT cells increased significantly (Figure 20C-D), whereas the proportion of B cells in JY-primed cells decreased sharply compared to their non-exposed counterparts (Figure 20B).

This study also examined the proportion of Pgp-expressing cells across different T-cell subsets in PBL-derived lymphocyte cultures. Within the T-cell population, there was a significant overall increase in the percentage of Pgp-positive cells (Figure 20G). Notably, the fraction of Pgp-expressing cells increased in both CD4+ and CD8+ T cells (Figure 20K and L), while it markedly decreased in NK and NKT cells (Figure 20I and J). Although there was a significant increase in Pgp-expressing B cells, this finding is less relevant due to the substantial reduction in the total number of B cells (Figure 20B and H).

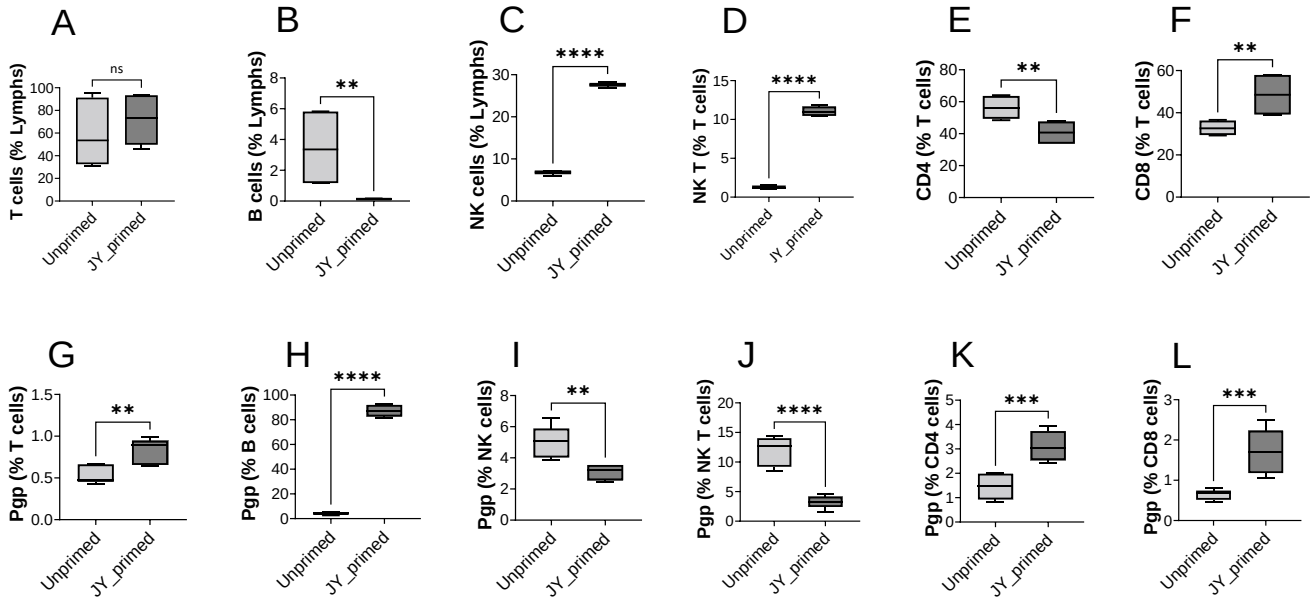

*Figure 20: Peripheral blood lymphocyte phenotypes and Pgp expression in unprimed and JY-primed cultures were detected. The rise in the population proportions of T cells, B cells, NK cells, NK T cells, and CD4+ and CD8+ T cell subsets in both JY-primed and unprimed cell cultures was evaluated using flow cytometric analysis. The percentage of Pgp-positive cells as well as variations in the concentrations of different immune cell types were computed and examined. After averaging the data, a Student's t-test was used to establish statistical significance (key: ns = non-significant), **p < 0.01, ***p < 0.001, ****p < 0.0001, n=4).*

4.2.2. Memory subpopulations identified during JY-primed CD8+ T cell maturation

Naive T cells are conventionally characterized as CD45RA+CD62L+, central memory T cells as CD45RA-CD62L+, effector T cells (Te) as CD45RA-CD62L-, and terminally differentiated effector T cells (Temra) as CD45RA+CD62L- (Murata et al., 2016). Additional subpopulations within these groups were identified based on previously published research (Cieri et al., 2015; Gattinoni et al., 2017; Lugli et al., 2013; Xia et al., 2021) (Figure 21A).

We utilized multi-parametric flow cytometry to analyze PBLs, and cultures stimulated with JY cells, labeling them with specific surface markers (Figure 21A). Immune clusters were determined based on the expression levels of these markers, visualized in a heat map (Figure 21A), and integrated into a comprehensive dataset. FlowSOM clustering was employed to identify immune

subsets, which were then mapped onto individual samples, allowing for comparison of their proportions among CD8+T cells. Dimensionality reduction using UMAP facilitated the visualization of the high-dimensional data (Figure 21B). Across both JY-exposed and non-exposed cytotoxic T lymphocytes, we identified 13 distinct CD8+ subsets: naive T cells, TeCD73+CD95+, TeCD95+, TemraCD127+, TemraCD127-, TymCD127+, TymCD127-, Tscm, TemCD95+, TcmCD95+CD127+, TcmCD73+CD95+, TcmCD95+, and TcmPD1+.

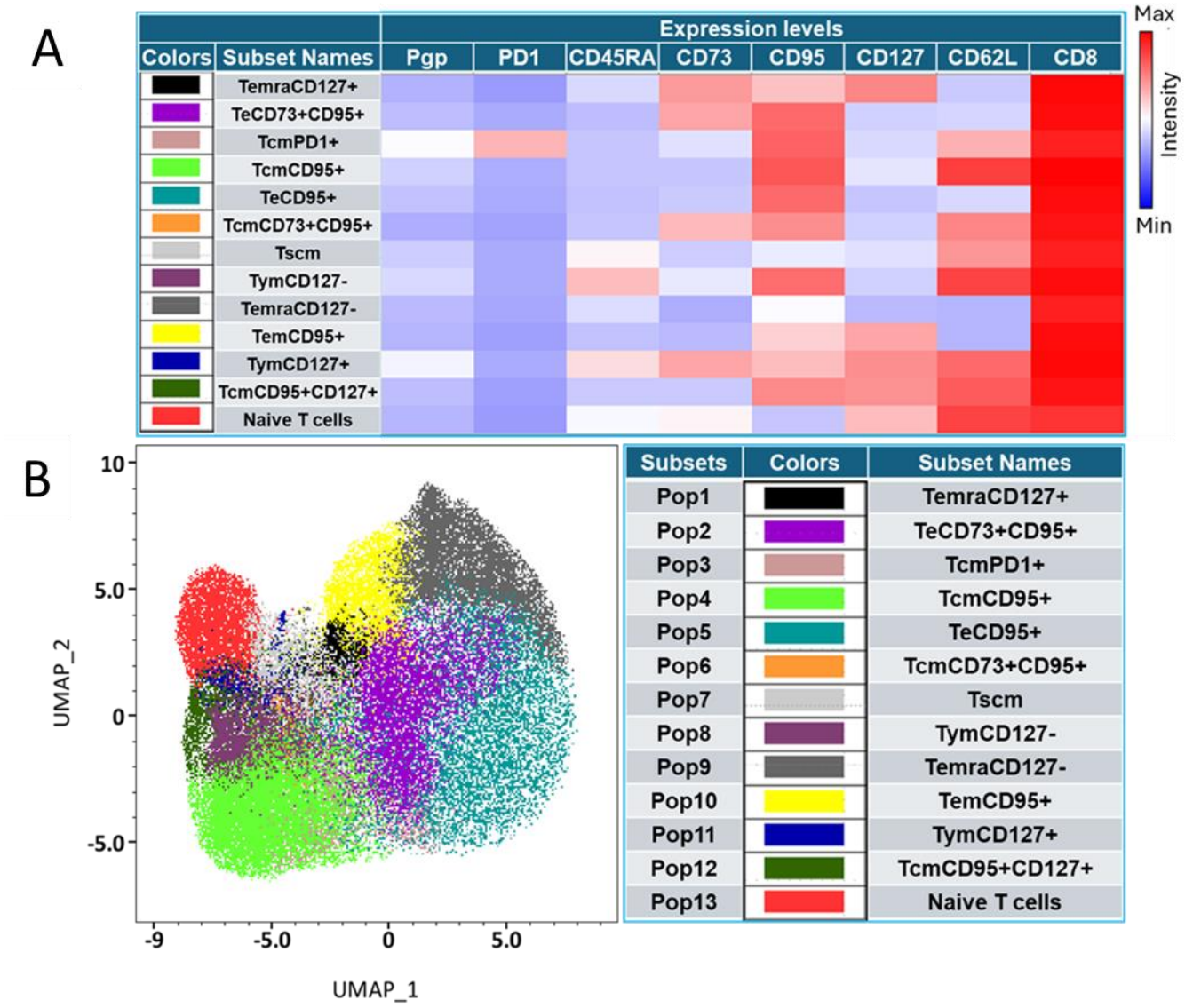

Figure 21: Heat map showing the expression of different markers and Pgp for each phenotype. (A) The flow cytometric data's dimensionality reduction (UMAP) and clustering (FlowSOM) are displayed. UMAP_1 and UMAP_2 are represented by the X and Y axes, respectively, and the cluster legends that demonstrated notable variations across treatments are displayed. TeCD73+CD95+, TeCD95+, TemraCD127+, TemraCD127-, TymCD127+, TymCD127-, Tscm, TemCD95+, TcmCD95+CD127+, TcmCD73+CD95+, TcmCD95+, and TcmPD1+ are CD8+ clusters that were recognized as naive T cells (B). The heat map's expression of surface markers served as the basis for its name. Central memory T cells are CD45RA-CDL62+, effectors are CD45RA-CD62L-, TemraCD127- are CD45RA+CD62L-, and conventional naive T cells are CD45RA+CD62L+.

4.2.3. P-glycoprotein-expressing CTL subsets were identified in both JY-primed and unprimed cultures

Among the 13 identified subsets, five exhibited significantly elevated levels of the multidrug resistance protein Pgp: TymCD127+, TymCD127-, Tscm, TcmCD95+, and TcmPD1+ (Figure 21). Notably, the TcmPD1+ subset, comprising central memory T cells expressing PD1, displayed the highest Pgp levels, representing a novel finding. This was followed by the young memory CD127+ subset (TymCD127+), consistent with previous observations (Murata et al., 2016). The remaining three subsets TymCD127-, Tscm, and TcmCD95+ showed progressively lower Pgp expression.

We further assessed the average Pgp expression across these memory subpopulations under different conditions of maturation, activation, and treatment (*Figure* 22). The analysis confirmed that TymCD127+ and TcmPD1+ subsets exhibited the highest Pgp levels. Notably, priming, activation, and RUX treatment consistently sustained significant Pgp expression, with RUX showing a tendency to further enhance Pgp levels.

It is important to note that elevated Pgp levels are not necessarily required for their physiological function. Even resting naive T cells exhibited detectable surface Pgp expression. The increased Pgp levels observed in cancer cells, however, represent a specific adaptation that supports multidrug resistance (MDR) during chemotherapy.

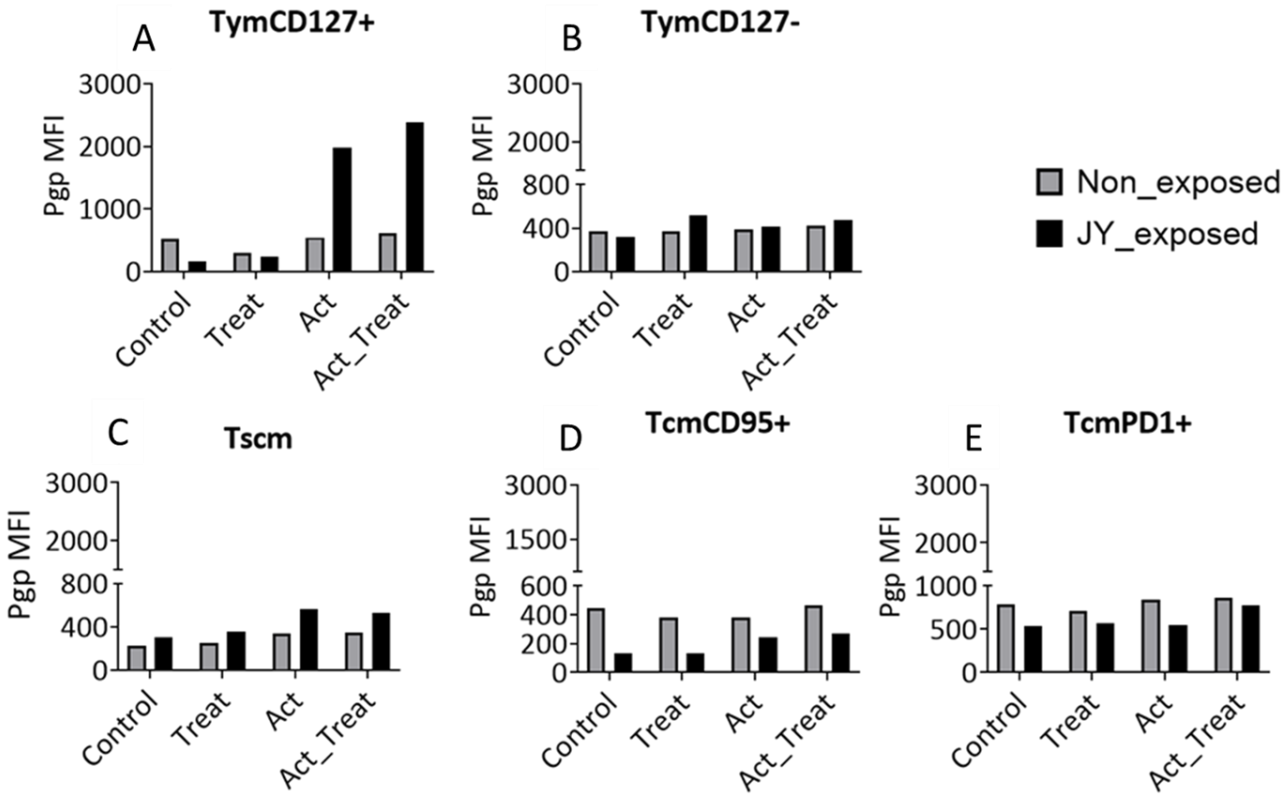

Figure 22: Pgp changes in immune clusters in JY-exposed and non-exposed CTLs following TCR activation and RUX treatment. TymCD127+ (A), TymCD127- (B), Tscm (C), TcmCD95+ (D), and TcmPD1+ (E) cells were found to express the greatest Pgp by UMAP of immunological CD8+ clusters. (Treat: RUX treatment; Act: activation of CD3/CD28 beads; Control: neither activation nor treatment).

4.2.4. Phenotypic polarization reflects typical adaptive immune responses in the JY-primed CTL maturation model following TCR activation.

Our goal was to distinguish between T-cell effector and memory phenotypes by exposing PBLs to antigen-presenting B cells, using the JY cell line to induce priming during the culture period. We analysed CD8+ T cell polarization under various activation conditions, resulting in a comprehensive dataset comprising 89,600 CD8+ cells. A contingency table was constructed to categorize each cytotoxic T lymphocyte phenotypic subset across different activation and treatment conditions. The changes observed in all subsets at various treatment and maturation stages are shown in Figure 23. Nearly all changes in CD8+ T cell activation were statistically significant, with non-significant changes labelled as ‘ns’ in the figures. We also calculated the effect sizes for these changes, emphasizing the biological significance of the statistically

significant variations. Subsets with large effect sizes, which suggest important immunological changes, are highlighted in bold in Figure 23 to Figure 26.

4.2.5. Differentiation of CD8+ T cell subsets derived from human peripheral blood lymphocytes in response to TCR activation

The subsets initially present in the PBL sample undergo notable changes following activation of the CD3/CD28 TCR signal. In the *in vitro* system, the absence of continuous naive T cell production from the thymus, as occurs *in vivo*, results in a decreased naive T cell fraction, leading to their differentiation into effector or memory cells. This transformation is evidenced by a reduced naive T cell fraction and an increased proportion of TeCD95+ and TeCD73+CD95+ subsets. While some cells may continue maturation from earlier stages initiated in the donor's body, most transformations are driven by the *in vitro* TCR signal. The robustness of our findings is supported by the use of healthy donors and a strong CD3/CD28 antibody-coated bead signal that targets all TCR-expressing cells.

Our study particularly focused on monitoring changes within the memory subsets, with special attention to the small intermediate memory subsets characterized by higher Pgp levels. As naive cells differentiate into effector and memory cells, they follow specific maturation pathways. Intermediate memory subsets such as TymCD127+, Tscm, TemCD95+, TcmCD95+CD127+, and TcmPD1+ decrease proportionally when insufficient precursor cells are supplied. Conversely, subsets derived from earlier differentiation states increase, including short-lived effectors that later undergo apoptosis. Notably, in the early stages of maturation, we observed a significant increase in Pgp-expressing TcmCD95+ cells, which rose from 9.5% to 36.5%. Additionally, the young memory TymCD127- subset, which expresses high levels of CD95 and is closely related to TcmCD95+ cells (Figure 23A), showed a slight increase, comprising nearly 10% of the earliest Pgp-expressing memory subset in PBL or TCR-activated PBL populations, rising from 9.9% to 12.7%; (Figure 23B).

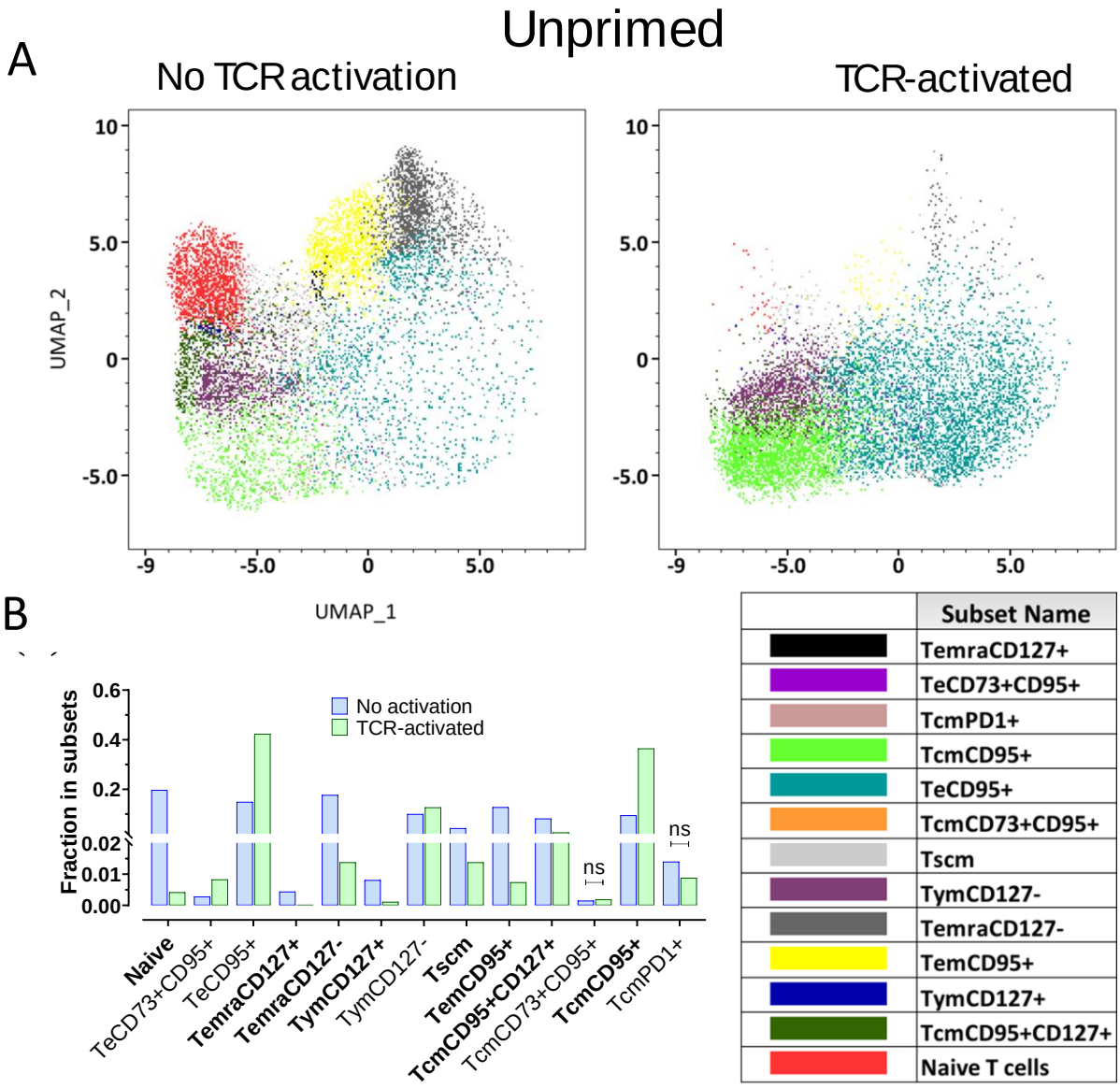

Figure 23: Changes in CD8+ T cell subset sizes from human peripheral blood lymphocytes in response to TCR activation after seventy-two hours (JY-non-exposed cells). *(A)The top panel features a UMAP cluster map with subpopulations distinguished by color, providing a visual representation of maturation changes. (B) The bottom panel shows a bar chart illustrating changes within the same dataset. All changes are statistically significant unless labelled "ns" (non-significant). Subsets highlighted in bold indicate a large effect size, reflecting notable immunological impacts, while non-bolded subsets correspond to medium or small effect sizes.*

4.2.6. Activation-dependent changes in the CD8+ subsets in JY-primed and unprimed CTLs

TCR activation of unprimed subsets led to a significant downregulation of TymCD127+ and Tscm subsets, while TymCD127- and TcmCD95+ subsets were upregulated. TcmPD1+ levels showed no significant change (*Figure* 24A). In unprimed versus JY-primed (JY-exposed) subsets of TCR-unactivated cells, TymCD127+ was upregulated, whereas Tscm, TymCD127-, TcmCD95+, and TcmPD1+ were downregulated (*Figure* 24B). In unprimed versus JY-primed subsets of TCR-activated cells, there was a significant increase in TcmPD1+ and significant downregulation of TymCD127+, Tscm, TymCD127-, and TcmCD95+ (*Figure* 24C). When comparing unactivated and TCR-activated subsets in JY-primed cells, we observed a significant increase in TcmPD1+ cells and a non-significant increase in TymCD127-, alongside significant downregulation of TcmCD95+. TymCD127+ and Tscm subsets exhibited non-significant downregulation (*Figure* 24D). The blue arrows (*Figure* 24) denote the direction of population changes in memory subsets expressing Pgp due to the treatment. Subsets listed in bold reflect large effect sizes, indicating significant immunological impacts, while non-bolded subsets represent medium or small effect size.

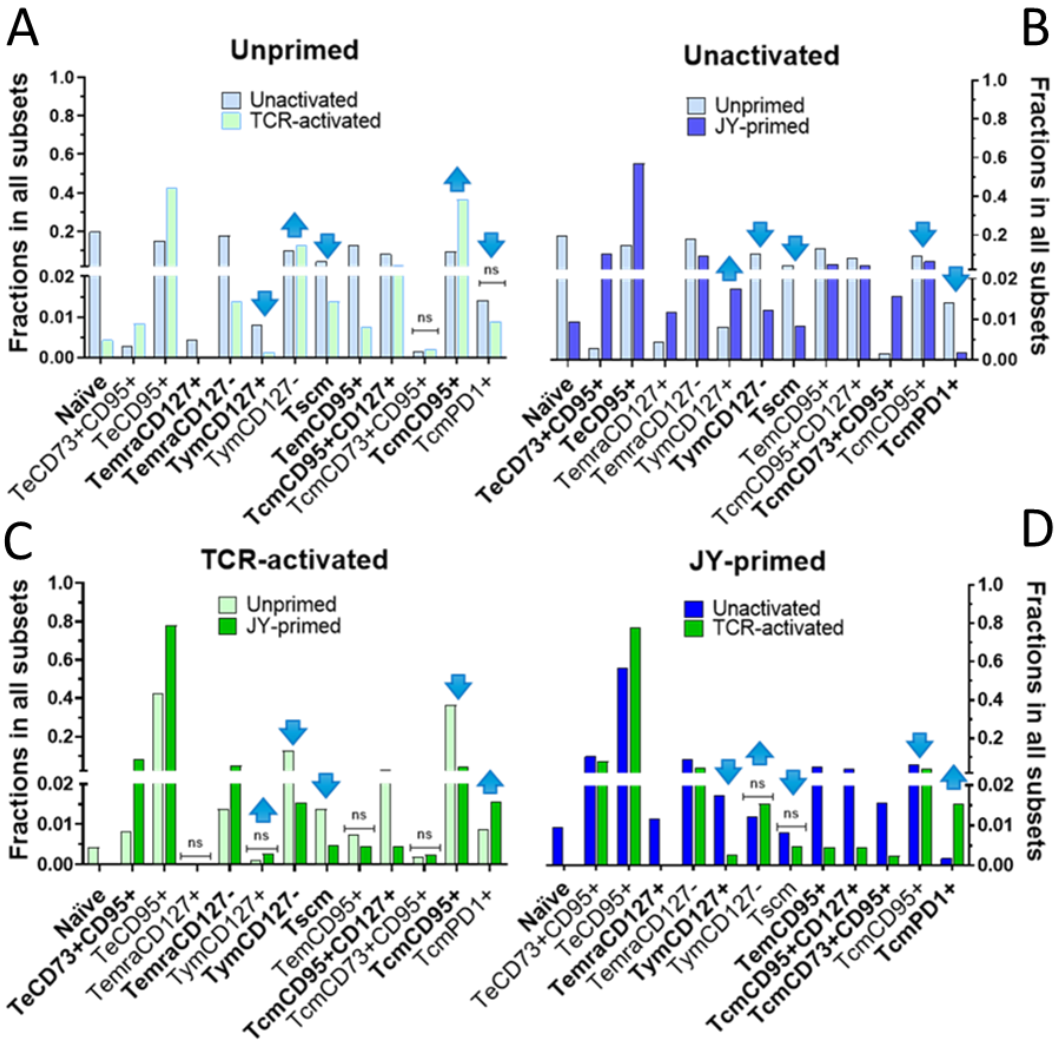

Figure 24: Activation-dependent changes in the CD8+ subsets in JY-primed and unprimed CTLs. (A) Comparison of TCR-unactivated and TCR-activated subsets in unprimed cells (JY-non-exposed). (B) Comparison of unprimed and JY-primed (JY-exposed) subsets in TCR-unactivated cells. (C) Comparison of unactivated and TCR-activated subsets in JY-primed cells. (D) Comparison of unprimed and JY-primed subsets in TCR-activated cells. Blue arrows indicate the direction of the changes in population size in memory subsets expressing Pgp due to the treatment. A contingency table was constructed from the number of CTLs in each subset. The level of association between these numbers was calculated using the Chi-square test to statistically evaluate changes under different experimental conditions. All changes are statistically significant, except those marked "ns", which denotes non-significant changes. Subsets in bold indicate a large effect size, suggesting significant immunological effects. Non-bolded subsets indicate medium or small effect sizes.

4.2.7. Differentiation of long-lived CD8+ T cell subsets in JY-primed human peripheral blood lymphocyte cultures

The next stage of differentiation was evaluated in one-month-old IL-2-expanded T cells, which were initially cultured through two cycles of JY-cell-primed mixed lymphocyte cultures. Within these cultures, CD8+ T cell subsets differentiated by recognizing allogeneic self-antigens presented by JY cells, leading to a robust CD8+ T cell response. The addition of IL-2 to the one-month culture facilitated the differentiation and accumulation of long-lived memory subpopulations (Kalia & Sarkar, 2018).

As shown in Figure 25A, there was a marked reduction in naive cells and subsets such as TymCD127-, TemCD95+, TemraCD127+, and TcmCD95+CD127+. Conversely, the most notable increases were observed in the TeCD95+ and TeCD73+CD95+ subsets. Figure 25B highlights more subtle changes, such as a decline in the small Pgp-expressing TcmPD1+ subset, alongside an increase in TemraCD127+ cells and Pgp-expressing TymCD127+ and TcmCD73+CD95+ subsets.

When comparing JY-primed T cells after one month of maturation to unprimed PBLs, there was a sustained loss of naive cells and a more pronounced rise in effector cells, exceeding the changes seen after 72 hours of acute TCR activation (Figure 23B, *Figure* 24A-B, and Figure 25B). The previously expanded TeCD95+ and TeCD73+CD95+ subsets continued to grow, while the smaller TemraCD127+ subset showed significant expansion. Additionally, other memory subsets changed, with long-lived memory cells emerging during the retraction phase. Early TymCD127+ and TcmCD73+CD95+ subsets increased, while the central memory population of TcmCD95+ cells and the larger TymCD127- subset, which primarily differentiates into effector cells, showed a decline. The smaller TymCD127+ subset, characterized by high Pgp expression, transitioned into TcmCD73+CD95+ memory subsets.

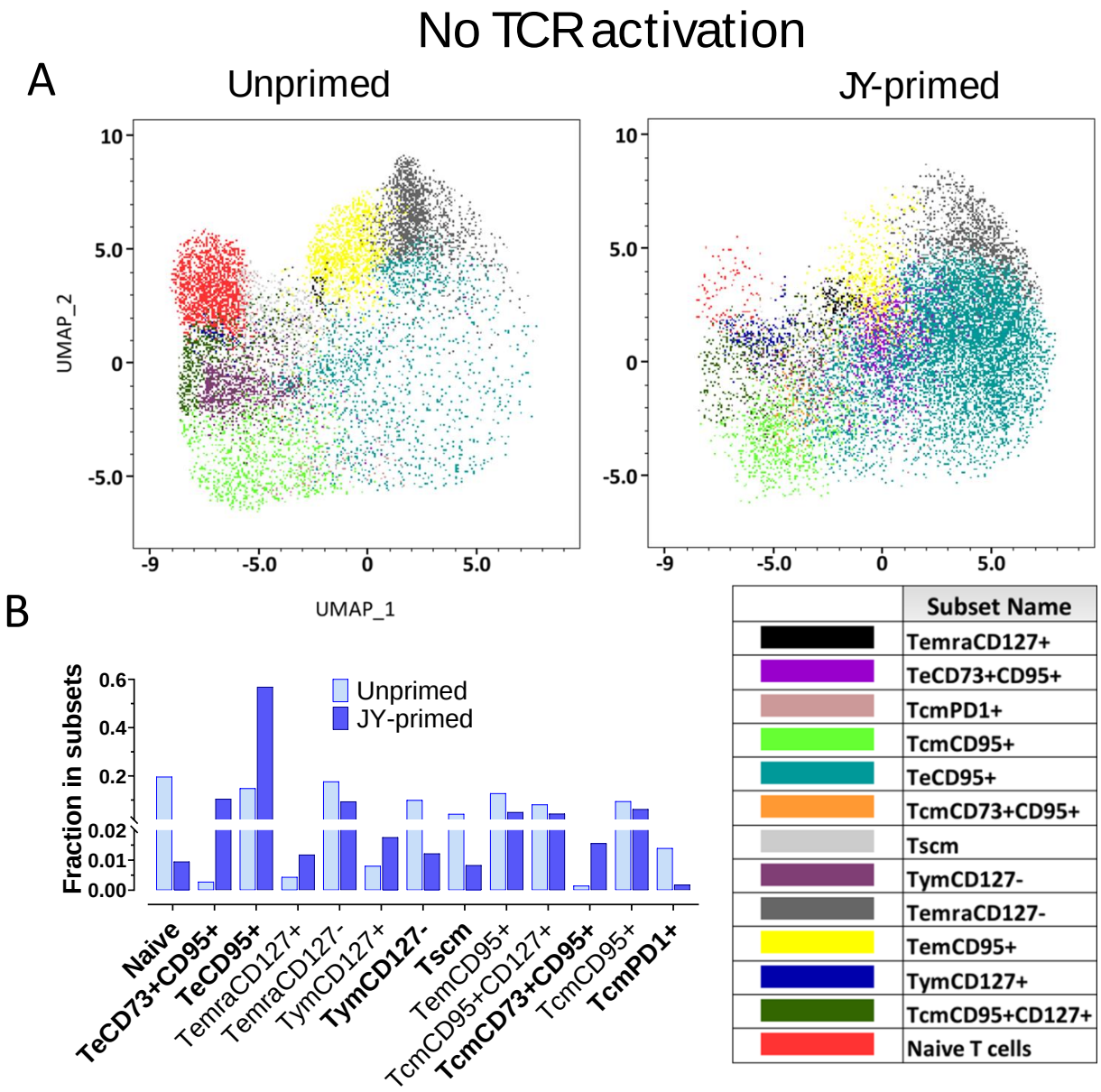

Figure 25: Changes in CD8+ T cell subset sizes from human peripheral blood lymphocytes in unprimed and in response to allogeneic activation after one month (JY-primed). Cells were cultured with IL-2, and allogeneic activation was repeated after two weeks. Samples were analyzed without acute CD3/CD28 activation. (A) The upper panel shows a UMAP cluster map with color-coded subpopulations, providing a visual representation of maturation changes. (B) The lower panel presents a bar chart illustrating changes in the same dataset. All changes are statistically significant. Subsets highlighted in bold indicate a large effect size, reflecting substantial immunological impacts, while non-bolded subsets denote medium or small effect sizes. Notably, no effect sizes were deemed statistically negligible.

4.2.8. Differentiation of late-stage CD8+ T cell subsets in TCR-reactivated, JY-primed cultures

To monitor the latest maturation changes in this system, we activated the TCR signal using CD3/CD28 beads in JY-primed one-month-old cultures.

In the upper panel of Figure 26A, the most significant observation is the repeated and substantial increase in the TeCD95+ short-lived effector population. Due to its brief lifespan, this population must be replenished from the smaller intermediate memory subsets, especially since naive precursors are nearly absent at this stage. This trend, characterized by the reduction of smaller intermediate populations, is also evident in the UMAP maps.

When comparing the TCR-activated and unactivated states of the JY-primed subset compositions in the lower panel of Figure 26B, it becomes clear that the recall response of the T-cell memory population is remarkably robust. This is demonstrated by the peak response of TeCD95+ effector CTLs, which rises to nearly 80%, compared to 40% observed under earlier unprimed conditions (Figure 23B). The established trend among memory subsets during both initial and recall TCR activation is consistent, with the long-lived, smaller memory subsets expressing high levels of Pgp.

The most intriguing finding in our study is the behavior of memory subsets during late TCR activation. Specifically, there is a notable decline in early maturation phase young memory TymCD127+ cells and their closely related central memory TcmCD73+CD95+ cells, both of which had previously increased. Strikingly, aside from the expanding CD95+ effectors, all other subpopulations decrease at this stage, with one exception: the small TcmPD1+ subset. This subset, which expresses the highest levels of Pgp, undergoes a significant and biologically meaningful expansion. Despite its modest size, remaining at just a few percent, this late-stage central memory TcmPD1+ T cell subpopulation demonstrates a prominent increase, mirroring the earlier behavior of TymCD127+ and TcmCD73+CD95+ small memory subsets, which also expressed high Pgp levels.

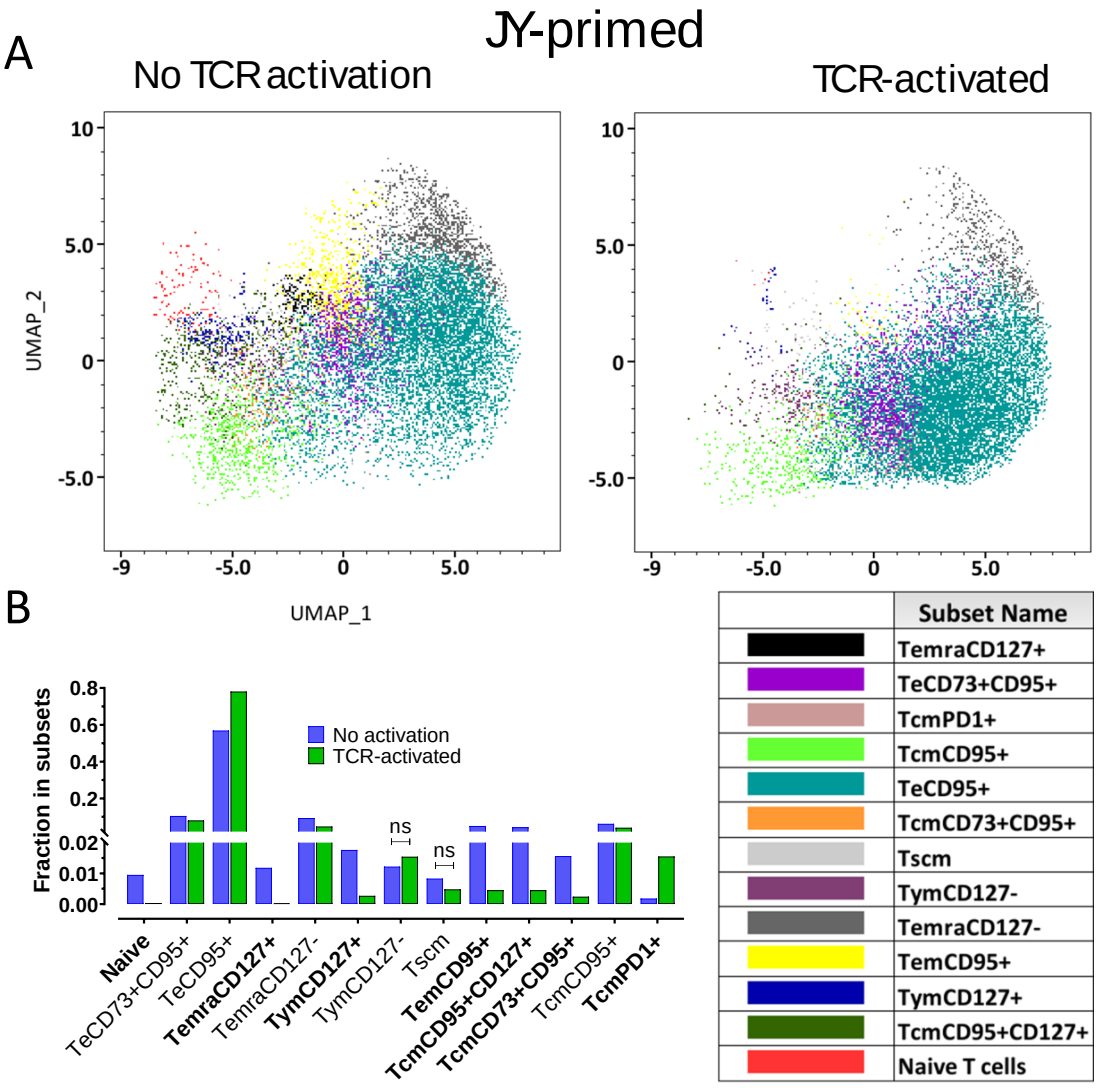

Figure 26: Changes in CD8+ T cell subset sizes from JY-primed human lymphocytes in response to TCR activation after 72 hours. (A) The upper panel presents a UMAP cluster map with color-coded subpopulations, visually confirming maturation changes. (B) The lower panel displays a bar chart showing changes in the same data set. All changes are statistically significant except those marked "ns" (non-significant). Subsets in bold indicate a large effect size, suggesting significant immunological effects. Non-bolded subsets represent medium or small effect sizes.

4.2.9. RUX delays CD8+ T cell maturation

RUX inhibits the Jak-1 and Jak-3 signaling pathways, critical for TCR activation and T-cell maturation (Appeldoorn et al., 2023). We examined RUX's impact on 13 identified CD8+ subsets maturation in unprimed and JY-primed systems, as shown in Figure 27. Multiple trials (control,

activated, treated, and treated-activated for 72 hours) assessed RUX's effects on CD8+ T-cell maturation. RUX was administered during TCR activation in both unprimed and JY-primed cells (Figure 27). UMAP analysis was used to evaluate outcomes, enabling visualization of RUX's effects. The UMAP plot for unprimed, activated, and treated cells (Figure 27) revealed that RUX preserved naive cells (red cluster) post-activation. Additionally, TCR activation increased TcmCD95+ cells in unprimed groups (light green clusters in UMAP plots), while JY-priming reduced naive cells and elevated TeCD95+ cells (Figure 27).

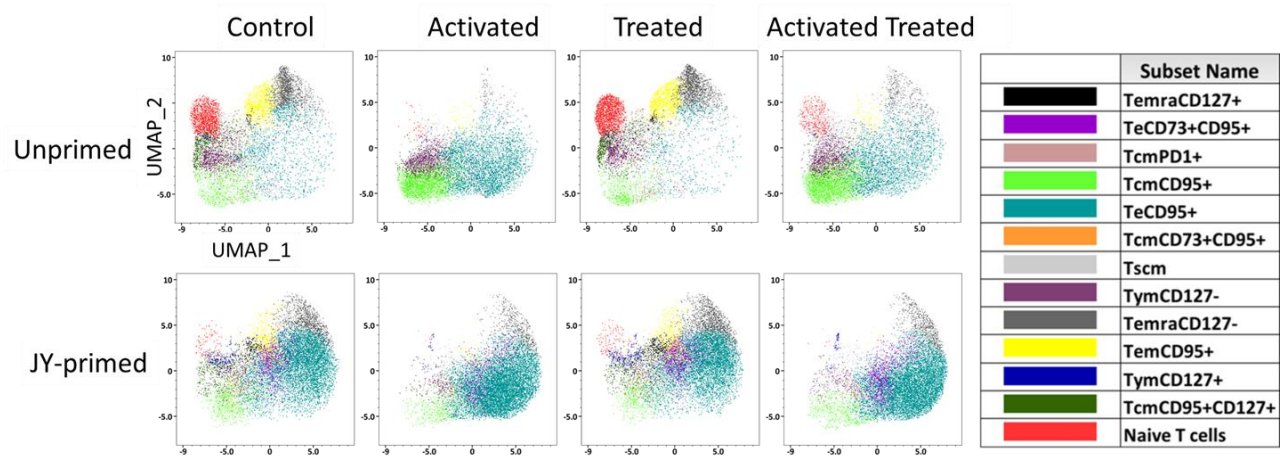

Figure 27: TCR activation and RUX-induced changes in human CD8+ T lymphocyte subsets in JY-primed and unprimed cells. On dimensionality-reduced UMAP plots based on various experimental conditions, immune clusters of unprimed and JY-primed cells were displayed: Activated (CD3/28 activated), Treated (RUX treated), Activated _Treated (CD3/28 activated and RUX treated), and Control (untreated, unstimulated) samples.

4.2.10. Effects of TCR-activation and RUX in the unprimed immune subsets

To investigate the impact of TCR activation on unprimed CTLs, we stimulated these cells with CD3/CD28 beads, both in the presence and absence of RUX in JY-primed samples. Figure 28A-M shows the 13 CD8+ subsets (shown in UMAP plot in Figure 21A and B) changes following TCR activation and RUX treatment. TCR activation resulted in an increase in Pgp-expressing subsets, notably TcmPD1+, as well as non-Pgp-expressing subsets such as TeCD95+ and TcmCD95+ (Figure 28). Conversely, TCR activation caused a decrease in the frequencies of subsets such asTemraCD127+, TemCD95+, TcmCD95+CD127+, and TemCD95+ subsets (Figure 28).

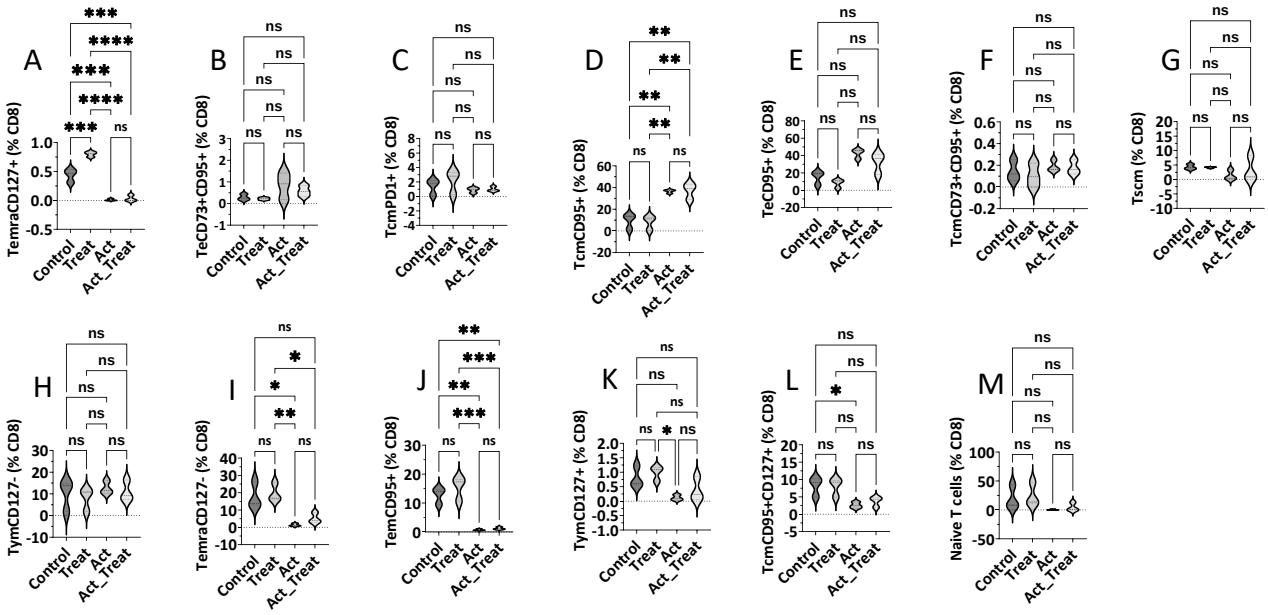

*Figure 28: Effects of TCR-activation and ruxolitinib in the unprimed immune subsets. The X-axis represents different treatment groups. Control (untreated, unstimulated), Activated (CD3/28 activated), Treated (RUX treated), and Activated _Treated (CD3/28 activated and RUX treated). The Y-axis represents subsets % within CD8+ cells. TemraCD127+ (A), TeCD73+CD95+ (B), TcmPD1+ (C), TcmCD95+ (D), TeCD95+ (E), TcmCD73+CD95+ (F), Tscm (G), TymCD127- (H), TemraCD127- (I), TemCD95+ (J), TymCD127+ (K), TcmCD95+CD127+ (L), Naive T cells (M). One-way ANOVA with Tukey's multiple comparison tests was used, and their statistical significance is given within the plots. (Statistical significance key: ns non-significant, *p < 0.05, **p < 0.01, ****p < 0.0001).*

4.2.11. Effects of TCR-activation and RUX in the JY-primed immune subsets

The impact of TCR activation on JY-primed CTLs was assessed, as shown in Figure 29A-M which depicts the 13 CD8+ subsets (shown in UMAP plot in Figure 21A and B) changes following TCR activation and RUX treatment in JY-primed CTLs. TCR activation resulted in an increase in the Pgp-expressing TcmPD1+ subset, as well as in the non-Pgp-expressing TeCD95+ subset (Figure 29). Notably, a 72-hour exposure to RUX resulted in an increase in the Tscm subset, a result not observed in other multidrug-resistant populations, including TcmPD1+ (Figure 29C, G). Interestingly, TCR activation led to a striking upregulation of the TeCD95+ subset (Figure 29E), while RUX treatment inhibited this activation-induced increase compared to the activated group.

Non-Pgp-expressing subsets, including TemraCD127+, TemraCD127-, TcmCD95+, TcmCD95+CD127+, TcmCD73+CD95+, and naive CD8+ T cells, were downregulated during TCR activation. Surprisingly, the TeCD73+CD95+ subset exhibited activation-induced downregulation, whereas RUX treatment led to its upregulation (Figure 29B). Overall, the observed patterns (Figure 29) suggest a potential maturation delay due to RUX; however, these changes were not statistically significant.

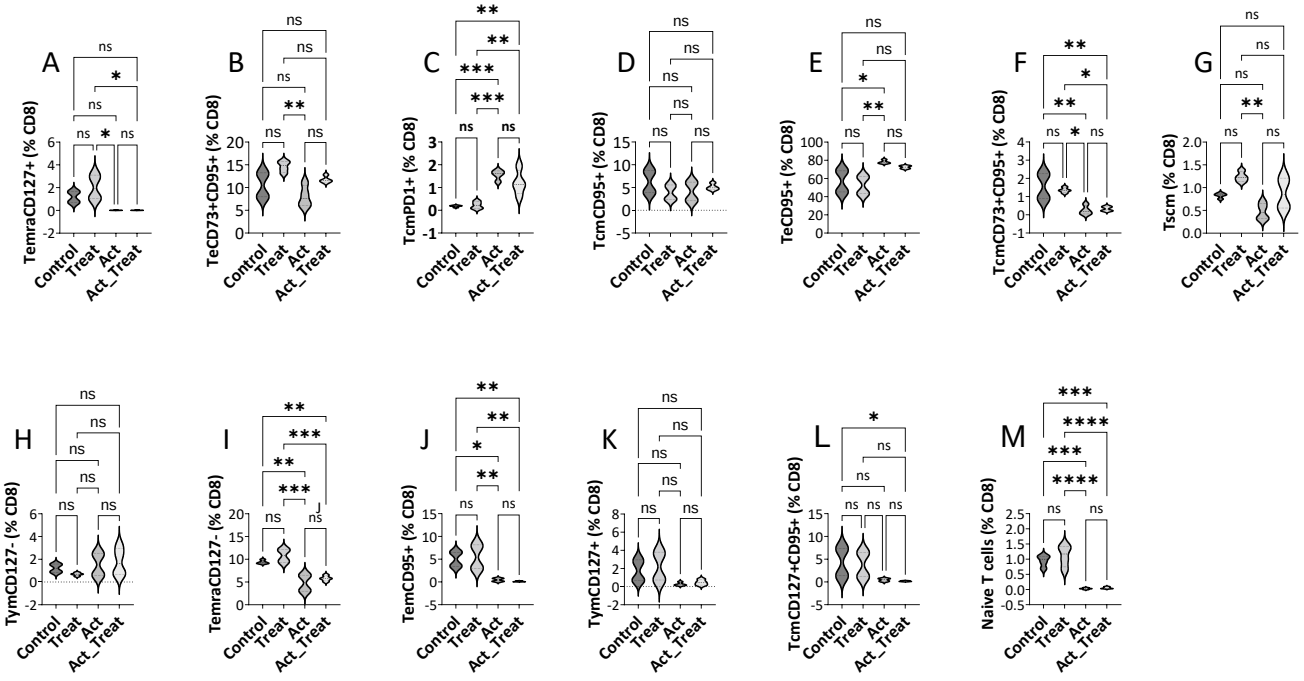

*Figure 29: Effects of TCR activation and RUX in JY-primed immune clusters. The X-axis represents different treatment groups. Control (untreated, unstimulated), Activated (CD3/28 activated), Treated (RUX treated), and Activated _Treated (CD3/28 activated and RUX treated). The Y-axis represents subsets % within CD8+ cells. TemraCD127+ (A), TeCD73+CD95+ (B), TcmPD1+ (C), TcmCD95+ (D), TeCD95+ (E), TcmCD73+CD95+ (F), Tscm (G), TymCD127- (H), TemraCD127- (I), TemCD95+ (J), TymCD127+ (K), TcmCD95+CD127+ (L), Naive T cells (M). One-way ANOVA with Tukey's multiple comparison tests was used, and their statistical significance is given within the plots. (Statistical significance key: ns non-significant, *p < 0.05, **p < 0.01, ****p < 0.0001).*

4.2.12. Effects of RUX on the maturation of CD8+ T cells

Contingency table analysis confirmed the maturation-delaying effect of RUX, revealing significant differences in cell numbers. Notably, naive cell counts were consistently higher in

RUX-treated samples compared to those treated with pure TCR-activation samples, across both unprimed and JY-primed conditions.

The effects of RUX treatment during TCR activation were further quantified by assessing the normalized cumulative change across all subsets (Figure 30). This metric reflects the total differences observed at each of the four phases of the maturation process in JY-priming TCR activation experiments.

Notably, naive cells, as well as the TemraCD127+, TemraCD127-, and Pgp-expressing TymCD127+, Tscm, and TcmPD1+ subpopulations, showed significant positive cumulative differences (indicated in bold). Additionally, TeCD73+CD95+ cells also demonstrated a positive trend, although it was less significant. In contrast, the subpopulation most negatively affected was the TeCD95+ effector cells, which experienced a modest reduction, along with a decrease in TymCD127- cells (Figure 30).

These findings indicate that RUX treatment diminishes the main short-lived effector subpopulation while maintaining small, long-lived Pgp-expressing memory populations, consequently delaying CD8+ T cell maturation.

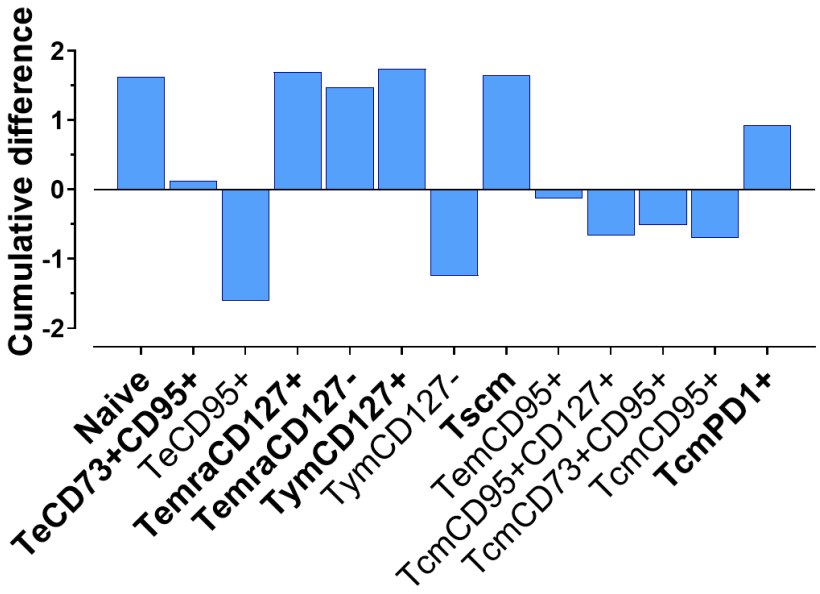

Figure 30: Effects of RUX on the maturation of CD8+ T cells. Subpopulations with positive values (in bold) increase their proportion to the end of the maturation process, and subpopulations with negative values decrease. To create this bar chart, the differences between RUX-treated and untreated values from the contingency table were first calculated. These differences were then summed across the four maturation phases: unprimed and unactivated, unprimed and TCR-activated, JY-primed and unactivated, JY-primed and TCR-activated. These summed differences were then normalized to the square root of the sum of squares. This normalization ensured that changes in the same direction were aggregated, resulting in larger values, while changes in opposite directions cancel each other.

4.2.13. Changes in the naive population across the maturation phases

Figure 31A illustrates that across the four major stages of maturation utilized in this study, and in conjunction with RUX treatments that alter maturation, significant changes in major subsets characterizing the adaptive CD8+ immune response were reliably identified. Specifically, during the acute TCR activation of PBLs, the initial population of naive cells experienced a reduction from 19.7% to 0.4%. These numerical changes are corroborated in *Figure* 24, while the trends are depicted in Figure 31. After the one-month mark, the percentage of naive cells was measured at 0.9%, which became negligible during the repeated "recall" TCR activation at 0.03%. Consequently, by the conclusion of the four maturation stages, the naive cell population had completely transitioned into more mature cell states, as there was no available cell supply from the thymus. At each stage shown Figure 31A, the samples treated with RUX exhibited a notable

upward trend relative to their previous untreated stages, thereby indicating that RUX treatment effectively delays the maturation of naive cells.

During the one-month culture period, which included two cycles of JY cell allogeneic antigen presentation, a substantial number of allogeneic T cell clones were generated due to the abundant allogeneic antigens. This phenomenon results in an increase in the effector population during the retraction phase, a phase typically marked by a decrease during the contraction phase of a standard immune response. The fourth maturation phase, responsible for generating a recall signal, involves reactivating all T cells using beads, similar to the activation process in the second phase of the maturation system. A limitation of this system is the continuous increase in effector cells, which deviates from the expected contraction phase and could obscure certain aspects of memory population behavior. However, a notable advantage is the robust and synchronous TCR activation facilitated by the abundance of allogeneic antigens via beads or JY cells, which allows for reliable monitoring of small memory populations.

4.2.14. Changes in the effector populations across the maturation phases

The two effector cell populations, TeCD95+ and TeCD73+CD95+, demonstrated significant increases across the four maturation stages. Initially, the TeCD95+ population was present at 15.2%, which further increased to 43.2% after acute TCR activation using anti-CD3/CD28 beads (Figure 31A and *Figure* 24). After one month of TCR activation with allogeneic JY cells, levels for this population increased further to 67.4%. A subsequent "recall" activation using anti-CD3/CD28 beads elevated their percentage to 86.1%.

In PBLs, the dominant effector population, TeCD95+, started at 14.9% and expanded to 42.4% following acute TCR activation. This population continued to grow, reaching 56.9% after one month (Figure 31B and *Figure* 24). During the recall phase, it peaked at 78%. In contrast, the other effector subset, TeCD73+CD95+, was initially negligible at just 0.3%. It increased modestly to between 8-11% but remained approximately one-tenth the size of the TeCD95+ population.

Treatment with RUX consistently reduced the overall production of effector cells, particularly impacting the dominant TeCD95+ subset. Across the four stages, the proportions of TeCD95+ and

TeCD73+CD95+ rose from 15.2% after acute TCR activation to 67.4% after one month of JY-cell stimulation, ultimately reaching 86.1% following recall activation with anti-CD3/CD28 beads.

In the dominant TeCD95^{+} population within PBLs, proportions showed a progressive increase across all stages, in the end peaking at 78% during the recall phase (*Figure* 24 and Figure 31B). Meanwhile, the TeCD73+CD95+ subset, which started at 0.3%, increased to between 8-11%, although it remained significantly smaller than the TeCD95+ population.

RUX treatment consistently suppressed effector cell generation, with the most pronounced effect on the major TeCD95+ subset (Figure 31A-B). Overall, effector populations declined under RUX treatment, while naive cells exhibited consistent growth during this period. Most memory cell subsets reflected a similar trend, showing increases at various stages despite RUX treatment.

Interestingly, the smaller TeCD73+CD95+ subset deviated from the general effector cell pattern. Although it declined in the initial phases, it expanded substantially after one month and, like naive cells, increased in response to RUX treatment (Figure 31B).

4.2.15. Changes in the memory subsets across the maturation phases

As PBLs progress through their maturation phases, the naive subset diminishes, while effector populations expand significantly. Over the four maturation phases, the total percentage of the ten memory subsets collectively decreases from 65.2% to 56.4%, then to 31.7%, and finally to 13.9% (Figure 21 and Figure 31A). Initially, in PBLs, the six most prominent memory pools comprised of 62.4% of the total: TemraCD127- (17.7%), TemCD95+ (12.8%), TymCD127- (10%), TcmCD95+ (9.5%), TcmCD95+CD127+ (8.2%), and the smaller Tscm subset (4.3%). The remaining four memory subsets each accounted for less than 3%: TcmPD1+ (1.4%), TymCD127+ (0.8%), TemraCD127+ (0.4%), and TcmCD73+CD95+ (0.1%; *Figure* 24 and Figure 31 C and D).

Among the larger memory populations, the TcmCD95+ subset exhibited the most significant early increase during the "expansion" phase, rising from 9.5% to 36.5%. In contrast, the TymCD127- subset showed only a modest increase, going from 10% to 12.7% across the 72-hour acute signal phase (*Figure* 24A and Figure 31C and D). Notably, all other memory subsets decreased during this phase. However, the early increases in TcmCD95+ and TymCD127- were

transient, as both subsets experienced a decline over one month. While TcmCD95+ remained a significant subset throughout the maturation process, TymCD127- eventually nearly disappeared.

During the third phase, known as the "contraction" phase, the ten memory subsets collectively decreased to 31.7%, down from 65.1% and 56.4% (*Figure* 24 B, Figure 31C and D). The four major memory subpopulations that persisted were TemraCD127- (which declined from 17.7% to 9.4%), TemCD95+ (dropping from 12.8% to 5.0%), TcmCD95+CD127+ (falling from 8.2% to 4.3%), and TcmCD95+ (decreasing from 9.5% to 6.2%). Together, these four subsets accounted for 24.9% of the total cells. While they comprised 78.5% of the overall memory subsets, all four experienced reductions during the retraction phase.

In contrast, three smaller memory subsets saw increases: TymCD127+ (rising from 0.08% to 1.8%), TcmCD73+CD95+ (increasing from 0.01% to 1.6%), and TemraCD127+ (growing from 0.4% to 1.2%). Of these, Tym expressed high levels of Pgp, while Tcm and Temra expressed low levels of Pgp, similar to naive cells. Meanwhile, the remaining three memory subsets, all characterized by high Pgp levels, decreased: TymCD127- (from 10% to 1.2%), Tscm (from 4.3% to 0.08%), and TcmPD1+ (from 1.4% to 0.02%).

In the final, fourth maturation phase, where cells are reactivated by CD3/CD28 beads, the highest Pgp-expressing memory subset, TcmPD1+, increased from 0.02% to 1.5%, alongside the other Pgp-high TymCD127- subset, which also rose to 1.5% from 1.2% (though this change was not statistically significant; *Figure* 24 D, Figure 31A, C and D). Meanwhile, the two most considerable memory subsets, TemraCD127- and TcmCD95+, declined to 4.8% and 4.1%, respectively. Together, these four subsets accounted for 86.3% of the total memory cells: out of these, TemraCD127- and TcmCD95+ made up 64.1%, while TcmPD1+ and TymCD127- comprised 22.2%. The remaining five memory subsets stabilized between 1.7% and 3.4%, except for TemraCD127+, which nearly disappeared, representing just 0.06% of the total memory population.

Figure 31C and D illustrate that during successive maturation stages, both TcmCD95+ and TymCD127- populations increase following acute TCR activation, though this expansion is dampened by the kinase inhibitor RUX. This behavior is characteristic of a transit-amplifying expansion curve during acute TCR activation. Similar to tissue stem cells, which renew

terminally differentiated tissue cells through asymmetric division, CD8+ T cells exhibit a comparable behavior. In this context, TcmCD95+ and TymCD127- likely represent rapidly dividing transit amplifying cells, potentially derived from activated naive T cells (or possibly from Tscm cells, though this was not evident in our results).

Another growth pattern in *Figure* 24 shows a decrease in certain cell populations following acute TCR activation, with RUX mitigating this decline. These memory subsets include the nearly disappeared TemraCD127+ subset, the small TymCD127+ subset, the medium-sized TcmCD95+CD127+ subset, and the large TemCD95+ memory subset. All these subsets express high levels of CD127, suggesting their potential transformation into other subsets, such as effectors, in response to TCR signaling. Notably, the literature suggests CD127 downregulates TCR signaling (Hammersen et al., 2023), which may partially explain the observed growth patterns. These cells exhibit a similar pattern to naive T cells, which also express CD127.

A different trend shown in Figure 31 is the increase in specific subsets after one month of culture, including TcmCD73+CD95+, TymCD127+, TemraCD127+, and TcmCD95+CD127+. Interestingly, except for TcmCD73+CD95+, which remained stable under acute TCR signaling, the other subsets exhibited a decrease following acute TCR activation. The final pattern in Figure 31 pertains to the TcmPD1+ memory cells, a small but relatively stable subset that significantly expands following repeated long-term TCR signals. These varied patterns suggest that while smaller memory subsets tend to increase, larger ones often decrease following repeated TCR signals.

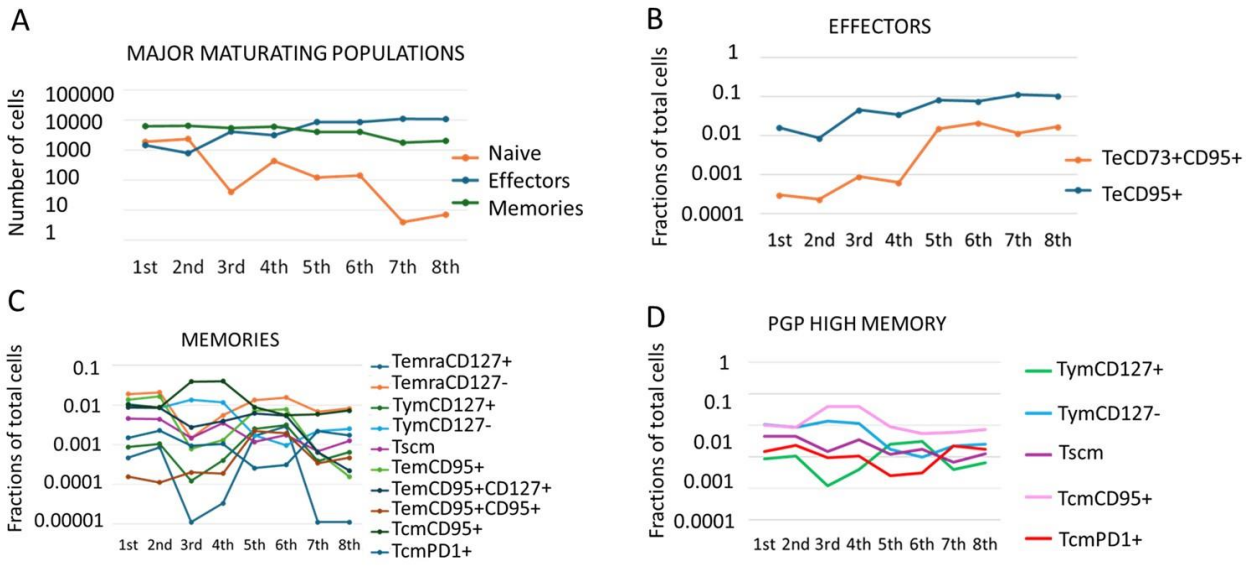

Figure 31: Illustrates the changes in CD8+ T cell subsets during in vitro differentiation and RUX treatment. The X-axis represents eight maturation phases of CD8+ T cells: unprimed unactivated (1st), unprimed unactivated treated with RUX (2nd), unprimed TCR-activated (3rd), unprimed TCR-activated treated with RUX (4th), JY-primed unactivated (5th), JY-primed unactivated treated with RUX (6th), JY-primed TCR-activated (7^{th}) and Y-primed TCR-activated treated with RUX(8th). The Y-axis, plotted on a log scale to capture changes in small memory subsets, displays either cell numbers (Panel A) or the fractional sizes of subsets within the total analyzed cells (Panels B, C, and D). Panel A shows the cell counts of primary CD8+ subsets across different differentiation stages. Panel B illustrates the proportions of two identified effector subtypes. Panel C depicts the proportions of ten memory subtypes across the maturation phases, while Panel D highlights the five memory subtypes with the highest Pgp expression from those identified in Panel C. Across repeated TCR activations, subset compositions undergo dynamic transformations, ultimately stabilizing in their numbers.

5. DISCUSSION

PART 1

Our research provides a new mechanistic understanding of how RUX affects Pgp expression and activity, T cell activation marker expression, and differentiation to affect cytotoxic T lymphocyte function. We show that RUX inhibits PD-1 upregulation and CD8 surface expression following TCR stimulation in addition to influencing Pgp transporter function at the transcriptional and protein activity levels. These results highlight the compound's complex effects on immune surveillance, memory T cell development, and therapeutic modulation.

We postulated that Pgp, whose expression is dynamically controlled during differentiation, contributes to the persistence of stem-like memory T cells. In comparison to unprimed cells, we observed a slight but significant decrease in Pgp protein levels in JY-primed cytotoxic T lymphocytes. The notion that Pgp is downregulated as T cells develop is supported by the observation that naive CD8+ T cells had ABCB1 mRNA levels that were around 20 times greater than those of long-term activated effector populations.

We looked more closely at the relationship between RUX and Pgp in light of earlier research that connected ABCB1 expression to RUX effectiveness both *in vitro* and *in vivo* (Caroline et al., 2016). the calcein-AM efflux test (Holló et al., 1994; Homolya et al., 1993). We measured the inhibitory levels of RUX in primary CD8+T-lymphocytes and NIH-3T3 MDR1-overexpressing cells. With an IC_{50} of roughly 13 µM in NIH-3T3 MDR1 cells and roughly 58 µM in CD8+ T cells, RUX suppressed Pgp function (Biwott et al., 2025a). These amounts are higher than normal therapeutic plasma concentrations. According to clinical reports, when Pgp expression is elevated, RUX efficacy is decreased (Caroline et al., 2016). This implies that local drug buildup may still result in Pgp inhibition. IC_{50} values obtained from fluorescent marker retention show that RUX and Pgp interact, even though they do not directly represent biological activity.

RUX significantly increased Pgp ATPase activity in a dose-dependent manner, with the highest stimulation seen at 100 µM, according to ATPase assays that also validated this interaction (Krasznai et al., 2014; Lowry et al., 1951; Sarkadi et al., 1992; Tarapcsák et al., 2017; Trencsényi et al., 2015). Additionally, RUX changed the activation of ATPase induced by verapamil,

indicating a modulatory or competitive role. Because of its smaller molecular weight and functional properties, RUX is a modulator in Seelig's classification of Pgp-interacting drugs (Seelig, 2020).

It functions as a substrate, increases ATPase activity, and probably competes with other Pgp substrates. Furthermore, it stimulates the expression of ABCB1 mRNA. In contrast to traditional inhibitors like cyclosporin A or ZQ, RUX increased rather than decreased basal ATPase activity, suggesting a complex regulatory relationship that may have consequences for drug-drug interactions and RUX bioavailability in T cell subsets that express Pgp.

In addition to regulating Pgp, RUX affected important indicators of T cell activation. RUX administration dramatically reduced the substantial upregulation of PD-1 expression that occurred during acute stimulation with CD3/CD28 beads. Similarly, RUX partially or completely suppressed the activation-induced elevation of CD8 and surface Pgp levels (Biwott et al., 2025a). These results are in line with other research showing that RUX interferes with PD-1 signaling pathways and persistent TCR stimulation increases PD-1 expression (Chu & Zehn, 2020; Zak et al., 2024).

ABCB1 mRNA expression changed more dramatically than Pgp protein levels, which changed very slightly after activation but increased by about 50% after 72 hours of CD3/CD28 stimulation and somewhat decreased after 30 days of JY priming. After short-term activation, we saw a ~20-fold decline, and after continuous stimulation, a ~50% reduction. The cellular heterogeneity of T cell populations is probably reflected in these variations between transcript and protein levels. The interpretation of bulk-level data is complicated by the different Pgp expression profiles displayed by the naive, effector, and memory subsets (Biwott et al., 2025b). All things considered, these findings imply that RUX inhibits activation-associated signaling, delaying T cell maturation and possibly maintaining a less differentiated or more naive phenotype.

There is substantial therapeutic value in RUX's ability to control Pgp expression and function, inhibit T cell activation signals, and affect exhaustion processes by lowering PD-1 levels. RUX may be helpful in autoimmune diseases, transplant tolerance induction, or immunological memory reprogramming during cancer immunotherapy because of these properties.

However, RUX's interaction with Pgp also raises questions about pharmacokinetics and drug interactions, especially because it may compete with other substrates and change the local concentrations of drugs in tissues.

One significant drawback of this work is its reliance on *in vitro* systems, which might not adequately represent the complexity of immune responses *in vivo*. Future research should evaluate long-term effects on T cell memory development and function and validate these findings using clinical specimens or animal models. Additionally, improving therapeutic approaches will require an understanding of the distinct effects of Pgp regulation on naive, effector, and memory subsets.

PART 2

Pgp, a human cell-surface ABC transporter, is best known for its role in conferring multidrug resistance (MDR) in cancer cells, posing significant challenges to chemotherapy (Gottesman et al., 2002). However, Pgp is also expressed in immune cells and plays a critical role in immune function (Bossennec et al., 2018). Notably, a recent mouse study highlighted Pgp's importance in the development of immune memory (Chen et al., 2020). Building on this knowledge, the present study investigates the expression of Pgp in human CD8+ memory T-cell subtypes at the single-cell protein level, aiming to deepen our understanding of its role in immune cell memory.

Human cytotoxic T lymphocytes are primarily categorized into naive, effector, and memory cells based on their primary function and characteristics (Lugli et al., 2020). During the expansion phase of the immune response, short-lived and quickly activated antigen-specific effector clones proliferate and eliminate antigen-carrying cells. In the contraction phase, these short-lived effector cells die, while memory cells of the same specificity persist, enabling future antigen recognition (Lugli et al., 2020). These long-lived memory cells exist in higher numbers and can quickly differentiate into effectors compared to their naive counterparts (Jameson & Masopust, 2018; Restifo & Gattinoni, 2013).

To explore the dynamics of memory T-cell differentiation, we established an *in vitro* model system to differentiate memory cells from peripheral blood and reconstitute the human adaptive CD8+ T-cell immune response. Using a long-term, IL-2-supplemented mixed lymphocyte culture, we co-cultured growth-arrested antigen-presenting cells (APCs) with peripheral lymphocytes. The APCs

were derived from the B-lymphoblastoid cell line JY, which expresses high levels of HLA-I A2 and co-receptors, thereby triggering robust allogeneic cellular immune responses. Flow cytometry analysis indicated that this JY-cell-based culture upregulated CD8+, NK, and NK-T cells while downregulating B and CD4+ T cells. This MHC-I-restricted immune reaction notably increased Pgp expression on CD8+, CD4+, and B cells but decreased it on NK and NK-T cells, consistent with prior research (Bossennec et al., 2018; Pendse et al., 2003; Zhang et al., 2014).

We observed the expected fractions of CD8+ T-cell subsets in peripheral blood: 40% naive, 20–25% effector, and Temra, with Tcm comprising the remainder (Reading et al., 2018). Our *in vitro* CTL maturation system generated four primary differentiation stages: unprimed and unactivated, unprimed and TCR-activated (CD3/CD28-bead triggered), JY-primed (JY-cell-activated) and unactivated, and JY-primed and TCR-activated. Additionally, we monitored the effects of RUX on each of these four stages. Stages 1 and 2 represent the acute phase of the adaptive immune response, while stage 3 models the memory phase, and stage 4 represents memory reactivation.

To classify CD8+ T-cell subsets, we used conventional surface markers: CD45RA+CD62L+ (naive), CD45RA-CD62L+ (central memory, Tcm), CD45RA-CD62L- (effector), and CD45RA+CD62L- (Temra). However, memory cells remain heterogeneous, requiring additional markers for finer distinction. We incorporated CD73, CD95, CD127, and CD279 to identify 13 human CTL subsets, including effector cells (TeCD95+ and TeCD73+CD95+) and memory populations (TymCD127+, TymCD127-, Tscm, TcmCD95+, TcmCD73+CD95+, TcmCD95+CD127+, TcmPD1+, TemCD95+, TemraCD127+, and TemraCD127-) (Biwott et al., 2025b).

During the acute phase, the central memory subset TcmCD95 + exhibited the highest generation rate, followed by a smaller proportion of the young TymCD127- subset, which likely precedes it. In the memory phase, the young TymCD127 + subset contributed the most (Biwott et al., 2025b). Meanwhile, the TcmPD1 + central memory subset, characterized by a late-stage marker, significantly expanded in the later stages of the memory-recall phase following TCR reactivation. The Tscm population maintained a stable 2–4% subpopulation throughout the maturation process within the dynamically evolving memory pool.

CD73 was used as a marker to identify young memory cells, which are known for their expression of Pgp, as previously described (Murata et al., 2016). Tym cells were initially characterized by high ALDH1 expression, a well-established marker of stemness (Gomez-Salazar et al., 2023). Further classification of these cells was based on their elevated levels of CD73, ALDH1, and Pgp, all of which are associated with stem cell-like properties. CD73, an ectonucleotidase, generates immunosuppressive adenosine from ATP released by damaged cells and functions as a co-signaling molecule in tissue-resident cells (Fang et al., 2021; Schneider et al., 2021). Additionally, it modulates T-cell activation. Tym populations exhibit high proliferative capacity, self-renewal ability, ALDH1 activity, and drug resistance (Murata et al., 2016). Notably, TCR activation leads to a reduction in CD127 expression in chemo-resistant CTL subsets, distinguishing activated TymCD127- cells from their non-activated TymCD127+ counterparts (Kudernatsch et al., 2014).

To identify the Tscm subset, the CD95 marker was employed. While primarily known for its role in inducing apoptosis in T cells, CD95 can also promote cell survival (Risso et al., 2022). Initially identified in graft-versus-host disease (Zhang et al., 2005) Tscm cells are commonly distinguished by markers such as CD45RA, CD62L, CD127, and CD95. These cells exhibit self-renewal, multipotency, and proliferative capacity (Alsuliman et al., 2017; Gattinoni et al., 2011; Xu et al., 2015). The Tscm and Tym populations are closely linked, with Tym representing an earlier stage of memory development (Murata et al., 2016). Both subsets express CD95, Pgp, and other shared markers, making it possible for slight contamination between these populations to bias the classification of memory subsets as long-lived memory subclasses. Previous studies have demonstrated that Tym and Tscm cells can differentiate into central and effector memory cells, contributing to the diversity of the memory population (Gattinoni et al., 2011; Murata et al., 2016).

CD127 was used as a marker for IL-7 receptor-expressing cells, which play a crucial role in transmitting survival signals and maintaining homeostatic proliferation in naive and memory effector T cells (Huster et al., 2004; Kudernatsch et al., 2014). CD127 also serves as a memory and effector T cell marker, with its downregulation observed during activation or IL-15 exposure (Kudernatsch et al., 2014; Parween et al., 2023). Identifying CTL subsets through this marker provides insights into distinct maturing CTL subtypes, which could be utilized for immunotherapeutic applications.

PD-1 (CD279) was employed to identify late-stage mature T cells. This marker is overexpressed in exhausted CTLs during chronic infections and cancer (Lugli et al., 2020). PD-1 inhibits TCR signaling to prevent autoimmunity during prolonged activation and repeated TCR stimulation, marking the late maturation stage of Tex (Terrabuio et al., 2023). Although Tex cells are often considered unresponsive, checkpoint blockade therapies and the discovery of stem-like Tex cells (Tex-stem) highlight their potential functionality. Tex-stem cells, which are self-renewing and proliferative, sustain long-term responses within the terminal Tex subset (Gounari & Khazaie, 2022).

The TcmPD1 + population we identified likely belongs to these exhausted stem cells. Similar cells in other studies have been categorized as exhausted precursors (Tex-pre) due to their persistent CD62L expression (Terrabuio et al., 2023). In our experiments, TcmPD1 + cells exhibited comparable characteristics, including the highest Pgp expression levels. This phenomenon is likely attributable to their preserved or acquired stemness, which enables them to undergo asymmetric division.

Exhausted T cell precursors share surface markers and transcriptional profiles with long-lived memory cells. Tym, Tscm, and Tcm subsets, which exhibit long-lived characteristics, express markers such as CD27, CD28, and CXCR3 as Tex precursors (Lugli et al., 2020; Murata et al., 2016).

The role of Pgp, a multidrug-resistant protein, in CTL subsets remains an area of active research. This study indicates that Pgp expression is most pronounced in the TcmPD1 +, Tscm, TymCD127, and TymCD127 + subsets. The presence of Pgp in these subsets suggests its critical role in chemo-immune efflux capacity, oxidative stress protection, and quiescence maintenance while retaining proliferative potential. Collectively, these properties may contribute to the stem-like nature of memory cells (Bossennec et al., 2018; Chen et al., 2020; Kudernatsch et al., 2014).

TCR, co-stimulatory, and interleukin receptor signals, via the JAK/STAT signaling pathways, influence CTL maturation. To assess the impact of JAK1/JAK2 signaling on memory differentiation, we used the kinase inhibitor RUX. JAK/STAT signaling modulation influences differentiation toward effector or memory cells. Diseases such as MF and GVHD, characterized

by hyperactive JAK/STAT signaling and premature exhaustion of adaptive immune responses, may benefit from RUX treatment, which alleviates the JAK1/JAK2 signaling burden, leading to decreased effector activation (Chen et al., 2020; Teshima & Hashimoto, 2023). Our findings suggest that inhibiting JAK1/JAK2 reduces effector cell production while promoting memory cell differentiation. IL-12, which signals via JAK1/JAK2, enhances effector cell production, whereas IL-7 and IL-15, signaling through JAK1/JAK3, sustain memory cell maintenance and proliferation (Curtsinger et al., 2003; Curtsinger et al., 1999; Kang et al., 2023). Therefore, JAK1/JAK2 inhibition shifts differentiation toward memory cells, as supported by our data. Notably, IL-7 and IL-12 co-administration in tumor-targeted therapies enhances anti-tumor efficacy while minimizing interleukin-associated side effects (Kang et al., 2023). Future studies should explore JAK2-specific inhibitors such as fedratinib and pacritinib in CTL maturation models.

In Figure 30, RUX delayed T-cell differentiation by increasing the number of naive cells while reducing effector cells. Memory subsets responded differently: smaller subsets expanded upon activation, mimicking naive cells, while larger subsets contracted following repeated TCR stimulation, resembling effector cells. These findings suggest that a small, quiescent core memory population matures heterogeneously in response to repeated TCR signals, sustaining long-term stability through asymmetric division and cytokine modulation.

In the context of COVID-19, RUX has been shown to improve outcomes in patients with high inflammation scores, indicating that it inhibits effector CTL maturation (Hammersen et al., 2023). Our data aligns with these observations, showing that while effector differentiation decreases, the functional memory subset expands during TCR activation, potentially enhancing CTL persistence in later inflammatory responses.

Our findings emphasize that memory T cell subsets are continuously generated and dynamically maintained over time. The small Pgp-expressing memory populations, including TymCD127+ and TcmPD1+ subsets, form a core group of self-renewing, slowly dividing quiescent memory cells (Boddupalli et al., 2016). These populations reside in low-redox environments, such as the bone marrow, ensuring long-term immune memory (Alsuliman et al., 2017; Boddupalli et al., 2016; Thurm et al., 2021). Moreover, PD-1, despite its association with exhaustion, does not entirely

restrict cell division, allowing memory T cells to surpass the Hayflick limit and support durable adaptive immunity, potentially improving cancer vaccine strategies (Soerens et al., 2023).

In conclusion, our study provides insights into CD8+ T cell maturation patterns following TCR activation. Long-lived naive T cells differentiate into effector and central memory cells, with an increase in short-lived TeCD95+ subsets and long-lived, high-Pgp-expressing TcmCD95+ cells. Over a month-long maturation period, advanced memory subsets, such as Temra, emerge. These findings have significant implications for optimizing immune responses in chemotherapy, vaccination, and immunotherapy.

6. SUMMARY

In this study, investigations were performed to assess the interaction between RUX, an FDA-approved JAK1/2 inhibitor, and Pgp, a key ATP-binding cassette transporter involved in multidrug resistance and immune regulation. Pgp, also known as ABCB1 or MDR-1, plays a crucial role in exporting xenobiotic compounds from cells, including chemotherapeutic agents, and is implicated in immune cell function. It is expressed by various immune cells, including T lymphocytes, whose elevated expression has been associated with poor treatment responses in autoimmune diseases. However, Pgp expression also confers resilience to chemotherapy, particularly in memory T cells, which can mount effective immune responses against infections post-treatment.

To explore this interaction, I first examined the effects of RUX on Pgp activity. This study used human primary T cells and 3T3 NIH-MDR1 cells to assess how RUX impacts Pgp function. The results indicated that RUX inhibited Pgp in a dose-dependent manner, although the concentrations used were not pharmacologically relevant. Additionally, RUX led to the downregulation of both Pgp and PD-1 expression in activated T cells, and it activated the ATPase activity of Pgp while interfering with verapamil-induced ATPase activity.

Next, this study analyzed the expression of ABCB1 in T cells. Through molecular analysis, it was found that ABCB1 mRNA expression was elevated in unprimed T cells, while TCR-activated and JY-primed cytotoxic T lymphocytes showed reduced levels of ABCB1 expression. Treatment with RUX increased ABCB1 expression in these activated T cells, suggesting that RUX functions as a regulator of Pgp expression. These findings have potential implications for improving chemotherapy efficacy and managing conditions like graft-versus-host disease.

An investigation into the impact of RUX on T-cell maturation and memory subsets was conducted. My study explored how RUX influences T-cell maturation, particularly the differentiation of CD8+ T-cell subsets. I found that RUX promoted a shift towards CD8+ T-cell phenotypes, enhancing the proportions of T cells and central memory T cells while reducing effector memory T cells and effector T cells. This shift in T-cell subsets is essential for its therapeutic efficacy in managing myelofibrosis and other immune-related diseases.

In vitro models were employed to track T-cell maturation and Pgp expression to explore these dynamics further. I utilized an *in vitro* model for CTL differentiation, which involved priming T cells from peripheral blood mononuclear cells with JY antigen-presenting cells. Over a one-month culture period, I tracked changes in T-cell maturation, comparing the baseline PBMC subsets with those at later stages of differentiation. I also monitored Pgp expression across the developing T-cell subsets and found that long-lived memory T cells expressing Pgp were maintained throughout maturation.

Finally, I explored the role of Pgp in sustaining long-term memory cells. My study showed that exposure to RUX delayed the differentiation of effector T cells and promoted the expansion of CD127-expressing memory T cells. The results suggest that elevated Pgp expression is crucial for the long-term survival and maintenance of memory cells in human CTLs.

In conclusion, this study provides valuable insights into the role of RUX in modulating T-cell maturation and Pgp expression, which could have significant implications for the treatment of immune-related diseases and hematologic malignancies. By understanding how RUX regulates Pgp activity and memory T-cell subsets, I have contributed to the broader understanding of immune modulation, which may enhance the therapeutic potential of RUX in chemotherapy, transplantation, and autoimmune disease management. The findings underscore the complex role of Pgp in memory T-cell biology and suggest that targeting Pgp could improve the efficacy of immunotherapies and cancer treatments.

7. REFERENCES

Abroun, S., Saki, N., Ahmadvand, M., Asghari, F., Salari, F., & Rahim, F. (2015). STATs: An Old Story, Yet Mesmerizing. *Cell Journal (Yakhteh)*, *17*(3), 395-411. https://doi.org/10.22074/cellj.2015.1

Ahmed Juvale, I. I., Abdul Hamid, A. A., Abd Halim, K. B., & Che Has, A. T. (2022). P-glycoprotein: new insights into structure, physiological function, regulation and alterations in disease. *Heliyon*, *8*(6), e09777. https://doi.org/https://doi.org/10.1016/j.heliyon.2022.e09777

Ahmed, R., & Gray, D. (1996). Immunological Memory and Protective Immunity: Understanding Their Relation. *Science*, *272*(5258), 54-60. https://doi.org/doi:10.1126/science.272.5258.54

Alsuliman, A., Muftuoglu, M., Khoder, A., Ahn, Y.-O., Basar, R., Verneris, M. R., Muranski, P., Barrett, A. J., Liu, E., Li, L., Stringaris, K., Armstrong-James, D., Shaim, H., Kondo, K., Imahashi, N., Andersson, B., Marin, D., Champlin, R. E., Shpall, E. J., & Rezvani, K. (2017). A subset of virus-specific CD161+ T cells selectively express the multidrug transporter MDR1 and are resistant to chemotherapy in AML. *Blood*, *129*(6), 740-758. https://doi.org/10.1182/blood-2016-05-713347

Ambudkar, S. V., Kim, I.-W., Xia, D., & Sauna, Z. E. (2006). The A-loop, a novel conserved aromatic acid subdomain upstream of the Walker A motif in ABC transporters, is critical for ATP binding. *FEBS Letters*, *580*(4), 1049-1055. https://doi.org/https://doi.org/10.1016/j.febslet.2005.12.051

Appeldoorn, T. Y. J., Munnink, T. H. O., Morsink, L. M., Hooge, M. N. L.-d., & Touw, D. J. (2023). Pharmacokinetics and Pharmacodynamics of Ruxolitinib: A Review. *Clinical Pharmacokinetics*, *62*(4), 559-571. https://doi.org/10.1007/s40262-023-01225-7

Arsenio, J., Metz, P. J., & Chang, J. T. (2015). Asymmetric Cell Division in T Lymphocyte Fate Diversification. *Trends in Immunology*, *36*(11), 670-683. https://doi.org/https://doi.org/10.1016/j.it.2015.09.004

Bacsó, Z., Bene, L., Bodnár, A., Matkó, J., & Damjanovich, S. (1996). A photobleaching energy transfer analysis of CD8MHC-I and LFA-1ICAM-1 interactions in CTL-target cell conjugates. *Immunology Letters*, *54*(2), 151-156. https://doi.org/https://doi.org/10.1016/S0165-2478(96)02665-X

Bader, M. S., & Meyer, S. C. (2022). JAK2 in Myeloproliferative Neoplasms: Still a Protagonist. *Pharmaceuticals*, *15*(2), 160. https://www.mdpi.com/1424-8247/15/2/160

Banerjee, A., Gordon, S. M., Intlekofer, A. M., Paley, M. A., Mooney, E. C., Lindsten, T., Wherry, E. J., & Reiner, S. L. (2010). Cutting Edge: The Transcription Factor Eomesodermin Enables CD8+ T Cells To Compete for the Memory Cell Niche. *The Journal of Immunology*, *185*(9), 4988-4992. https://doi.org/10.4049/jimmunol.1002042

Bársony, O., Szalóki, G., Türk, D., Tarapcsák, S., Gutay-Tóth, Z., Bacsó, Z., Holb, I. J., Székvölgyi, L., Szabó, G., Csanády, L., Szakács, G., & Goda, K. (2016). A single active catalytic site is sufficient to promote transport in P-glycoprotein. *Scientific Reports*, *6*(1), 24810. https://doi.org/10.1038/srep24810

Bello-Reuss, E., Ernest, S., Holland, O. B., & Hellmich, M. R. (2000). Role of multidrug resistance P-glycoprotein in the secretion of aldosterone by human adrenal NCI-H295 cells. *American Journal of Physiology-Cell Physiology*, *278*(6), C1256-C1265. https://doi.org/10.1152/ajpcell.2000.278.6.C1256

Biwott, K., Lkhamkhuu, A., Ghaffar, N., Papp, A. B., Tarban, N., Goda, K., & Bacso, Z. (2025a). Ruxolitinib Modulates P-Glycoprotein Function, Delays T Cell Activation, and Impairs CCL19 Chemokine-Directed Migration in Human Cytotoxic T Lymphocytes. *International Journal of Molecular Sciences*, *26*(13). https://doi.org/10.3390/ijms26136123

Biwott, K., Singh, P., Baráth, S., Nyariki, J. N., Hevessy, Z., & Bacso, Z. (2025b). Dynamic P-glycoprotein expression in early and late memory states of human CD8 + T cells and the protective role of ruxolitinib. *Biomedicine & Pharmacotherapy*, *182*, 117780. https://doi.org/https://doi.org/10.1016/j.biopha.2024.117780

Blackburn, S. D., Shin, H., Haining, W. N., Zou, T., Workman, C. J., Polley, A., Betts, M. R., Freeman, G. J., Vignali, D. A. A., & Wherry, E. J. (2009). Coregulation of CD8+ T cell exhaustion by multiple inhibitory receptors during chronic viral infection. *Nature Immunology*, *10*(1), 29-37. https://doi.org/10.1038/ni.1679

Boddupalli, C. S., Nair, S., Gray, S. M., Nowyhed, H. N., Verma, R., Gibson, J. A., Abraham, C., Narayan, D., Vasquez, J., Hedrick, C. C., Flavell, R. A., Dhodapkar, K. M., Kaech, S. M., & Dhodapkar, M. V. (2016). ABC transporters and NR4A1 identify a quiescent subset of tissue-resident memory T cells. *The Journal of Clinical Investigation*, *126*(10), 3905-3916. https://doi.org/10.1172/JCI85329

Borsa, M., Barandun, N., Gräbnitz, F., Barnstorf, I., Baumann, N. S., Pallmer, K., Baumann, S., Stark, D., Balaz, M., Oetiker, N., Wagen, F., Wolfrum, C., Simon, A. K., Joller, N., Barral, Y., Spörri, R., & Oxenius, A. (2021). Asymmetric cell division shapes naive and virtual memory T-cell immunity during ageing. *Nature Communications*, *12*(1), 2715. https://doi.org/10.1038/s41467-021-22954-y

Bossennec, M., Anthony, D. R., Christophe, C., & and Ménétrier-Caux, C. (2018). MDR1 in immunity: friend or foe? *OncoImmunology*, *7*(12), e1499388. https://doi.org/10.1080/2162402X.2018.1499388

Böhm, J. W., Sia, K. C. S., Jones, C., Evans, K., Mariana, A., Pang, I., Failes, T., Zhong, L., Mayoh, C., Landman, R., Collins, R., Erickson, S. W., Arndt, G., Raftery, M. J., Wilkins, M. R., Norris, M. D., Haber, M., Marshall, G. M., & Lock, R. B. (2021). Combination efficacy of ruxolitinib with standard-of-care drugs in CRLF2-rearranged Ph-like acute

lymphoblastic leukemia. *Leukemia*, *35*(11), 3101-3112. https://doi.org/10.1038/s41375-021-01248-8

Caroline, E., Florian, P., Denise, W., Tina, M. S., Thomas, F., & Florian, H. H. (2016). Expression and function of ABC-transporter protein ABCB1 correlates with inhibitory capacity of Ruxolitinib in vitro and in vivo. *Haematologica*, *101*(3), e81-e85. https://doi.org/10.3324/haematol.2015.136754

Chaudhary, P. M., Mechetner, E. B., & Roninson, I. B. (1992). Expression and activity of the multidrug resistance P-glycoprotein in human peripheral blood lymphocytes. *Blood*, *80*(11), 2735-2739.

Chen, M. L., Sun, A., Cao, W., Eliason, A., Mendez, K. M., Getzler, A. J., Tsuda, S., Diao, H., Mukori, C., Bruno, N. E., Kim, S. Y., Pipkin, M. E., Koralov, S. B., & Sundrud, M. S. (2020). Physiological expression and function of the MDR1 transporter in cytotoxic T lymphocytes. *Journal of Experimental Medicine*, *217*(5). https://doi.org/10.1084/jem.20191388

Chen, Y., Zander, R., Khatun, A., Schauder, D. M., & Cui, W. (2018). Transcriptional and Epigenetic Regulation of Effector and Memory CD8 T Cell Differentiation [Review]. *Frontiers in Immunology*, *Volume 9 - 2018*. https://doi.org/10.3389/fimmu.2018.02826

Chu, T., & Zehn, D. (2020). Charting the Roadmap of T Cell Exhaustion. *Immunity*, *52*(5), 724-726. https://doi.org/https://doi.org/10.1016/j.immuni.2020.04.019

Cieri, N., Oliveira, G., Greco, R., Forcato, M., Taccioli, C., Cianciotti, B., Valtolina, V., Noviello, M., Vago, L., Bondanza, A., Lunghi, F., Marktel, S., Bellio, L., Bordignon, C., Bicciato, S., Peccatori, J., Ciceri, F., & Bonini, C. (2015). Generation of human memory stem T cells after haploidentical T-replete hematopoietic stem cell transplantation. *Blood*, *125*(18), 2865-2874. https://doi.org/10.1182/blood-2014-11-608539

Cory, T. J., He, H., Winchester, L. C., Kumar, S., & Fletcher, C. V. (2016). Alterations in P-Glycoprotein Expression and Function Between Macrophage Subsets. *Pharmaceutical Research*, *33*(11), 2713-2721. https://doi.org/10.1007/s11095-016-1998-x

Curtsinger , J. M., Lins , D. C., & Mescher , M. F. (2003). Signal 3 Determines Tolerance versus Full Activation of Naive CD8 T Cells : Dissociating Proliferation and Development of Effector Function. *Journal of Experimental Medicine*, *197*(9), 1141-1151. https://doi.org/10.1084/jem.20021910

Curtsinger, J. M., Schmidt, C. S., Mondino, A., Lins, D. C., Kedl, R. M., Jenkins, M. K., & Mescher, M. F. (1999). Inflammatory Cytokines Provide a Third Signal for Activation of Naive CD4+ and CD8+ T Cells1. *The Journal of Immunology*, *162*(6), 3256-3262. https://doi.org/10.4049/jimmunol.162.6.3256

Curtsinger, J. M., Valenzuela, J. O., Agarwal, P., Lins, D., & Mescher, M. F. (2005). Cutting Edge: Type I IFNs Provide a Third Signal to CD8 T Cells to Stimulate Clonal Expansion

and Differentiation1. *The Journal of Immunology*, *174*(8), 4465-4469. https://doi.org/10.4049/jimmunol.174.8.4465

Dean, M., Hamon, Y., & Chimini, G. (2001). The human ATP-binding cassette (ABC) transporter superfamily. *J Lipid Res*, *42*(7), 1007-1017.

Dean, M., Moitra, K., & Allikmets, R. (2022). The human ATP-binding cassette (ABC) transporter superfamily. *Human Mutation*, *43*(9), 1162-1182. https://doi.org/https://doi.org/10.1002/humu.24418

Devine, K., Villalobos, E., Kyle, C. J., Andrew, R., Reynolds, R. M., Stimson, R. H., Nixon, M., & Walker, B. R. (2023). The ATP-binding cassette proteins ABCB1 and ABCC1 as modulators of glucocorticoid action. *Nature Reviews Endocrinology*, *19*(2), 112-124. https://doi.org/10.1038/s41574-022-00745-9

Doan Ngoc, T.-M., Tilly, G., Danger, R., Bonizec, O., Masset, C., Guérif, P., Bruneau, S., Glemain, A., Harb, J., Cadoux, M., Vivet, A., Mai, H. L., Garcia, A., Laplaud, D., Liblau, R., Giral, M., Blandin, S., Feyeux, M., Dubreuil, L.,…Degauque, N. o. b. o. t. D. C. (2022). Effector Memory–Expressing CD45RA (TEMRA) CD8+ T Cells from Kidney Transplant Recipients Exhibit Enhanced Purinergic P2X4 Receptor–Dependent Proinflammatory and Migratory Responses. *Journal of the American Society of Nephrology*, *33*(12), 2211-2231. https://doi.org/10.1681/asn.2022030286

Eadie, L. N., Hughes, T. P., & White, D. L. (2014). Interaction of the Efflux Transporters ABCB1 and ABCG2 With Imatinib, Nilotinib, and Dasatinib. *Clinical Pharmacology & Therapeutics*, *95*(3), 294-306. https://doi.org/https://doi.org/10.1038/clpt.2013.208

Elli, E. M., Baratè, C., Mendicino, F., Palandri, F., & Palumbo, G. A. (2019). Mechanisms Underlying the Anti-inflammatory and Immunosuppressive Activity of Ruxolitinib [Review]. *Frontiers in Oncology*, *Volume 9 - 2019*. https://doi.org/10.3389/fonc.2019.01186

Fan, J., To, K. K. W., Chen, Z.-S., & Fu, L. (2023). ABC transporters affects tumor immune microenvironment to regulate cancer immunotherapy and multidrug resistance. *Drug Resistance Updates*, *66*, 100905. https://doi.org/https://doi.org/10.1016/j.drup.2022.100905

Fang, F., Cao, W., Zhu, W., Lam, N., Li, L., Gaddam, S., Wang, Y., Kim, C., Lambert, S., Zhang, H., Hu, B., Farber, D. L., Weyand, C. M., & Goronzy, J. J. (2021). The cell-surface 5′-nucleotidase CD73 defines a functional T memory cell subset that declines with age. *Cell Reports*, *37*(6), 109981. https://doi.org/https://doi.org/10.1016/j.celrep.2021.109981

Ferrao, R., & Lupardus, P. J. (2017). The Janus Kinase (JAK) FERM and SH2 Domains: Bringing Specificity to JAK–Receptor Interactions [Review]. *Frontiers in Endocrinology*, *Volume 8 - 2017*. https://doi.org/10.3389/fendo.2017.00071

Flynn, J. K., & Gorry, P. R. (2014). Stem memory T cells (TSCM)—their role in cancer and HIV immunotherapies. *Clinical & Translational Immunology*, *3*(7), e20. https://doi.org/https://doi.org/10.1038/cti.2014.16

Garrido-Trigo, A., & Salas, A. (2019). Molecular Structure and Function of Janus Kinases: Implications for the Development of Inhibitors. *Journal of Crohn's and Colitis*, *14*(Supplement_2), S713-S724. https://doi.org/10.1093/ecco-jcc/jjz206

Gattinoni, L., Lugli, E., Ji, Y., Pos, Z., Paulos, C. M., Quigley, M. F., Almeida, J. R., Gostick, E., Yu, Z., Carpenito, C., Wang, E., Douek, D. C., Price, D. A., June, C. H., Marincola, F. M., Roederer, M., & Restifo, N. P. (2011). A human memory T cell subset with stem cell–like properties. *Nature Medicine*, *17*(10), 1290-1297. https://doi.org/10.1038/nm.2446

Gattinoni, L., Speiser, D. E., Lichterfeld, M., & Bonini, C. (2017). T memory stem cells in health and disease. *Nature Medicine*, *23*(1), 18-27. https://doi.org/10.1038/nm.4241

Ge, C., Xu, D., Yu, P., Fang, M., Guo, J., Xu, D., Qiao, Y., Chen, S., Zhang, Y., & Wang, H. (2021). P-gp expression inhibition mediates placental glucocorticoid barrier opening and fetal weight loss. *BMC Medicine*, *19*(1), 311. https://doi.org/10.1186/s12916-021-02173-4

Gellen, G., Klement, E., Biwott, K., Schlosser, G., Kalló, G., Csősz, É., Medzihradszky, K. F., & Bacso, Z. (2023). Cross-Linking Mass Spectrometry on P-Glycoprotein. *International Journal of Molecular Sciences*, *24*(13), 10627. https://www.mdpi.com/1422-0067/24/13/10627

Goda, K., Dönmez-Cakil, Y., Tarapcsák, S., Szalóki, G., Szöllősi, D., Parveen, Z., Türk, D., Szakács, G., Chiba, P., & Stockner, T. (2020). Human ABCB1 with an ABCB11-like degenerate nucleotide binding site maintains transport activity by avoiding nucleotide occlusion. *PLOS Genetics*, *16*(10), e1009016. https://doi.org/10.1371/journal.pgen.1009016

Gomez-Salazar, M. A., Wang, Y., Thottappillil, N., Hardy, R. W., Alexandre, M., Höller, F., Martin, N., Gonzalez-Galofre, Z. N., Stefancova, D., Medici, D., James, A. W., & Péault, B. (2023). Aldehyde Dehydrogenase, a Marker of Normal and Malignant Stem Cells, Typifies Mesenchymal Progenitors in Perivascular Niches. *Stem Cells Translational Medicine*, *12*(7), 474-484. https://doi.org/10.1093/stcltm/szad024

Gottesman, M. M., & Ambudkar, S. V. (2001). Overview: ABC Transporters and Human Disease. *Journal of Bioenergetics and Biomembranes*, *33*(6), 453-458. https://doi.org/10.1023/A:1012866803188

Gottesman, M. M., Fojo, T., & Bates, S. E. (2002). Multidrug resistance in cancer: role of ATP–dependent transporters. *Nature Reviews Cancer*, *2*(1), 48-58. https://doi.org/10.1038/nrc706

Gounari, F., & Khazaie, K. (2022). TCF-1: a maverick in T cell development and function. *Nature Immunology*, *23*(5), 671-678. https://doi.org/10.1038/s41590-022-01194-2

Hammersen, J., Birndt, S., Döhner, K., Reuken, P., Stallmach, A., Sauerbrey, P., La Rosée, F., Pfirrmann, M., Fabisch, C., Weiss, M., Träger, K., Bremer, H., Russo, S., Illerhaus, G., Drömann, D., Schneider, S., La Rosée, P., & Hochhaus, A. (2023). The JAK1/2 inhibitor ruxolitinib in patients with COVID-19 triggered hyperinflammation: the RuxCoFlam trial. *Leukemia*, *37*(9), 1879-1886. https://doi.org/10.1038/s41375-023-01979-w

Harris, T. J., & Drake, C. G. (2013). Primer on tumor immunology and cancer immunotherapy. *Journal for ImmunoTherapy of Cancer*, *1*(1), 12. https://doi.org/10.1186/2051-1426-1-12

Heemskerk, S., van Koppen, A., van den Broek, L., Poelen, G. J. M., Wouterse, A. C., Dijkman, H. B. P. M., Russel, F. G. M., & Masereeuw, R. (2007). Nitric oxide differentially regulates renal ATP-binding cassette transporters during endotoxemia. *Pflügers Archiv - European Journal of Physiology*, *454*(2), 321-334. https://doi.org/10.1007/s00424-007-0210-x

Higgins, C. F. (1992). ABC Transporters: From Microorganisms to Man. *Annual Review of Cell and Developmental Biology*, *8*(Volume 8, 1992), 67-113. https://doi.org/https://doi.org/10.1146/annurev.cb.08.110192.000435

Holló, Z., Homolya, L., Davis, C. W., & Sarkadi, B. (1994). Calcein accumulation as a fluorometric functional assay of the multidrug transporter. *Biochimica et Biophysica Acta (BBA) - Biomembranes*, *1191*(2), 384-388. https://doi.org/https://doi.org/10.1016/0005-2736(94)90190-2

Homolya, L., Holló, Z., Germann, U. A., Pastan, I., Gottesman, M. M., & Sarkadi, B. (1993). Fluorescent cellular indicators are extruded by the multidrug resistance protein. *Journal of Biological Chemistry*, *268*(29), 21493-21496. https://doi.org/https://doi.org/10.1016/S0021-9258(20)80566-3

Hu, Y., Zhang, Y., Shi, F., Yang, R., Yan, J., Han, T., & Guan, L. (2024). Reversal of T-cell exhaustion: Mechanisms and synergistic approaches. *International Immunopharmacology*, *138*, 112571. https://doi.org/https://doi.org/10.1016/j.intimp.2024.112571

Hudson, W. H., Gensheimer, J., Hashimoto, M., Wieland, A., Valanparambil, R. M., Li, P., Lin, J.-X., Konieczny, B. T., Im, S. J., Freeman, G. J., Leonard, W. J., Kissick, H. T., & Ahmed, R. (2019). Proliferating Transitory T Cells with an Effector-like Transcriptional Signature Emerge from PD-1+ Stem-like CD8+ T Cells during Chronic Infection. *Immunity*, *51*(6), 1043-1058.e1044. https://doi.org/https://doi.org/10.1016/j.immuni.2019.11.002

Hui, E., Cheung, J., Zhu, J., Su, X., Taylor, M. J., Wallweber, H. A., Sasmal, D. K., Huang, J., Kim, J. M., Mellman, I., & Vale, R. D. (2017). T cell costimulatory receptor CD28 is a primary target for PD-1–mediated inhibition. *Science*, *355*(6332), 1428-1433. https://doi.org/doi:10.1126/science.aaf1292

Huster, K. M., Busch, V., Schiemann, M., Linkemann, K., Kerksiek, K. M., Wagner, H., & Busch, D. H. (2004). Selective expression of IL-7 receptor on memory T cells identifies early CD40L-dependent generation of distinct CD8⁺ memory T cell subsets. *Proceedings of the National Academy of Sciences*, *101*(15), 5610-5615. https://doi.org/doi:10.1073/pnas.0308054101

Ichii, H., Sakamoto, A., Kuroda, Y., & Tokuhisa, T. (2004). Bcl6 Acts as an Amplifier for the Generation and Proliferative Capacity of Central Memory CD8+ T Cells1. *The Journal of Immunology*, *173*(2), 883-891. https://doi.org/10.4049/jimmunol.173.2.883

Intlekofer, A. M., Banerjee, A., Takemoto, N., Gordon, S. M., DeJong, C. S., Shin, H., Hunter, C. A., Wherry, E. J., Lindsten, T., & Reiner, S. L. (2008). Anomalous Type 17 Response to Viral Infection by CD8⁺ T Cells Lacking T-bet and Eomesodermin. *Science*, *321*(5887), 408-411. https://doi.org/doi:10.1126/science.1159806

Isberner, N., Kraus, S., Grigoleit, G. U., Aghai, F., Kurlbaum, M., Zimmermann, S., Klinker, H., & Scherf-Clavel, O. (2021). Ruxolitinib exposure in patients with acute and chronic graft versus host disease in routine clinical practice—a prospective single-center trial. *Cancer Chemotherapy and Pharmacology*, *88*(6), 973-983. https://doi.org/10.1007/s00280-021-04351-w

Ivo, V., Sanja, P., Taghi, M., Graciela, M. N.-G., Srdan, V., & Zeev, E. (2021). Altered T-cell subset repertoire affects treatment outcome of patients with myelofibrosis. *Haematologica*, *106*(9), 2384-2396. https://doi.org/10.3324/haematol.2020.249441

Jameson, S. C., & Masopust, D. (2018). Understanding Subset Diversity in T Cell Memory. *Immunity*, *48*(2), 214-226. https://doi.org/https://doi.org/10.1016/j.immuni.2018.02.010

Johnston, C. U., & Kennedy, C. J. (2024). A Review of P-Glycoprotein Function and Regulation in Fish. *Fishes*, *9*(2), 51. https://www.mdpi.com/2410-3888/9/2/51

Joshi, N. S., Cui, W., Chandele, A., Lee, H. K., Urso, D. R., Hagman, J., Gapin, L., & Kaech, S. M. (2007). Inflammation Directs Memory Precursor and Short-Lived Effector CD8+ T Cell Fates via the Graded Expression of T-bet Transcription Factor. *Immunity*, *27*(2), 281-295. https://doi.org/https://doi.org/10.1016/j.immuni.2007.07.010

June, C. H. (2007). Principles of adoptive T cell cancer therapy. *The Journal of Clinical Investigation*, *117*(5), 1204-1212. https://doi.org/10.1172/JCI31446

Kaech, S. M., & Cui, W. (2012). Transcriptional control of effector and memory CD8+ T cell differentiation. *Nature Reviews Immunology*, *12*(11), 749-761. https://doi.org/10.1038/nri3307

Kaech, S. M., Tan, J. T., Wherry, E. J., Konieczny, B. T., Surh, C. D., & Ahmed, R. (2003). Selective expression of the interleukin 7 receptor identifies effector CD8 T cells that give rise to long-lived memory cells. *Nature Immunology*, *4*(12), 1191-1198. https://doi.org/10.1038/ni1009

Kaech, S. M., & Wherry, E. J. (2007). Heterogeneity and Cell-Fate Decisions in Effector and Memory CD8+ T Cell Differentiation during Viral Infection. *Immunity*, *27*(3), 393-405. https://doi.org/https://doi.org/10.1016/j.immuni.2007.08.007

Kalia, V., & Sarkar, S. (2018). Regulation of Effector and Memory CD8 T Cell Differentiation by IL-2—A Balancing Act [Mini Review]. *Frontiers in Immunology*, *Volume 9 - 2018*. https://doi.org/10.3389/fimmu.2018.02987

Kallies, A., Xin, A., Belz, G. T., & Nutt, S. L. (2009). Blimp-1 Transcription Factor Is Required for the Differentiation of Effector CD8+ T Cells and Memory Responses. *Immunity*, *31*(2), 283-295. https://doi.org/https://doi.org/10.1016/j.immuni.2009.06.021

Kang, S., Mansurov, A., Kurtanich, T., Chun, H. R., Slezak, A. J., Volpatti, L. R., Chang, K., Wang, T., Alpar, A. T., Refvik, K. C., Hansen, O. I., Borjas, G. J., Shim, H.-N., Hultgren, K. T., Gomes, S., Solanki, A., Ishihara, J., Swartz, M. A., & Hubbell, J. A. (2023). Engineered IL-7 synergizes with IL-12 immunotherapy to prevent T cell exhaustion and promote memory without exacerbating toxicity. *Science Advances*, *9*(48), eadh9879. https://doi.org/doi:10.1126/sciadv.adh9879

Karthika, C., Sureshkumar, R., Zehravi, M., Akter, R., Ali, F., Ramproshad, S., Mondal, B., Tagde, P., Ahmed, Z., Khan, F. S., Rahman, M. H., & Cavalu, S. (2022). Multidrug Resistance of Cancer Cells and the Vital Role of P-Glycoprotein. *Life*, *12*(6), 897. https://www.mdpi.com/2075-1729/12/6/897

Kawaguchi, K., & Morita, M. (2016). ABC Transporter Subfamily D: Distinct Differences in Behavior between ABCD1–3 and ABCD4 in Subcellular Localization, Function, and Human Disease. *BioMed Research International*, *2016*(1), 6786245. https://doi.org/https://doi.org/10.1155/2016/6786245

Khanniche, A., Yang, Y., Zhang, J., Liu, S., Xia, L., Duan, H., Yao, Y., Zhao, B., Zhao, G.-P., Hu, C., Wang, Y., & Lu, S. (2022). Early-like differentiation status of systemic PD-1+CD8+ T cells predicts PD-1 blockade outcome in non-small cell lung cancer. *Clinical & Translational Immunology*, *11*(7), e1406. https://doi.org/https://doi.org/10.1002/cti2.1406

Koh, C.-H., Lee, S., Kwak, M., Kim, B.-S., & Chung, Y. (2023). CD8 T-cell subsets: heterogeneity, functions, and therapeutic potential. *Experimental & Molecular Medicine*, *55*(11), 2287-2299. https://doi.org/10.1038/s12276-023-01105-x

Kooij, G., Kroon, J., Paul, D., Reijerkerk, A., Geerts, D., van der Pol, S. M. A., van het Hof, B., Drexhage, J. A., van Vliet, S. J., Hekking, L. H. P., van Buul, J. D., Pachter, J. S., & de Vries, H. E. (2014). P-glycoprotein regulates trafficking of CD8+ T cells to the brain parenchyma. *Acta Neuropathologica*, *127*(5), 699-711. https://doi.org/10.1007/s00401-014-1244-8

Krasznai, Z. T., Trencsényi, G., Krasznai, Z., Mikecz, P., Nizsalóczki, E., Szalóki, G., Szabó, J. P., Balkay, L., Márián, T., & Goda, K. (2014). 18FDG a PET tumor diagnostic tracer is not a substrate of the ABC transporter P-glycoprotein. *European Journal of*

Pharmaceutical Sciences, *64*, 1-8. https://doi.org/https://doi.org/10.1016/j.ejps.2014.08.002

Kudernatsch, R. F., Letsch, A., Guerreiro, M., Löbel, M., Bauer, S., Volk, H.-D., & Scheibenbogen, C. (2014). Human bone marrow contains a subset of quiescent early memory CD8+ T cells characterized by high CD127 expression and efflux capacity. *European Journal of Immunology*, *44*(12), 3532-3542. https://doi.org/https://doi.org/10.1002/eji.201344180

Kurachi, M. (2019). CD8+ T cell exhaustion. *Seminars in Immunopathology*, *41*(3), 327-337. https://doi.org/10.1007/s00281-019-00744-5

La Rosée, F., Bremer, H. C., Gehrke, I., Kehr, A., Hochhaus, A., Birndt, S., Fellhauer, M., Henkes, M., Kumle, B., Russo, S. G., & La Rosée, P. (2020). The Janus kinase 1/2 inhibitor ruxolitinib in COVID-19 with severe systemic hyperinflammation. *Leukemia*, *34*(7), 1805-1815. https://doi.org/10.1038/s41375-020-0891-0

Lee, J. S., Jung, I. D., Lee, C.-M., Noh, K. T., Park, J. W., Son, K. H., Heo, D. R., Shin, Y. K., Kim, D., & Park, Y.-M. (2011). Venlafaxine inhibits the development and differentiation of dendritic cells through the regulation of p-glycoprotein. *International Immunopharmacology*, *11*(9), 1348-1357. https://doi.org/https://doi.org/10.1016/j.intimp.2011.04.019

Liau, N. P. D., Laktyushin, A., Morris, R., Sandow, J. J., Nicola, N. A., Kershaw, N. J., & Babon, J. J. (2019). Enzymatic Characterization of Wild-Type and Mutant Janus Kinase 1. *Cancers*, *11*(11), 1701. https://www.mdpi.com/2072-6694/11/11/1701

Liu, Q., Sun, Z., & Chen, L. (2020). Memory T cells: strategies for optimizing tumor immunotherapy. *Protein & Cell*, *11*(8), 549-564. https://doi.org/10.1007/s13238-020-00707-9

Lowry, O., Rosebrough, N., Farr, A. L., & Randall, R. (1951). Protein measurement with the folin phenol reagent. *Journal of Biological Chemistry*, *193*(1), 265-275. https://doi.org/https://doi.org/10.1016/S0021-9258(19)52451-6

Lugli, E., Galletti, G., Boi, S. K., & Youngblood, B. A. (2020). Stem, Effector, and Hybrid States of Memory CD8+ T Cells. *Trends in Immunology*, *41*(1), 17-28. https://doi.org/https://doi.org/10.1016/j.it.2019.11.004

Lugli, E., Gattinoni, L., Roberto, A., Mavilio, D., Price, D. A., Restifo, N. P., & Roederer, M. (2013). Identification, isolation and in vitro expansion of human and nonhuman primate T stem cell memory cells. *Nature Protocols*, *8*(1), 33-42. https://doi.org/10.1038/nprot.2012.143

Mackay, L. K., Stock, A. T., Ma, J. Z., Jones, C. M., Kent, S. J., Mueller, S. N., Heath, W. R., Carbone, F. R., & Gebhardt, T. (2012). Long-lived epithelial immunity by tissue-resident memory T (T_{RM}) cells in the absence of persisting local antigen

presentation. *Proceedings of the National Academy of Sciences*, *109*(18), 7037-7042. https://doi.org/doi:10.1073/pnas.1202288109

Mahnke, Y. D., Brodie, T. M., Sallusto, F., Roederer, M., & Lugli, E. (2013). The who's who of T-cell differentiation: Human memory T-cell subsets. *European Journal of Immunology*, *43*(11), 2797-2809. https://doi.org/https://doi.org/10.1002/eji.201343751

Maranghi, M., Truglio, G., Gallo, A., Grieco, E., Verrienti, A., Montali, A., Gallo, P., Alesini, F., Arca, M., & Lucarelli, M. (2019). A novel splicing mutation in the ABCA1 gene, causing Tangier disease and familial HDL deficiency in a large family. *Biochemical and Biophysical Research Communications*, *508*(2), 487-493. https://doi.org/https://doi.org/10.1016/j.bbrc.2018.11.064

McInnes, L., Healy, J., Saul, N., & Großberger, L. (2018). UMAP: Uniform Manifold Approximation and Projection. *J. Open Source Softw.*, *3*(29), 861. https://doi.org/10.21105/joss.00861

Min, X., Ungureanu, D., Maxwell, S., Hammarén, H., Thibault, S., Hillert, E.-K., Ayres, M., Greenfield, B., Eksterowicz, J., Gabel, C., Walker, N., Silvennoinen, O., & Wang, Z. (2015). Structural and Functional Characterization of the JH2 Pseudokinase Domain of JAK Family Tyrosine Kinase 2 (TYK2)*. *Journal of Biological Chemistry*, *290*(45), 27261-27270. https://doi.org/https://doi.org/10.1074/jbc.M115.672048

Moore, J. M., Bell, E. L., Hughes, R. O., & Garfield, A. S. (2023). ABC transporters: human disease and pharmacotherapeutic potential. *Trends in Molecular Medicine*, *29*(2), 152-172. https://doi.org/https://doi.org/10.1016/j.molmed.2022.11.001

Mora Lagares, L., Pérez-Castillo, Y., Minovski, N., & Novič, M. (2022). Structure–Function Relationships in the Human P-Glycoprotein (ABCB1): Insights from Molecular Dynamics Simulations. *International Journal of Molecular Sciences*, *23*(1), 362. https://www.mdpi.com/1422-0067/23/1/362

Morita, M., & Imanaka, T. (2012). Peroxisomal ABC transporters: Structure, function and role in disease. *Biochimica et Biophysica Acta (BBA) - Molecular Basis of Disease*, *1822*(9), 1387-1396. https://doi.org/https://doi.org/10.1016/j.bbadis.2012.02.009

Murata, K., Tomohide, T., Makoto, E., Yuji, S., Emi, M., Hiroshi, M., Keiji, Y., Mitsunori, K., Yoshihiko, H., Takayuki, K., Terufumi, K., Tetsuo, H., Shingo, I., Toshihiko, Y., Noriyuki, S., & and Torigoe, T. (2016). Identification of a novel human memory T-cell population with the characteristics of stem-like chemo-resistance. *OncoImmunology*, *5*(6), e1165376. https://doi.org/10.1080/2162402X.2016.1165376

Muroyama, Y., & Wherry, E. J. (2021). Memory T-Cell Heterogeneity and Terminology. *Cold Spring Harbor Perspectives in Biology*, *13*(10). https://doi.org/10.1101/cshperspect.a037929 (P a037929)

Neubauer, D. N. (2007). The Evolution and Development of Insomnia Pharmacotherapies. *Journal of Clinical Sleep Medicine*, *3*(5 suppl), S11-S16. https://doi.org/doi:10.5664/jcsm.26930

Neudeck, B. L., Loeb, J. M., Faith, N. G., & Czuprynski, C. J. (2004). Intestinal P Glycoprotein Acts as a Natural Defense Mechanism against Listeria monocytogenes. *Infection and Immunity*, *72*(7), 3849-3854. https://doi.org/doi:10.1128/iai.72.7.3849-3854.2004

O'Shea, J. J., Husa, M., Li, D., Hofmann, S. R., Watford, W., Roberts, J. L., Buckley, R. H., Changelian, P., & Candotti, F. (2004). Jak3 and the pathogenesis of severe combined immunodeficiency. *Molecular Immunology*, *41*(6), 727-737. https://doi.org/https://doi.org/10.1016/j.molimm.2004.04.014

Oiwa, K., & Sakakibara, H. (2005). Recent progress in dynein structure and mechanism. *Current Opinion in Cell Biology*, *17*(1), 98-103. https://doi.org/https://doi.org/10.1016/j.ceb.2004.12.006

Ortega, M. A., Boaru, D. L., De Leon-Oliva, D., Fraile-Martinez, O., García-Montero, C., Rios, L., Garrido-Gil, M. J., Barrena-Blázquez, S., Minaya-Bravo, A. M., Rios-Parra, A., Álvarez-Mon, M., Jiménez-Álvarez, L., López-González, L., Guijarro, L. G., Diaz, R., & Saez, M. A. (2024). PD-1/PD-L1 axis: implications in immune regulation, cancer progression, and translational applications. *Journal of Molecular Medicine*, *102*(8), 987-1000. https://doi.org/10.1007/s00109-024-02463-3

Ostojic, A., Radovan, V., & and Verstovsek, S. (2011). Ruxolitinib: A New JAK1/2 Inhibitor That Offers Promising Options for Treatment of Myelofibrosis. *Future Oncology*, *7*(9), 1035-1043. https://doi.org/10.2217/fon.11.81

Parween, F., Singh, S. P., Zhang, H. H., Kathuria, N., Otaizo-Carrasquero, F. A., Shamsaddini, A., Gardina, P. J., Ganesan, S., Kabat, J., Lorenzi, H. A., Myers, T. G., & Farber, J. M. (2023). Chemokine positioning determines mutually exclusive roles for their receptors in extravasation of pathogenic human T cells. *bioRxiv*, 2023.2001.2025.525561. https://doi.org/10.1101/2023.01.25.525561

Pavlova, E. N., Lepekha, L. N., Rybalkina, E. Y., Tarasov, R. V., Sychevskaya, K. A., Voronezhskaya, E. E., Masyutin, A. G., Ergeshov, A. E., & Erokhina, M. V. (2023). High and Low Levels of ABCB1 Expression Are Associated with Two Distinct Gene Signatures in Lung Tissue of Pulmonary TB Patients with High Inflammation Activity. *International Journal of Molecular Sciences*, *24*(19), 14839. https://www.mdpi.com/1422-0067/24/19/14839

Pendse, S. S., Briscoe, D. M., & Frank, M. H. (2003). P-glycoprotein and alloimmune T-cell activation. *Clinical and Applied Immunology Reviews*, *4*(1), 3-14. https://doi.org/https://doi.org/10.1016/S1529-1049(03)00007-2

Ramos, A., Sadeghi, S., & Tabatabaeian, H. (2021). Battling Chemoresistance in Cancer: Root Causes and Strategies to Uproot Them. *International Journal of Molecular Sciences*, *22*(17), 9451. https://www.mdpi.com/1422-0067/22/17/9451

Randolph, G. J., Beaulieu, S., Pope, M., Sugawara, I., Hoffman, L., Steinman, R. M., & Muller, W. A. (1998). A physiologic function for p-glycoprotein (MDR-1) during the migration of dendritic cells from skin via afferent lymphatic vessels. *Proceedings of the National Academy of Sciences, 95*(12), 6924-6929. https://doi.org/doi:10.1073/pnas.95.12.6924

Raskov, H., Orhan, A., Christensen, J. P., & Gögenur, I. (2021). Cytotoxic CD8+ T cells in cancer and cancer immunotherapy. *British Journal of Cancer, 124*(2), 359-367. https://doi.org/10.1038/s41416-020-01048-4

Reading, J. L., Gálvez-Cancino, F., Swanton, C., Lladser, A., Peggs, K. S., & Quezada, S. A. (2018). The function and dysfunction of memory CD8+ T cells in tumor immunity. *Immunological Reviews, 283*(1), 194-212. https://doi.org/https://doi.org/10.1111/imr.12657

Rekik, R., Belhadj Hmida, N., Ben Hmid, A., Zamali, I., Kammoun, n., & Ben Ahmed, M. (2015). PD-1 induction through TCR activation is partially regulated by endogenous TGF-β. *Cellular & Molecular Immunology*, *12*(5), 648-649. https://doi.org/10.1038/cmi.2014.104

Restifo, N. P., & Gattinoni, L. (2013). Lineage relationship of effector and memory T cells. *Current Opinion in Immunology, 25*(5), 556-563. https://doi.org/https://doi.org/10.1016/j.coi.2013.09.003

Risso, V., Lafont, E., & Le Gallo, M. (2022). Therapeutic approaches targeting CD95L/CD95 signaling in cancer and autoimmune diseases. *Cell Death & Disease*, *13*(3), 248. https://doi.org/10.1038/s41419-022-04688-x

Sallusto, F., Lenig, D., Förster, R., Lipp, M., & Lanzavecchia, A. (1999). Two subsets of memory T lymphocytes with distinct homing potentials and effector functions. *Nature, 401*(6754), 708-712. https://doi.org/10.1038/44385

Sandu, I., Cerletti, D., Oetiker, N., Borsa, M., Wagen, F., Spadafora, I., Welten, S. P. M., Stolz, U., Oxenius, A., & Claassen, M. (2020). Landscape of Exhausted Virus-Specific CD8 T Cells in Chronic LCMV Infection. *Cell Reports, 32*(8), 108078. https://doi.org/https://doi.org/10.1016/j.celrep.2020.108078

Sarkadi, B., Homolya, L., Szakács, G., & Váradi, A. (2006). Human Multidrug Resistance ABCB and ABCG Transporters: Participation in a Chemoimmunity Defense System. *Physiological Reviews, 86*(4), 1179-1236. https://doi.org/10.1152/physrev.00037.2005

Sarkadi, B., Price, E. M., Boucher, R. C., Germann, U. A., & Scarborough, G. A. (1992). Expression of the human multidrug resistance cDNA in insect cells generates a high activity drug-stimulated membrane ATPase. *Journal of Biological Chemistry, 267*(7), 4854-4858. https://doi.org/https://doi.org/10.1016/S0021-9258(18)42909-2

Schneider, E., Winzer, R., Rissiek, A., Ricklefs, I., Meyer-Schwesinger, C., Ricklefs, F. L., Bauche, A., Behrends, J., Reimer, R., Brenna, S., Wasielewski, H., Lauten, M., Rissiek, B., Puig, B., Cortesi, F., Magnus, T., Fliegert, R., Müller, C. E., Gagliani, N., & Tolosa,

E. (2021). CD73-mediated adenosine production by CD8 T cell-derived extracellular vesicles constitutes an intrinsic mechanism of immune suppression. *Nature Communications*, *12*(1), 5911. https://doi.org/10.1038/s41467-021-26134-w

Seelig, A. (2020). P-Glycoprotein: One Mechanism, Many Tasks and the Consequences for Pharmacotherapy of Cancers [Review]. *Frontiers in Oncology*, *Volume 10 - 2020*. https://doi.org/10.3389/fonc.2020.576559

Shakiba, M., Zumbo, P., Espinosa-Carrasco, G., Menocal, L., Dündar, F., Carson, S. E., Bruno, E. M., Sanchez-Rivera, F. J., Lowe, S. W., Camara, S., Koche, R. P., Reuter, V. P., Socci, N. D., Whitlock, B., Tamzalit, F., Huse, M., Hellmann, M. D., Wells, D. K., Defranoux, N. A.,…Schietinger, A. (2021). TCR signal strength defines distinct mechanisms of T cell dysfunction and cancer evasion. *Journal of Experimental Medicine*, *219*(2). https://doi.org/10.1084/jem.20201966

Shawky, A. M., Almalki, F. A., Abdalla, A. N., Abdelazeem, A. H., & Gouda, A. M. (2022). A Comprehensive Overview of Globally Approved JAK Inhibitors. *Pharmaceutics*, *14*(5), 1001. https://www.mdpi.com/1999-4923/14/5/1001

Singh, K., Tarapcsák, S., Gyöngy, Z., Ritter, Z., Batta, G., Bosire, R., Remenyik, J., & Goda, K. (2021). Effects of Polyphenols on P-Glycoprotein (ABCB1) Activity. *Pharmaceutics*, *13*(12), 2062. https://www.mdpi.com/1999-4923/13/12/2062

Skinner, K. T., Palkar, A. M., & Hong, A. L. (2023). Genetics of ABCB1 in Cancer. *Cancers*, *15*(17), 4236. https://www.mdpi.com/2072-6694/15/17/4236

Soerens, A. G., Künzli, M., Quarnstrom, C. F., Scott, M. C., Swanson, L., Locquiao, J. J., Ghoneim, H. E., Zehn, D., Youngblood, B., Vezys, V., & Masopust, D. (2023). Functional T cells are capable of supernumerary cell division and longevity. *Nature*, *614*(7949), 762-766. https://doi.org/10.1038/s41586-022-05626-9

Sorf, A., Sucha, S., Morell, A., Novotna, E., Staud, F., Zavrelova, A., Visek, B., Wsol, V., & Ceckova, M. (2020). Targeting Pharmacokinetic Drug Resistance in Acute Myeloid Leukemia Cells with CDK4/6 Inhibitors. *Cancers*, *12*(6), 1596. https://www.mdpi.com/2072-6694/12/6/1596

Srikant, S. (2020). Evolutionary history of ATP-binding cassette proteins. *FEBS Letters*, *594*(23), 3882-3897. https://doi.org/https://doi.org/10.1002/1873-3468.13985

St. Paul, M., & Ohashi, P. S. (2020). The Roles of CD8+ T Cell Subsets in Antitumor Immunity. *Trends in Cell Biology*, *30*(9), 695-704. https://doi.org/https://doi.org/10.1016/j.tcb.2020.06.003

Stemberger, C., Neuenhahn, M., Gebhardt, F. E., Schiemann, M., Buchholz, V. R., & Busch, D. H. (2009). Stem cell-like plasticity of naïve and distinct memory CD8+ T cell subsets. *Seminars in Immunology*, *21*(2), 62-68. https://doi.org/https://doi.org/10.1016/j.smim.2009.02.004

Stratford, Fiona L. L., Ramjeesingh, M., Cheung, Joanne C., Huan, L.-J., & Bear, Christine E. (2006). The Walker B motif of the second nucleotide-binding domain (NBD2) of CFTR plays a key role in ATPase activity by the NBD1–NBD2 heterodimer. *Biochemical Journal*, *401*(2), 581-586. https://doi.org/10.1042/bj20060968

Sun, L., Su, Y., Jiao, A., Wang, X., & Zhang, B. (2023). T cells in health and disease. *Signal Transduction and Targeted Therapy*, *8*(1), 235. https://doi.org/10.1038/s41392-023-01471-y

Tarapcsák, S., Szalóki, G., Telbisz, Á., Gyöngy, Z., Matúz, K., Csősz, É., Nagy, P., Holb, I. J., Rühl, R., Nagy, L., Szabó, G., & Goda, K. (2017). Interactions of retinoids with the ABC transporters P-glycoprotein and Breast Cancer Resistance Protein. *Scientific Reports*, *7*(1), 41376. https://doi.org/10.1038/srep41376

Terrabuio, E., Zenaro, E., & Constantin, G. (2023). The role of the CD8+ T cell compartment in ageing and neurodegenerative disorders [Review]. *Frontiers in Immunology*, *Volume 14 - 2023*. https://doi.org/10.3389/fimmu.2023.1233870

Teshima, T., & Hashimoto, D. (2023). Separation of GVL from GVHD -location, location, location [Mini Review]. *Frontiers in Immunology*, *Volume 14 - 2023*. https://doi.org/10.3389/fimmu.2023.1296663

Thurm, C., Schraven, B., & Kahlfuss, S. (2021). ABC Transporters in T Cell-Mediated Physiological and Pathological Immune Responses. *International Journal of Molecular Sciences*, *22*(17), 9186. https://www.mdpi.com/1422-0067/22/17/9186

Trencsényi, G., Kertész, I., Krasznai, Z. T., Máté, G., Szalóki, G., Szabó Judit, P., Kárpáti, L., Krasznai, Z., Márián, T., & Goda, K. (2015). 2′[18F]-fluoroethylrhodamine B is a promising radiotracer to measure P-glycoprotein function. *European Journal of Pharmaceutical Sciences*, *74*, 27-35. https://doi.org/https://doi.org/10.1016/j.ejps.2015.03.026

Tsui, C., Kretschmer, L., Rapelius, S., Gabriel, S. S., Chisanga, D., Knöpper, K., Utzschneider, D. T., Nüssing, S., Liao, Y., Mason, T., Torres, S. V., Wilcox, S. A., Kanev, K., Jarosch, S., Leube, J., Nutt, S. L., Zehn, D., Parish, I. A., Kastenmüller, W.,…Kallies, A. (2022). MYB orchestrates T cell exhaustion and response to checkpoint inhibition. *Nature*, *609*(7926), 354-360. https://doi.org/10.1038/s41586-022-05105-1

Türk, L., Filippov, I., Arnold, C., Zaugg, J., Tserel, L., Kisand, K., & Peterson, P. (2024). Cytotoxic CD8+ Temra cells show loss of chromatin accessibility at genes associated with T cell activation [Original Research]. *Frontiers in Immunology*, *Volume 15 - 2024*. https://doi.org/10.3389/fimmu.2024.1285798

Turtle, C. J., Swanson, H. M., Fujii, N., Estey, E. H., & Riddell, S. R. (2009). A Distinct Subset of Self-Renewing Human Memory CD8+ T Cells Survives Cytotoxic Chemotherapy. *Immunity*, *31*(5), 834-844. https://doi.org/https://doi.org/10.1016/j.immuni.2009.09.015

Ueda, K., Cornwell, M. M., Gottesman, M. M., Pastan, I., Roninson, I. B., Ling, V., & Riordan, J. R. (1986). The mdrl gene, responsible for multidrug-resistance, codes for P-glycoprotein. *Biochemical and Biophysical Research Communications*, *141*(3), 956-962. https://doi.org/https://doi.org/10.1016/S0006-291X(86)80136-X

Vainchenker, W., Leroy, E., Gilles, L., Marty, C., Plo, I., & Constantinescu, S. (2018). JAK inhibitors for the treatment of myeloproliferative neoplasms and other disorders [version 1; peer review: 2 approved]. *F1000Research*, *7*(82). https://doi.org/10.12688/f1000research.13167.1

van den Broek, T., Borghans, J. A. M., & van Wijk, F. (2018). The full spectrum of human naive T cells. *Nature Reviews Immunology*, *18*(6), 363-373. https://doi.org/10.1038/s41577-018-0001-y

Van Gassen, S., Callebaut, B., Van Helden, M. J., Lambrecht, B. N., Demeester, P., Dhaene, T., & Saeys, Y. (2015). FlowSOM: Using self-organizing maps for visualization and interpretation of cytometry data. *Cytometry Part A*, *87*(7), 636-645. https://doi.org/https://doi.org/10.1002/cyto.a.22625

Verbeke, D., Gielen, O., Jacobs, K., Boeckx, N., De Keersmaecker, K., Maertens, J., Uyttebroeck, A., Segers, H., & Cools, J. (2019). Ruxolitinib Synergizes With Dexamethasone for the Treatment of T-cell Acute Lymphoblastic Leukemia. *HemaSphere*, *3*(6), e310. https://doi.org/10.1097/hs9.0000000000000310

Wang, D., Fang, J., Wen, S., Li, Q., Wang, J., Yang, L., Dai, W., Lu, H., Guo, J., Shan, Z., Xie, W., Liu, X., Wen, L., Shen, J., Wang, A., Chen, Q., & Wang, Z. (2022). A comprehensive profile of TCF1+ progenitor and TCF1− terminally exhausted PD-1+CD8+ T cells in head and neck squamous cell carcinoma: implications for prognosis and immunotherapy. *International Journal of Oral Science*, *14*(1), 8. https://doi.org/10.1038/s41368-022-00160-w

Wang, L., Huang, Q.-H., Li, Y.-X., Huang, Y.-F., Xie, J.-H., Xu, L.-Q., Dou, Y.-X., Su, Z.-R., Zeng, H.-F., & Chen, J.-N. (2018). Protective effects of silymarin on triptolide-induced acute hepatotoxicity in rats. *Mol Med Rep*, *17*(1), 789-800. https://doi.org/10.3892/mmr.2017.7958

Wang, L., Shah, S. M., Mangwani-Mordani, S., & Gregori, N. Z. (2023). Updates on Emerging Interventions for Autosomal Recessive ABCA4-Associated Stargardt Disease. *Journal of Clinical Medicine*, *12*(19), 6229. https://www.mdpi.com/2077-0383/12/19/6229

Wherry, E. J., Blattman, J. N., Murali-Krishna, K., Most, R. v. d., & Ahmed, R. (2003). Viral Persistence Alters CD8 T-Cell Immunodominance and Tissue Distribution and Results in Distinct Stages of Functional Impairment. *Journal of Virology*, *77*(8), 4911-4927. https://doi.org/doi:10.1128/jvi.77.8.4911-4927.2003

Wherry, E. J., Ha, S.-J., Kaech, S. M., Haining, W. N., Sarkar, S., Kalia, V., Subramaniam, S., Blattman, J. N., Barber, D. L., & Ahmed, R. (2007). Molecular Signature of CD8+ T Cell

Exhaustion during Chronic Viral Infection. *Immunity*, *27*(4), 670-684. https://doi.org/https://doi.org/10.1016/j.immuni.2007.09.006

Willinger, T., Freeman, T., Herbert, M., Hasegawa, H., McMichael, A. J., & Callan, M. F. C. (2006). Human Naive CD8 T Cells Down-Regulate Expression of the WNT Pathway Transcription Factors Lymphoid Enhancer Binding Factor 1 and Transcription Factor 7 (T Cell Factor-1) following Antigen Encounter In Vitro and In Vivo1. *The Journal of Immunology*, *176*(3), 1439-1446. https://doi.org/10.4049/jimmunol.176.3.1439

Xia, Y., Liu, A., Li, W., Liu, Y., Zhang, G., Ye, S., Zhao, Z., Shi, J., Jia, Y., Liu, X., Guo, Y., Chen, H., & Yu, J. (2021). Reference range of naïve T and T memory lymphocyte subsets in peripheral blood of healthy adult. *Clinical and Experimental Immunology*, *207*(2), 208-217. https://doi.org/10.1093/cei/uxab038

Xin, A., Masson, F., Liao, Y., Preston, S., Guan, T., Gloury, R., Olshansky, M., Lin, J.-X., Li, P., Speed, T. P., Smyth, G. K., Ernst, M., Leonard, W. J., Pellegrini, M., Kaech, S. M., Nutt, S. L., Shi, W., Belz, G. T., & Kallies, A. (2016). A molecular threshold for effector CD8+ T cell differentiation controlled by transcription factors Blimp-1 and T-bet. *Nature Immunology*, *17*(4), 422-432. https://doi.org/10.1038/ni.3410

Xu, L., Zhang, Y., Luo, G., & Li, Y. (2015). The roles of stem cell memory T cells in hematological malignancies. *Journal of Hematology & Oncology*, *8*(1), 113. https://doi.org/10.1186/s13045-015-0214-5

Yang, C. Y., Best, J. A., Knell, J., Yang, E., Sheridan, A. D., Jesionek, A. K., Li, H. S., Rivera, R. R., Lind, K. C., D'Cruz, L. M., Watowich, S. S., Murre, C., & Goldrath, A. W. (2011). The transcriptional regulators Id2 and Id3 control the formation of distinct memory CD8+ T cell subsets. *Nature Immunology*, *12*(12), 1221-1229. https://doi.org/10.1038/ni.2158

Yin, L., Castagnino, P., & Assoian, R. K. (2008). ABCG2 Expression and Side Population Abundance Regulated by a Transforming Growth Factor β–Directed Epithelial-Mesenchymal Transition. *Cancer Research*, *68*(3), 800-807. https://doi.org/10.1158/0008-5472.Can-07-2545

Zak, J., Pratumchai, I., Marro, B. S., Marquardt, K. L., Zavareh, R. B., Lairson, L. L., Oldstone, M. B. A., Varner, J. A., Hegerova, L., Cao, Q., Farooq, U., Kenkre, V. P., Bachanova, V., & Teijaro, J. R. (2024). JAK inhibition enhances checkpoint blockade immunotherapy in patients with Hodgkin lymphoma. *Science*, *384*(6702), eade8520. https://doi.org/doi:10.1126/science.ade8520

Zhang, J.-C., Xie, F., Yu, X.-H., Deng, Z.-Y., Wang, Y., Liang, P., Sun, L., & Zhang, F.-X. (2014). Expression levels of P-glycoprotein in peripheral blood CD8+ T lymphocytes from HIV-1-infected patients on antiretroviral therapy. *Int J Mol Med*, *33*(2), 431-440. https://doi.org/10.3892/ijmm.2013.1584

Zhang, N., & Bevan, Michael J. (2011). CD8+ T Cells: Foot Soldiers of the Immune System. *Immunity*, *35*(2), 161-168. https://doi.org/https://doi.org/10.1016/j.immuni.2011.07.010

Zhang, Y., Joe, G., Hexner, E., Zhu, J., & Emerson, S. G. (2005). Host-reactive CD8+ memory stem cells in graft-versus-host disease. *Nature Medicine*, *11*(12), 1299-1305. https://doi.org/10.1038/nm1326

Zhao, X., Shan, Q., & Xue, H.-H. (2022). TCF1 in T cell immunity: a broadened frontier. *Nature Reviews Immunology*, *22*(3), 147-157. https://doi.org/10.1038/s41577-021-00563-6

Zhou, X., Yu, S., Zhao, D.-M., Harty, J. T., Badovinac, V. P., & Xue, H.-H. (2010). Differentiation and Persistence of Memory CD8+ T Cells Depend on T Cell Factor 1. *Immunity*, *33*(2), 229-240. https://doi.org/https://doi.org/10.1016/j.immuni.2010.08.002

Zook, E. C., Li, Z.-Y., Xu, Y., de Pooter, R. F., Verykokakis, M., Beaulieu, A., Lasorella, A., Maienschein-Cline, M., Sun, J. C., Sigvardsson, M., & Kee, B. L. (2018). Transcription factor ID2 prevents E proteins from enforcing a naïve T lymphocyte gene program during NK cell development. *Science Immunology*, *3*(22), eaao2139. https://doi.org/doi:10.1126/sciimmunol.aao2139

Zu, H., & Chen, X. (2024). Epigenetics behind CD8+ T cell activation and exhaustion. *Genes & Immunity*, *25*(6), 525-540. https://doi.org/10.1038/s41435-024-00307-1

8. KEYWORDS

P-glycoprotein; Cytotoxic T lymphocytes; CTL memory subsets; Ruxolitinib; JY cells; T cell activation; JAK-STAT signaling immune modulation; TCR activation; UMAP; flow cytometer; Subsets.

9. ACKNOWLEDGEMENTS

Earning a Ph.D. represents years of dedication, perseverance, and learning. I am profoundly grateful to God for the gift of life, good health, and abundant provisions. His unmerited favor has been my strength throughout this journey, allowing me to come this far and accomplish so much. Along the way, I have been fortunate to cross paths with individuals who have guided me, pointed me toward opportunities, and encouraged me to stay focused. While it is impossible to name each one of them, I extend my heartfelt gratitude to all who have contributed to my success.

I wish to express my sincere gratitude to my supervisor, Dr. Zsolt Bacsó, for graciously welcoming me into his lab and providing invaluable guidance over the past four years. His unwavering support, mentorship, and open-door policy have been pivotal in shaping both my research and academic growth. His dedication and commitment have had a profound impact on my journey, and I am deeply grateful for the opportunity to work under his supervision.

I extend my appreciation to my colleagues Batta Ágnes, Anass Benzaine, Nimrah Ghaffar, Algirmaa Lkhamkhuu, Timea Hajdu, Kuljeet Singh, Bilakovics Noémi, and Varga-Tóth Katic from whom I learned essential techniques and with whom I shared insightful conversations. Their presence in the lab was a great source of motivation. I also sincerely thank Marianna Száraz-Széles, Rita Katalin Utasi-Szabó, and Edina Nagy for their tireless efforts in ensuring that I always had the materials needed for my experiments and the entire Department of Biophysics and cell Biology.

A special thank you goes to the friends who made my time in Debrecen truly memorable**:** Aron Rop, Maureen Jelagat, Sanchez Noemi, Komen Boaz, and you became my family away from home, offering unwavering support and companionship. I also thank Amos Siwoi for his constant encouragement and motivation.

I am immensely grateful to our collaborators who generously shared their expertise and resources, contributing significantly to the completion of my research. My appreciation goes to Dr. Parvind Singh, Dr. Sándor Baráth, and Dr. Zsuzsanna Hevessy for their valuable contributions to my work. A heartfelt thank you to Dr. Rosevalentine Bosire, Postdoctoral Fellow at Fred Hutch, Seattle, Washington, United States, whose mentorship and encouragement played a crucial role in my

academic journey. Her guidance during my scholarship application process was invaluable, and her ongoing support has been deeply appreciated.

I am also grateful to the Tempus Foundation for awarding me the scholarship that made this academic pursuit possible, and to the Technical University of Kenya for granting me study leave to focus fully on my Ph.D.

Finally, my deepest gratitude goes to my family for their unwavering prayers, encouragement, and belief in me. Their high expectations have been a driving force throughout my academic journey. Special thanks to my parents, Dad and Mum, for their sacrifices, steadfast support, and unconditional love. Their dedication to my education and well-being have been the bedrock of my success.

10. FUNDING

Stipendium Hungaricum Scholarship grant for Kipchumba Biwott ID 409037 funded this project

11. LIST OF PUBLICATIONS RELATED TO THE DESSERTATION

UNIVERSITY AND NATIONAL LIBRARY
UNIVERSITY OF DEBRECEN
H-4002 Egyetem tér 1, Debrecen
Phone: +3652/410-443, email: publikaciok@lib.unideb.hu

Registry number: DEENK/439/2025.PL
Subject: PhD Publication List

Candidate: Kipchumba Biwott
Doctoral School: Doctoral School of Molecular Cellular and Immune Biology
MTMT ID: 10090211

List of publications related to the dissertation

1. **Biwott, K.**, Singh, P., Baráth, S., Nyariki, J. N., Hevessy, Z., Bacsó, Z.: Dynamic P-glycoprotein expression in early and late memory states of human CD8+T cells and the protective role of ruxolitinib.
Biomed. Pharmacother. 182, 1-14, 2025.
DOI: http://dx.doi.org/10.1016/j.biopha.2024.117780
IF: 7.5 (2024)

2. **Biwott, K.**, Lkhamkhuu, A., Ghaffar, N., Papp, A. B., Tarban, N., Goda, K., Bacsó, Z.: Ruxolitinib Modulates P-Glycoprotein Function, Delays T Cell Activation, and Impairs CCL19 Chemokine-Directed Migration in Human Cytotoxic T Lymphocytes.
Int. J. Mol. Sci. 26 (13), 1-21, 2025.
DOI: http://dx.doi.org/10.3390/ijms26136123
IF: 4.9 (2024)

List of other publications

3. **Biwott, K.**, Gitonga, F., Jepchirchir, C., Gitau, G. W., Wafula, O. P., Amwayi, P. W., Isaac, A. O., Nyariki, J. N.: Alcohol spiked with zolpidem and midazolam potentiates inflammation, oxidative stress and organ damage in a mouse model.
Forensic Toxicol. 42, 55-61, 2024.
DOI: http://dx.doi.org/10.1007/s11419-023-00674-w
IF: 3

4. Gellén, G., Klement, É., **Biwott, K.**, Schlosser, G., Kalló, G., Csősz, É., Medzihradszky-Fölkl, K., Bacsó, Z.: Cross-Linking Mass Spectrometry on P-Glycoprotein.
Int. J. Mol. Sci. 24 (13), 1-24, 2023.
DOI: http://dx.doi.org/10.3390/ijms241310627
IF: 4.9

UNIVERSITY AND NATIONAL LIBRARY
UNIVERSITY OF DEBRECEN
H-4002 Egyetem tér 1, Debrecen
Phone: +3652/410-443, email: publikaciok@lib.unideb.hu

5. **Biwott, K.**, Isaac, A. O., Mwaeni, V. K., Omwenga, G., Ngugi, M., Nyariki, J. N.: Vitamin B12 and coenzyme Q10 ameliorated alcohol-driven impairment of hematological parameters, inflammation, and organ damage in a mouse model.
Nutrire. 48 (1), 1-19, 2023.
DOI: http://dx.doi.org/10.1186/s41110-023-00197-9

6. Gitonga, F., **Biwott, K.**, Gitau, G. W., Wafula, O. P., Amwayi, P. W., Isaac, A. O., Nyariki, J. N.: Coenzyme Q10 Ameliorates potassium cyanide-induced toxicosis in a mouse model.
Sci. Afr. 12, 1-10, 2021.
DOI: http://dx.doi.org/10.1016/j.sciaf.2021.e00815

Total IF of journals (all publications): 20,3
Total IF of journals (publications related to the dissertation): 12,4

The Candidate's publication data submitted to the Tudóstér have been validated by DEENK on the basis of the Journal Citation Report (Impact Factor) database.

04 July, 2025